# RADIATIONAL PARAMETERIZATION FOR THE FNWC PRIMITIVE EQUATION MODEL USING DATA OVER THE OCEANS FOR 16 JULY 1974.

Terry William Beahan

# NAVAL POSTGRADUATE SCHOOL
## Monterey, California


# THESIS

RADIATIONAL PARAMETERIZATION FOR THE
FNWC PRIMITIVE EQUATION MODEL USING DATA
OVER THE OCEANS FOR 16 JULY 1974

by

Terry William Beahan

September 1975

Thesis Advisor: F. L. Martin

Approved for public release; distribution unlimited.

SECURITY CLASSIFICATION OF THIS PAGE (When Data Entered)

| REPORT DOCUMENTATION PAGE | | READ INSTRUCTIONS BEFORE COMPLETING FORM |
|---|---|---|
| 1. REPORT NUMBER | 2. GOVT ACCESSION NO. | 3. RECIPIENT'S CATALOG NUMBER |
| 4. TITLE (and Subtitle)<br>Radiational Parameterization for the FNWC Primitive Equation Model Using Data Over the Oceans for 16 July 1974 | | 5. TYPE OF REPORT & PERIOD COVERED<br>Master's Thesis<br>September 1975<br>6. PERFORMING ORG. REPORT NUMBER |
| 7. AUTHOR(s)<br>Terry William Beahan | | 8. CONTRACT OR GRANT NUMBER(s) |
| 9. PERFORMING ORGANIZATION NAME AND ADDRESS<br>Naval Postgraduate School<br>Monterey, California 93940 | | 10. PROGRAM ELEMENT, PROJECT, TASK AREA & WORK UNIT NUMBERS |
| 11. CONTROLLING OFFICE NAME AND ADDRESS<br>Naval Postgraduate School<br>Monterey, California 93940 | | 12. REPORT DATE<br>September 1975<br>13. NUMBER OF PAGES<br>123 |
| 14. MONITORING AGENCY NAME & ADDRESS(if different from Controlling Office)<br>Naval Postgraduate School<br>Monterey, California 93940 | | 15. SECURITY CLASS. (of this report)<br>Unclassified<br>15a. DECLASSIFICATION/DOWNGRADING SCHEDULE |

16. DISTRIBUTION STATEMENT (of this Report)

Approved for public release; distribution unlimited.

17. DISTRIBUTION STATEMENT (of the abstract entered in Block 20, if different from Report)

18. SUPPLEMENTARY NOTES

19. KEY WORDS (Continue on reverse side if necessary and identify by block number)

20. ABSTRACT (Continue on reverse side if necessary and identify by block number)

This study employs a radiational model, with large-scale cloud parameterization in several layers, in order to compute the absorption of solar insolation by the ocean's surface and by atmospheric layers, and to compute the planetary albedo for the FNWC primitive equation model. Solar insolation dispositions were computed on a gridpoint basis using water-vapor mass and cloud amounts. Using emissivity formulas after Sasamori, the long-wave cooling effects were calculated at the earth's surface and over the tropospheric

DD FORM 1 JAN 73 1473 EDITION OF 1 NOV 65 IS OBSOLETE
S/N 0102-014-6601 |
(Page 1)



SECURITY CLASSIFICATION OF THIS PAGE (When Data Entered)

layers, and were found to be dependent upon the cloud parameterization.

FNWC data over oceanic gridpoints for 16 July 1974 were used to test two forms of the cloud parameterization. The objective was to determine the parameterization which better verified the radiational balance at the top of the atmosphere as a function of latitude as compared with satellite climatology. The smaller cloud parameterization gave the better verification.

# Radiational Parameterization for the FNWC Primitive Equation Model Using Data Over the Oceans for 16 July 1974

by

Terry William Beahan
Lieutenant, United States Navy
B.S., University of Montana, 1967

Submitted in partial fulfillment of the
requirements for the degree of

MASTER OF SCIENCE IN METEOROLOGY

ABSTRACT

This study employs a radiational model, with large-scale cloud parameterization in several layers, in order to compute the absorption of solar insolation by the ocean's surface and by atmospheric layers, and to compute the planetary albedo for the FNWC primitive equation model. Solar insolation dispositions were computed on a gridpoint basis using water-vapor mass and cloud amounts. Using emissivity formulas after Sasamori, the long-wave cooling effects were calculated at the earth's surface and over the tropospheric layers, and were found to be dependent upon the cloud parameterization.

FNWC data over oceanic gridpoints for 16 July 1974 were used to test two forms of the cloud parameterization. The objective was to determine the parameterization which better verified the radiational balance at the top of the atmosphere as a function of latitude as compared with satellite climatology. The smaller cloud parameterization gave the better verification.

TABLE OF CONTENTS


I. INTRODUCTION - - - - - - - - - - - - - - - - - - - - - - - - 16

II. DATA PREPARATION - - - - - - - - - - - - - - - - - - - - - - 19

A. INITIAL DATA FIELDS- - - - - - - - - - - - - - - - - - - 19

B. INTERPOLATIVE PROCESSING TO K-LEVELS IN RADIATIVE SOUNDINGS- - - - - - - - - - - - - - - - - - - 25

1. Temperature Profiles - - - - - - - - - - - - - - - - - 25

2. Moisture Profiles- - - - - - - - - - - - - - - - - - - 25

3. Pressure-Scaled Absorber Masses- - - - - - - - - - - - 26

C. CLOUD PARAMETERIZATION - - - - - - - - - - - - - - - - - - 27

D. CLOUD-AREA COVERAGES - - - - - - - - - - - - - - - - - - - 28

III. TERRESTRIAL RADIATION- - - - - - - - - - - - - - - - - - - 30

A. THEORETICAL AND EMPIRICAL BASIS- - - - - - - - - - - - - 30

B. NET FLUX FORMULATION - - - - - - - - - - - - - - - - - - - 31

1. At Level k=10- - - - - - - - - - - - - - - - - - - - 31

2. Net Flux $F_6^*$ - - - - - - - - - - - - - - - - - - - - 32

3. Net Flux $F_2^*$ - - - - - - - - - - - - - - - - - - - - 33

C. APPLICATIONS TO HEAT BALANCE COMPUTATIONS- - - - - - - - 34

1. At Upper and Lower Boundaries- - - - - - - - - - - - 34

2. Intermediate Levels- - - - - - - - - - - - - - - - - 35

D. STATISTICAL RESULTS AND COMPARISONS- - - - - - - - - - - 35

1. Net Flux $F_{10}^*(0,0)$ - - - - - - - - - - - - - - - - - 35

2. Modification of $F_{10}^*$ for Cloudiness $CL_1$, $CL_2$ - - - - 37

E. COMPARISONS OF FF2 WITH SATELLITE CLIMATOLOGY- - - - - - 41

F. COMPARISONS OF CROSS-SEASONAL RESULTS OF $F_{10}^*$- - - - - - 43

IV. SOLAR RADIATION - - - - - - - - - - - - - - - - - - - - - - - 46

A. PARTITION OF SOLAR INSOLATION - - - - - - - - - - - - - - 46

B. DISPOSITION OF F(S) INSOLATION- - - - - - - - - - - - - - 48

1. Clear Sky Case- - - - - - - - - - - - - - - - - - - - 49

2. Cloudy Sky Cases- - - - - - - - - - - - - - - - - - - 50

3. Composite F(S) Insolation - - - - - - - - - - - - - - 51

C. DISPOSITION OF F(A) INSOLATION- - - - - - - - - - - - - - 52

1. Clear Sky Case (0,0)- - - - - - - - - - - - - - - - - 52

2. Cloudy Cases- - - - - - - - - - - - - - - - - - - - - 53

3. Composite F(A) Layer-Absorptions and Surface Absorption Insolation - - - - - - - - - - - - 57

4. Absorptivity (ABA) by Layers- - - - - - - - - - - - - 58

D. ALBEDO (ALB) OF THE EARTH-TROPOSPHERE SYSTEM- - - - - - - 59

E. COMPOSITE ABSORPTIVITY (ABG) BY THE EARTH-SURFACE; COMPOSITE ATMOSPHERIC TRANSMISSIVITY (ATRAN) - 59

1. Absorptivity (ABG) of Earth - - - - - - - - - - - - - 59

2. Transmissivity (ATRAN) of the Troposphere - - - - - - 60

3. Computational Check - - - - - - - - - - - - - - - - - 61

F. STATISTICAL ANALYSIS- - - - - - - - - - - - - - - - - - - 61

1. Clear Sky Case- - - - - - - - - - - - - - - - - - - - 61

2. Statistical Relationships between ALB, ABA, and ATRAN in the Cloudy and Clear Sky Cases - - - - 62

G. ALBEDO COMPARISONS WITH PUBLISHED RESULTS - - - - - - - 66

V. SENSIBLE AND LATENT HEAT TRANSPORT AT THE SEA-AIR INTERFACE - - - - - - - - - - - - - - - - - - - - - 70

A. GENERAL PURPOSE - - - - - - - - - - - - - - - - - - - - 70

B. WINDSPEED COMPUTATION IN THE TURBULENT FLUX MODEL - - - 70

C. SENSIBLE HEAT TRANSPORT - - - - - - - - - - - - - - - - 73

D. EVAPORATIVE HEAT TRANSPORT- - - - - - - - - - - - - - - - 74

E. LARGE-SCALE TURBULENT HEAT FLUX ACROSS THE SEA-AIR INTERFACE - - - - - - - - - - - - - - - - - - - - - - 77

VI. MERIDIONAL CROSS-SECTIONAL DEPICTION OF THE HEAT-BALANCE COMPUTATIONS - - - - - - - - - - - - - - - - 79

A. GENERAL - - - - - - - - - - - - - - - - - - - - - - - - - 79

B. GEOGRAPHICAL REPRESENTATION OF THE HEAT-BALANCE DISTRIBUTION - - - - - - - - - - - - - - - - 79

C. EXPLANATION OF SYMBOLIC TERMS - - - - - - - - - - - - - - 80

1. Cross-Section at Level k=2 (Fig. 6) - - - - - - - - - 80

2. Cross-Section in Layer (2,6)- - - - - - - - - - - - - 82

3. Cross-Section in Layer (6,10) - - - - - - - - - - - - 83

4. Cross-Section at Air-Sea Interface (k=10) - - - - - - 83

D. MERIDIONAL CROSS-SECTIONS OF THE VERTICAL HEAT BALANCE- - - - - - - - - - - - - - - - - - - - - - - - 84

VII. THE LATITUDINAL DISTRIBUTION OF RADIATIONAL BALANCE TERMS OF THE OCEAN-ATMOSPHERE SYSTEM- - - - - - - - - - - - - 94

A. GENERAL - - - - - - - - - - - - - - - - - - - - - - - - - 94

B. EARTH-TROPOSPHERE SYSTEM RADIATIONAL BALANCE SUMMARY - - - - - - - - - - - - - - - - - - - - - - 95

C. CROSS-SEASONAL EFFECTS- - - - - - - - - - - - - - - - - - 104

D. COMPARISONS OF NET FLUX AT THE TOP OF THE MODEL ATMOSPHERE WITH SATELLITE OBSERVATIONS- - - - - - - - - 104

VIII. ZONALLY-AVERAGED TROPOSPHERIC AND OCEANIC HEAT BUDGETS FOR 16 JULY 1974 - - - - - - - - - - - - - - - - 112

A. THE TROPOSPHERIC HEAT BUDGET- - - - - - - - - - - - - - - 112

B. THE LATITUDINALLY-AVERAGED HEAT BUDGET OF THE OCEAN- - - - - - - - - - - - - - - - - - - - - - - - 115

IX. CONCLUSIONS - - - - - - - - - - - - - - - - - - - - - - - - 118

LIST OF REFERENCES - - - - - - - - - - - - - - - - - - - - - - - 120

INITIAL DISTRIBUTION LIST- - - - - - - - - - - - - - - - - - - - 123

LIST OF TABLES


I. a. Example of a Typical FNWC Sounding for Gridpoint (2,2) - - - - - - - - - - - - - - - - - - - - - 22

b. Example of Corresponding Radiative Sounding with Temperatures, Mixing Ratios, Water-Vapor and $CO_2$ Absorber Masses and Cloud Amounts ($CL_1$ and $CL_2$) Listed- - - - - - - - - - - - - - - - - - 23

II. Example Listing of Gridpoint Values of the Terrestrial Radiation Fluxes Computed at Gridpoint (2,2) - - - - - - - - - - - - - - - - - - - - - - - 38

III. Statistical Cross-Seasonal Comparisons of the Downward Flux at the Surface as Given by the Coefficients of the Brunt Formula for Both Cloud Models- - - - - - - - - - - - - - - - - - - - - - - 40

IV. Statistical Cross-Seasonal Comparison of the Coefficient d in the Net Surface Flux $F_{10}^*$, Against CL for Both Cloud Models- - - - - - - - - - - - - 40

V. Comparison of Zonally-Averaged Net Flux to Space, FF2, Between this Study and Satellite Climatology After Raschke. Composite CL Amounts for Both Model Cases are Included- - - - - - - - - - - - - - - - - - 42

VI. Cross-Seasonal Comparison of the Zonally-Averaged Net Fluxes at the Surface, $F_{10}^*$, and the Cloud Amounts for the 2/3-CL Parameterization - - - - - 44

VII. Sample Listing of the F(S) Insolational Dispositions Computed at Gridpoint (2,2) - - - - - - - - - - - - 52

VIII. Sample Listing of the F(A) Insolational Dispositions Computed at Gridpoint (2,2) - - - - - - - - - - - - 58

IX. Comparison of Planetary Albedo between this Study and Raschke, Including a Listing of Composite Cloud Amounts Both Cases - - - - - - - - - - - - - 67

X. Cross-Seasonal Comparison of the Ocean-Troposphere Net Radiation $R_s$ for Both Cloud Parameterizations - - - - - 108

XI. Cross-Seasonal Comparison of the Surface Net Radiation R for Both Cloud Parameterizations- - - - - - - - 109

XII. Cross-Seasonal Comparison of the Atmospheric Net Radiation Loss-Rate $R_a$ for Both Cloud Parameterizations - - - - - - - - - - - - - - - - - - - - - 110

XIII. Comparison of the Ocean-Troposphere Net Radiation $R_s$ and RNMOD for Both Cloud-Cases in this Study and RNRAS by Raschke et al (1973) - - - - - - - - - - - - - - 111

XIV. Zonally-Averaged Values of $E+H_\Gamma$ as a Function of Latitude - - - - - - - - - - - - - - - - - - - - - - 112

LIST OF FIGURES


1. FNWC Polar Stereographic Grid Meridians Selected for Study- - - - - - - - - - - - - - - - - - - - - - 20

2. Five-Layer Radiative Sounding Used in this Study- - - - - - 24

3. Schematic Representation of F(A) Insolation Disposition in the Case of Two Overcast Layers- - - - - - - 55

4. Section of FNWC Stereographic Grid Illustrating the Method of Obtaining Contour Gradients - - - - - - - - - 72

5. Schematic Representation of the Distribution of Convergence of Sensible and Latent Heat - - - - - - - - - - 75

6. Key to Meridional Cross-Sections for Radiative and Turbulent Transfer Values - - - - - - - - - - - - - - - 85

7. 125W Longitudinal Cross-Section (2/3-CL Model)

   a. Tropical Latitudes- - - - - - - - - - - - - - - - - - - 86

   b. Higher Latitudes- - - - - - - - - - - - - - - - - - - - 87

8. 170W Longitudinal Cross-Section (2/3-CL Model)

   a. Tropical Latitudes- - - - - - - - - - - - - - - - - - - 88

   b. Higher Latitudes- - - - - - - - - - - - - - - - - - - - 89

9. 145E Longitudinal Cross-Section (2/3-CL Model)

   a. Tropical Latitudes- - - - - - - - - - - - - - - - - - - 90

   b. Higher Latitudes- - - - - - - - - - - - - - - - - - - - 91

10. 35W Longitudinal Cross-Section (2/3-CL Model)

   a. Tropical Latitudes- - - - - - - - - - - - - - - - - - - 92

   b. Higher Latitudes- - - - - - - - - - - - - - - - - - - - 93

11. Key to Zonally-Averaged Radiational Cross-Sections- - - - - 97

12. Zonally-Averaged Radiational Cross-Section for 2/3-CL Model

a. Tropical Latitudes- - - - - - - - - - - - - - - - - - - - 98

b. Higher Latitudes- - - - - - - - - - - - - - - - - - - - - 99

13. Zonally-Averaged Radiational Cross-Section for 2/3-CL Model

a. Tropical Latitudes- - - - - - - - - - - - - - - - - - - - 100

b. Higher Latitudes- - - - - - - - - - - - - - - - - - - - - 101

14. Radiational Balance at the Tropopause, the Ocean Surface and in the Tropospheric Column for Both the Full-CL and 2/3-CL Models for 16 July 1974- - - - - - - - - - - - - - - - - - - - - - - - - - 102

15. Tropospheric Heat Budget Disposition of Both the 2/3-CL Case Model and the Full-CL Case Model for 16 July 1974- - - - - - - - - - - - - - - - - - - - 113

16. Surface Heat Budget Disposition of Both the 2/3-CL Case Model and the Full-CL Model for 16 July 1974- - - - - - - - - - - - - - - - - - - - - - - - - 116

## LIST OF SYMBOLS AND ABBREVIATIONS

| | |
|---|---|
| $A(m,n)$ | solar insolation absorbed in the layer (m,n) |
| $\bar{a}(m,n)$ | Manabe-Möller absorptivity function |
| $a^*$ | turbulent transfer coefficient |
| ABA | absorptivity of the troposphere |
| ABG | fractional absorptivity of solar insolation by earth's surface |
| ALB | earth-atmosphere system albedo |
| ATRAN | transmissivity of the troposphere |
| $B_k$ | Stefan-Boltzmann blackbody flux at $T_k$ |
| BALB | 24-hour averaged radiational balance at earth's surface |
| $BALk_1k_2$ | 24-hour averaged radiational balance for layer $(k_1,k_2)$ |
| BALT | 24-hour averaged radiational balance at tropopause |
| BBB | ice conduction coefficient |
| C | carbon dioxide layer absorber mass |
| cal $cm^{-2}$ $min^{-1}$ | calories per centimeter squared per minute |
| CL | total opaque cloud cover |
| CL(I) | fractional cloud amount for layer:<br>I = 1 in 600 to 400 mb;<br>I = 2 in 900 to 800 mb |
| CL'(I) | two-thirds of cloud amount CL(I) |
| E | East longitude; evaporational heat transport |
| $e_x$ | vapor pressure at top of constant flux layer |
| F(A) | solar insolation subject to water vapor absorption only |

| | |
|---|---|
| FADJ | total incoming insolation at top of atmosphere |
| $F_d$ | net downward flux at the earth |
| $Fk_1k_2$ | net infrared flux divergence between level $k_1, k_2$ |
| $F_k^*$ | net infrared flux at level k |
| FNWC | Fleet Numerical Weather Central |
| F(S) | solar insolation subject to Rayleigh scattering only |
| g | gravity = 9.8067 m $sec^2$ |
| h | hour angle |
| H | height of homogeneous atmosphere; 24-hour averaged hour angle |
| $H_\Gamma$ | sensible heat transport |
| I | abscissa grid location |
| IAlO(m,n) | solar insolation absorbed at surface with cloud condition (m,n) |
| ISlO(m,n) | solar insolation at surface subject to Rayleigh scatter with cloud condition (m,n) |
| J | ordinate grid location |
| k | pressure level used in this study equal to 10σ |
| K* | eddy turbulent transfer coefficient |
| L | latent heat of vaporization |
| ly $min^{-1}$ | langleys per minute |
| M | water-vapor mass path length |
| N | North latitude |
| P | pressure |
| $P_k$ | pressure in millibars (mb) at level k |
| $q_k$ | mixing ratio at level k |
| $q_{s_k}$ | saturated mixing ratio at level k |

| | |
|---|---|
| QAVE | 24-hour averaged insolation at the tropopause |
| r | Bowen ratio |
| R | correlation coefficient; net radiation balance at the surface |
| $R_a$ | mean radiative cooling rate in troposphere |
| $R_d$ | universal gas constant |
| REF | total insolation reflected back to space |
| REFA | F(A) insolation reflected back to space |
| REFS | F(S) insolation reflected back to space |
| R.H. | relative humidity |
| $R_s$ | mean radiative energy gain (loss) rate at ocean-troposphere system |
| S | South latitude; effective solar constant |
| $S_o$ | heat storage in oceanic water mass |
| $S_a$ | heat storage term for the troposphere |
| St | Stefan-Boltzmann constant |
| $T_k$ | temperature at level k |
| $T_o$ | freezing point of sea water |
| TRAN | total insolation incident at the earth's surface |
| $T_x$ | temperature at the top of constant flux layer |
| U | water-vapor layer absorber mass |
| $V_g$ | geostrophic windspeed |
| $V_s$ | surface windspeed |
| W | West latitude |
| W(m,n) | cloud fractional weight for cloud condition (m,n) |
| Z | Zenith angle |
| $\alpha(G)$ | surface albedo |

| | |
|---|---|
| $\alpha(R)$ | Rayleigh clear sky albedo |
| $\gamma_c$ | critical lapse rate |
| $\delta$ | solar declination angle |
| $\varepsilon_{wc}$ | emissivity due to water and carbon dioxide absorber mass at indicated layer |
| $\theta_k$ | potential temperature at level k |
| $\Lambda$ | longitude |
| $\pi$ | surface pressure; pi = 3.1416 |
| $\rho$ | density |
| $\sigma$ | sigma pressure level used by FNWC, normalized to surface pressure |
| $\phi$ | latitude |
| FF2 | total long-wave flux to space by model |
| F2(RAS) | total long-wave flux to space at level k=0 based upon NIMBUS III measurements by Raschke et al (1973) |
| RNMOD | solar net insolation minus outgoing terrestrial flux FF2 crossing level k=2 |
| RN(RAS) | total flux to space based upon NIMBUS III measurements after Raschke et al (1973) |

ACKNOWLEDGEMENT

The author wishes to express his appreciation and gratitude to his wife for her support, aid, and perseverance.

Appreciation is also expressed to his thesis advisor, Professor F. L. Martin, for his suggestions, advice, and guidance in this research and to Mr. Russell D. Schwanz for his expert programming assistance.

# I. INTRODUCTION

This thesis is a study of a radiative heating parameterization for use in the Fleet Numerical Weather Central (FNWC) prediction system. The study has as a primary objective, the analysis of the radiational and heat balance of the ocean-atmosphere system utilizing FNWC gridded data-fields at constant pressure levels for 16 July 1974. The grid-point data were selected along four oceanic meridians, three in the Pacific and one in the Atlantic, with most of the gridpoints located in the Northern Hemisphere (Fig. 1).

The specification of amounts of clouds in two designated layers has the most influence on the radiative-model dispositions (short- and long-wave). The initial specification of the fractional amounts of CL(1) and CL(2) were based on large-scale formulations developed by Smagorinsky (1960) and used in a similar study based on the data day 16 January 1974 by Spaeth (1975).

The governing equations of the radiational transfer of the model have been derived by Martin (1972, 1974), who modified both the solar and terrestrial radiation transfers to respond to the presence of clouds. These clouds were of specified amounts in the two layers, one of which is a mid-level cloud and the other a low-level cloud. The radiational model in use here has similarities to those in use in UCLA and NCAR General Circulation models.

The physical description of the radiative model may be applied to any scale of analysis for which there is adequate resolution of the

temperature and moisture data in the vertical. In the horizontal, the reliability of the data used here is consistent with that of the FNWC analysis to gridpoints, and is typically reported to the nearest tenth of a degree with regard to temperature and dewpoint. The radiational computations made here are applied to FNWC gridpoints and are designed to make a one-hour forward-time step applicable to the FNWC primitive equation forecast model, with special adaptations to their σ-levels.

The Smagorinsky (1960) cloud-specification of CL(1) and CL(2) when used with the model of this study resulted in global albedo estimates that were too high especially in the tropics as compared to the satellite data of Raschke (1973), thus leading to under-estimates of the net radiative balance at the top of the atmosphere and at the ocean surface. This could be a result of inadequately resolved relative humidities, which in reality might well be lower than inferred by the FNWC tropical analysis.

The comparative results afforded by the 2/3-CL parameterization gave reasonably close agreement with the radiative climatology of Raschke et al (1973), for the NIMBUS III period 16-31 July 1969. Oceanic and tropospheric balances were computed for both sets of cloud conditions (full-CL and 2/3-CL) for 16 July 1974. It was also necessary to augment the purely radiative model by including a turbulent boundary-layer model for sensible and latent heat transports over the ocean as adapted from Kaitala (1974).

The radiation package results computed with the 2/3-CL cloud model compared very favorably with satellite climatology, though only one data day (16 July 1974) was used as representative of mid-July soundings over the ocean, both for the model and the Raschke satellite

climatology. However, the latter climatology was based on the data period 16-31 July 1969.

The major effect noted by the use of the 2/3-CL as contrasted with full-CL parameterization was the reduction in global albedo and the resulting greater contribution to the surface net heating rates. This result is in general agreement with recent observations by Von der Haar and Hanson (1969), Von der Haar and Oort (1973) and Raschke et al (1973). However, the major discrepancies in the radiative model resulted from the specification of layered cloud amounts in the tropics (in a manner identical to that used poleward of the tropics) where the model gave somewhat excessive albedos. It is felt that the geometry of solar radiation streams impinging upon subgrid sized cumulus cells in the tropics should be remodeled so as to divert a greater percentage of solar radiation downward, as compared with the characteristic cloud-layering and resultant reflective effects which seem permissible in middle and high latitudes.

## II. DATA PREPARATION

### A. INITIAL DATA FIELDS

The temperature and humidity data used in this study were arranged in the form of soundings taken along four oceanic meridians (Fig. 1) of the Fleet Numerical Weather Central (FNWC) Northern Hemisphere analyses on 16 July 1974. Computation of radiational dispositions and of other heat budget terms were made at these gridpoints. Oceanic locations for these computations were chosen because:

1. The constant $\sigma$ surfaces (where $\sigma = \frac{P}{\pi}$ ) of the FNWC primitive equation system are close to being constant pressure levels.

2. The maritime-area heating rate computations are likely to be representative of the month of July 1974 as contrasted with computations made for 16 July 1974 for a corresponding set of gridpoints over land.

The three meridians (and their respective number of soundings) selected over the Pacific Ocean were located at 125W (25 soundings), 170W (25 soundings) and 145E (17 soundings). The Atlantic Ocean meridian was 35W (26 soundings). This method of selecting "soundings" along the indicated meridians of the FNWC polar stereographic map, made it unnecessary to employ spatial interpolation between original data gridpoints along the meridians. Data along line 3 in the Pacific was not extended southward of gridpoint (9,55) because they fell over land masses (New Guinea and Northern Australia) where the surface temperatures and other sounding features were unrepresentative of the oceanic values. For similar reason two other

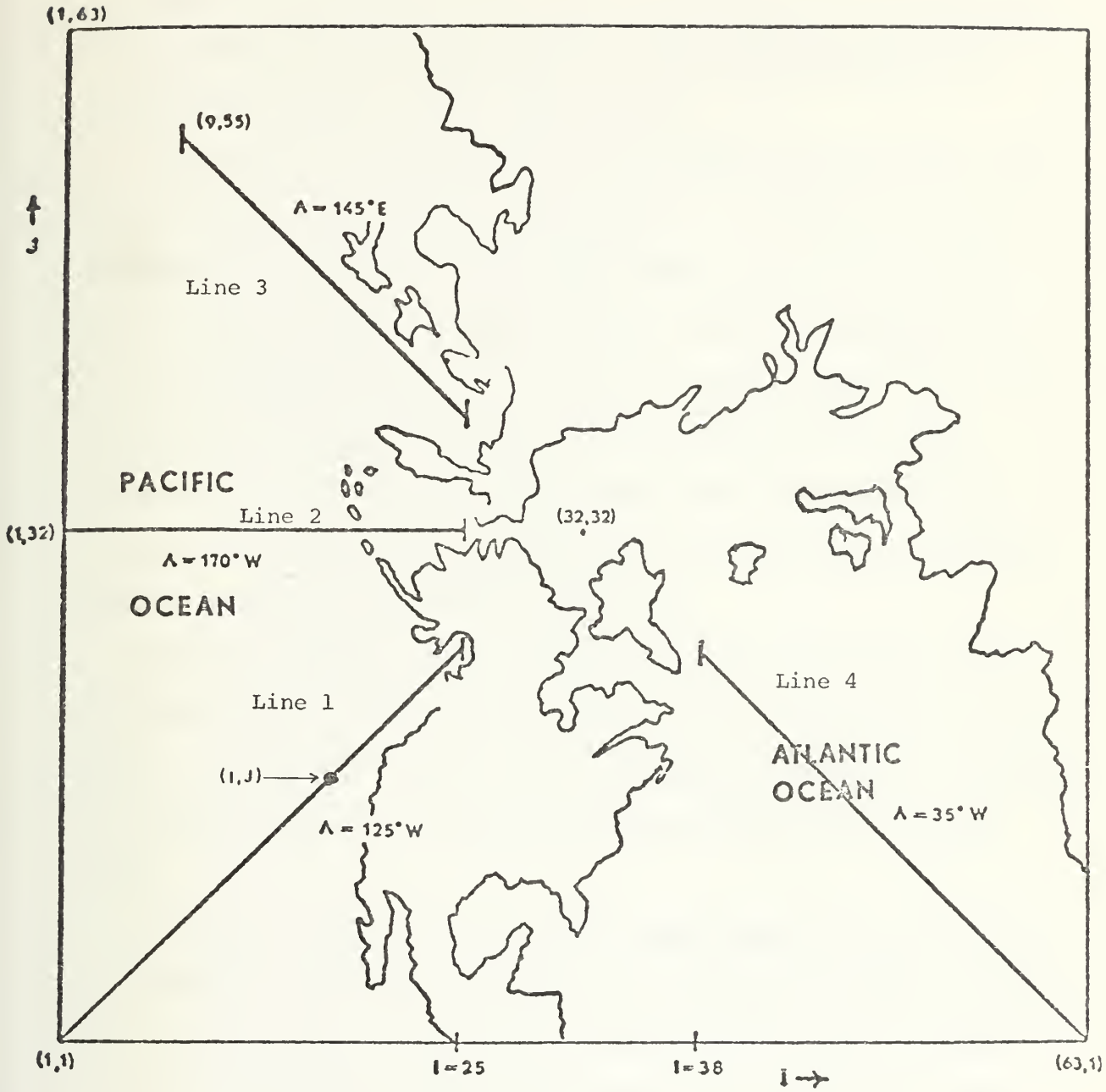


Figure 1. FNWC polar stereographic grid and meridians (lines 1, 2, 3, and 4) selected for study. The longitudes Λ are shown for each meridian as well as the extent considered of each meridian.

gridpoints at (24,24)and (56,6) which also fell just over land masses, were replaced with more representative oceanic soundings from the gridpoints (23,24)and (56,7), respectively.

The gridpoint soundings in the form of Table I(a) were taken from the original FNWC 63-by-63 surface analysis, as well as the vertical distribution of T(P) at ten additional levels ranging up to 100 millibars. Moisture parameters were provided as the vapor pressure at the top of the constant flux level, and as the dewpoint depression at five selected levels between the 925 millibar and 400 millibar levels. These original soundings were then modeled into a radiative sounding (Table I(b)) corresponding in the vertical to FNWC primitive equation prediction levels up to 100 mb (see Fig. 2).

Data from 0000GMT, 16 July 1974 were used for the Pacific soundings while 1200GMT, 16 July 1974 data were used for the Atlantic soundings. These times were used so that the analysis times would correspond as closely as possible to local solar noon in each of the indicated areas.

Since the standard instrument level vapor pressure ($e_{air}$) was missing from the original FNWC analysis at all gridpoints, $e_{air}$ was approximated using the FNWC field of $e_x$, a computed value of vapor pressure at about 20 meters above MSL in the turbulent boundary layer. FNWC values of $T_x$ and $e_x$ over the ocean had been made available using an operational planetary boundary layer model detailed by Kaitala (1974).

To perform radiative calculations, it is necessary to have water-vapor and $CO_2$ absorber masses and cloud amounts, CL(1) and CL(2) within certain k-level boundaries (Fig. 2). All soundings in this study start at sea level with the approximation of surface pressure

Table I(a). Example of typical FNWC sounding for gridpoint (2,2). The humidity parameters between 925, ...,400 mb are dewpoint depressions, whereas the values at the surface and the top of the constant flux layer (9999*) are vapor pressures.

| Pressure (mb) | T(°C) | Humidity Parameters |
|---|---|---|
| Surface, 1000 mb | 26.1 | $e_x$ = 23.8 mb |
| 925 | 17.5 | 5.4 °C |
| 850 | 13.7 | 7.7 |
| 700 | 4.8 | 12.7 |
| 500 | -11.8 | 13.5 |
| 400 | -23.4 | 15.3 |
| 300 | -38.2 | |
| 250 | -47.1 | |
| 200 | -56.9 | |
| 150 | -67.8 | |
| 100 | -81.0 | |
| 9999* | $T_x$ = 23.5 | |

* Code 9999 indicates data taken from the top of the constant flux level (CFL) of the FNWC initial data program.

Table I(b). Example of the corresponding radiative sounding with mixing ratio listed at odd k-levels (Fig. 2). Additionally, water-vapor and $CO_2$ absorber masses, and cloud amounts CL(1) and CL(2) (after Smagorinsky (1960)) are also listed, as these parameters have been modeled in the radiative theory presented in this study.

| Pressure (mb) | T(°C) | Mixing Ratio g/kg | Absorber Masses Water Vapor ($gm/cm^2$) | $CO_2$ ($cm/cm^2$) | Smagorinsky Cloud Amounts CL(1), CL(2) |
|---|---|---|---|---|---|
| 1000 | 26.1 | 14.93 | | | |
| 900 | 15.7 | 8.45 | | | 0.24, CL(2) |
| 800 | 10.9 | 0.0 | 1.58 | 45.53 | |
| 700 | 4.8 | 3.04 | | | |
| 600 | -2.4 | 0.0 | 2.06 | 83.53 | |
| 500 | -11.8 | 1.02 | | | 0.00, CL(1) |
| 400 | -23.4 | 0.36 | 2.18 | 113.35 | |
| 300 | -38.2 | 0.15 | | | |
| 200 | -56.9 | 0.0 | 2.20 | 133.99 | |
| 100 | -81.0 | 0.00 | 2.20 | 138.67 | |
| 0 | -81.0 | 0.0 | 2.20 | 143.35 | |

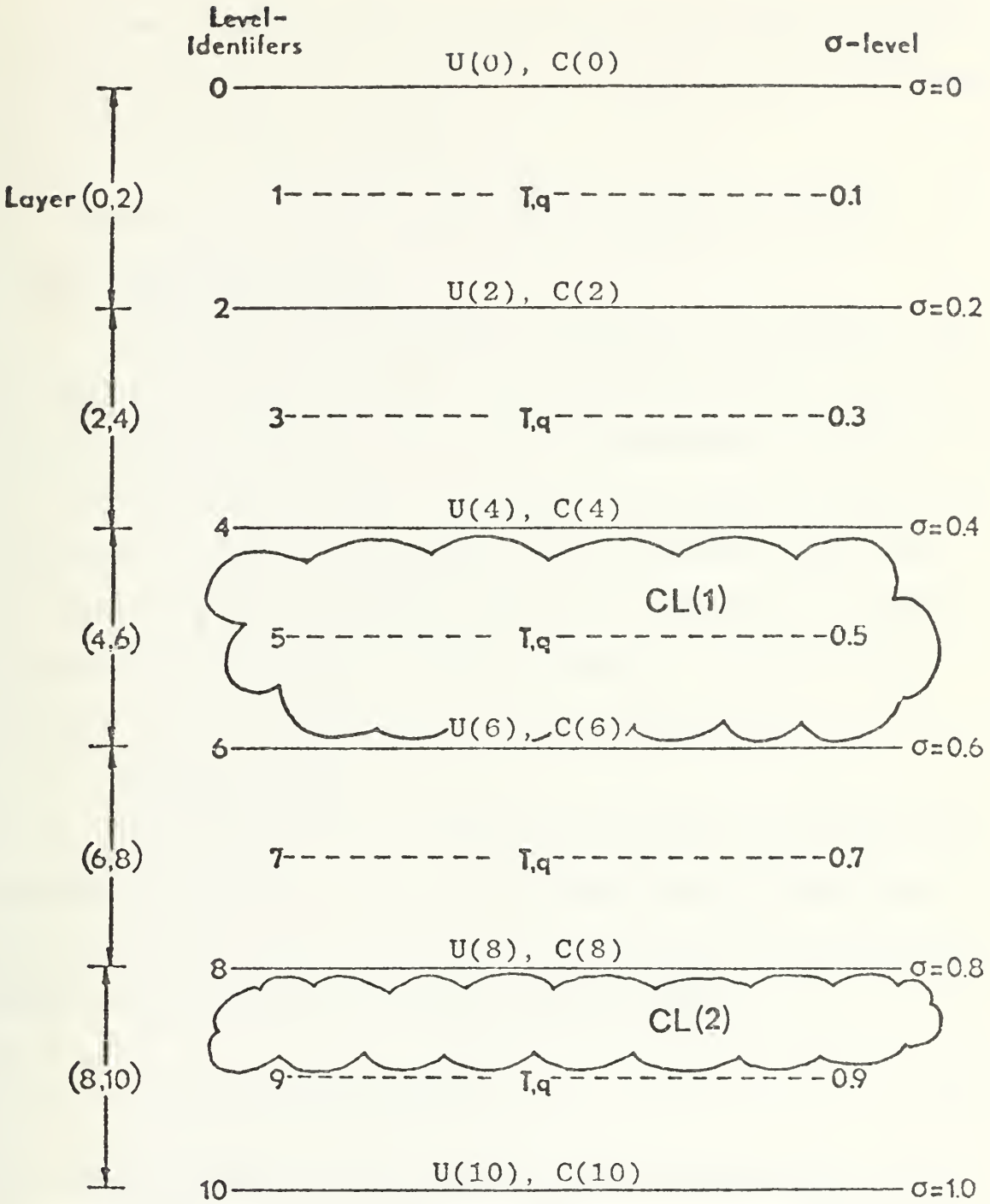


Figure 2. Five-layer radiative sounding used in this study. Levels are identified by their values on the k-scale, while layers are identified by their level boundary indices in parentheses, e.g. (8,10). Pressure-scaled water vapor and $CO_2$ mass increments $\Delta U$ and $\Delta C$, respectively are integrated relative to the surface and the resulting U and C are carried at even levels. The temperature T is retained at all levels. Amounts of clouds CL(1) and CL(2) in the layers shown have been parameterized for consideration of their radiative effects.

$\pi \doteq 1000$ mb. Therefore, the k-levels are associated approximately with the FNWC levels $P_k$ = 1000., 900., 800., ...., 200., 100., 0.0 mb respective to $\sigma_k$ = 1.0, 0.9, ..., 0.1, 0.0.

B. INTERPOLATIVE PROCESSING TO K-LEVELS IN RADIATIVE SOUNDINGS

1. Temperature Profiles

The gridpoint temperatures were listed at each mandatory level of Table I(a) between 1000., ..., 100 mb. The temperature was assumed to be isothermal from 100 mb to p=0.0 mb. The temperature $T_{10}$ was set equal to the FNWC listed sea-surface temperature. The radiative sounding temperatures for the remaining k-levels were obtained from either their corresponding listed temperature value or by a three-point Lagrangian interpolation scheme (Eq. 2-1, (Spaeth, 1975)), to level k when the listed temperature-profile does not include the value $T_k$.

2. Moisture Profiles

The moisture from the original FNWC soundings (Table I(a)) were converted into mixing ratios at each of the original sounding levels. The near-surface vapor pressure (taken as $e_x$) was used to calculate the mixing ratio at k=10, as described by Spaeth (1975):

$$q_{10} = 621.97\ (e_x/1000) \qquad (2\text{-}1)$$

The remaining mixing ratios q were calculated from the original FNWC sounding (Table I(a)), using a dewpoint depression formula (Spaeth, 1975, (Eq. 2-3)). The computed q-values were subsequently interpolated to k-levels using the previously mentioned three-point Lagrangian procedure applied to successive q-values in the original sounding. Resulting values of the interpolated q-values are shown for the case of the radiative sounding at gridpoint (2,2) (Table I(b)).

Due to the fact that most radiosonde humidity data for $p \leq 300$ mb is either unreliable or not available, a power-law extrapolation formula (Spaeth, 1975)

$$q_k/q_{500} = (P_k/500)^{\lambda} \qquad (2\text{-}2)$$

was used to obtain q-values at k=3,2,1.

This extrapolative procedure for obtaining q-values at high levels was first suggested by Smith (1966), utilizing the least squares estimation of $\lambda$ according to

$$\lambda = \frac{\sum_{i=1}^{6} y_i \, x_i}{\sum_i x_i^2} = R_{yx} \sqrt{\frac{\sum y_i^2}{\sum x_i^2}} \qquad (2\text{-}3)$$

with $y_i = \log (q_i/q_5)$ and $x_i = \log (p_i/p_5)$. The Smith method was then further tested by Spaeth (1975) for the vertical scale of the FNWC initial data soundings. The resulting correlation coefficient $R_{yx}$ was found here to lie in the range .95 to .99. Such high correlations indicate that the procedure described by Spaeth (1975) for determining upper atmosphere q-values has realistic estimation value for the vertical scale involved in the radiative sounding.

3. Pressure-Scaled Absorber Masses

The pressure-scaled water vapor absorber mass $\Delta U$ in a layer (Fig. 2) were calculated for the five odd k-levels by using the computed mixing ratio values (Eq. 2-7, Spaeth, (1975)). The equation for computing the integrated pressure-scaled water vapor mass is given by the algorithm described by Eq. 2-8 of Spaeth.

A similar routine was used in the computation of the carbon-dioxide scaled absorber mass (Spaeth, 1975, Eqs. 2-10,11). To be noted here is the fact that $CO_2$ absorber masses have been stated in terms of N.T.P. "pressure-scaled"cms, since the $CO_2$ absorption coefficients are generally stated in terms of the reciprocal of this $CO_2$ mass unit.

C. CLOUD PARAMETERIZATION

The relative humidities and thus the saturation vapor pressure at levels k=5 and k=9 are used in the calculations of the fractional cloud cover $CL_1$ and $CL_2$ in layers (4,6) and (8,9) respectively, as depicted in Fig. 2. From the computed relative humidity values at k=5 and k=9, the fractional cloud amounts for each layer were parameterized using the equation (after Smagorinsky, (1960)):

$$CL(1) = 2.0\ (RH(5)) - 0.7 \qquad (2\text{-}4(a))$$

$$CL(2) = 3.33(RH(9)) - 2.0 \qquad (2\text{-}4(b))$$

Smagorinsky's parameterization of CL(1) and CL(2) permits cloudiness fractions of 1.30 and 1.333 respectively with RH=1.0. Values of CL greater than 1.0 were considered initially by Smagorinsky (1960) to suggest the amount of supersaturation which accompanies precipitation.

All radiative models in use at the present time limit CL in accordance with $0 \leq CL \leq 1.0$. In the present radiative package there is little opportunity to deduce precipitation and/or supersaturation amounts. Hence, the formulations of $CL_1$ and $CL_2$ of Eqs. 2-4 were limited to a maximum of 1.0 in each layer in the "full-CL" case. In addition, the

Smagorinsky computations for $CL_1$ and $CL_2$ were reduced to

$$CL_1' = 2/3\ (CL_1) \qquad (2\text{-}5(a))$$

$$CL_2' = 2/3\ (CL_2) \qquad (2\text{-}5(b))$$

regardless of whether the original CL values exceeded 1.0 or not, so that the revised cloud-cover amounts could be considered for purposes of estimating shifts in the global radiative balance. Computations made with cloud parameterization of Eq. 2-5, are termed the 2/3-CL case.

The 1/3 reduction inherent in $CL_1'$, $CL_2'$ relative to Smagorinsky's $CL_1$, $CL_2$ were initiated in this study in an attempt to tune cloud amounts to give radiation results in closer agreement with recent satellite climatology of Raschke et al, (1973). This satellite climatology suggests the use of smaller cloud amounts than that specified by Smagorinsky. Fractional cloud amounts were considered to be functions of large scale effects only. Therefore, small scale convective activity, seasonal conditions (except for the soundings) and latitudinal effects were not considered in specifying the reduction factor of Eq. 2-5. The reduced cloud-parameterization was introduced here for estimating large scale radiational effects only.

D. CLOUD-AREA COVERAGES

Since Eqs. 2-4a,b or 2-5a,b gave the fractional-coverage of the gridpoint area by the appropriate cloud-type, the gridpoint area may be thought of as broken into random fractional segments of size

$$W(0,0) = (1\text{-}CL_1)*(1\text{-}CL_2) \qquad (2\text{-}6(a))$$

wherein there is a combination of clear-over-clear segments in the layers. Similarly, the gridpoint area has the fractional area of cloud coverage

$$W(1,1) = CL_1 * CL_2 \qquad (2\text{-}6(b))$$

of upper-cloud amount $CL_1$ overlying lower-cloud amount $CL_2$. Likewise the combinations of cloudy-over-clear and clear-over-cloudy, by layers, may be visualized as occurring with the weights

$$W(1,0) = CL_1 * (1-CL_2) \qquad (2\text{-}6(c))$$

and

$$W(0,1) = (1-CL_1) * CL_2 \qquad (2\text{-}6(d))$$

Regardless of whether the full-cloud amounts $CL_1$, $CL_2$ of Smagorinsky (Eq. 2-4), or the 2/3-CL amounts of Eq. 2-5 were utilized, it was useful to carry, for radiation computations of each sounding, the relative weights or fractions of the gridpoint area exposed to the specified cloud-layer combinations. Henceforth, the symbols are denoted by W(0,0), W(1,1), W(1,0), W(0,1) and as given by Eqs. 2-6(a,b,c,d) suggest overcast (1) or clear (0) cloud amounts in the indicated layers (Fig. 2), the first index referring to the level of $CL_1$ and the second to that of $CL_2$. The usefulness of this computational device will be exemplified in Sections III and IV, where the procedures for the terrestrial and solar radiational computations are discussed and the results are summarized over the full set of soundings.

## III. TERRESTRIAL RADIATION

### A. THEORETICAL AND EMPIRICAL BASIS

Empirical formulas were developed by Sasamori (1968) for flux emissivities in the atmosphere as associated with computations required for the heat balance requirement of the NCAR General Circulation Model. Sasamori derived the empirical emissivity formulas for water vapor and $CO_2$ by comparison with the theoretical values built into the Yamamoto Radiation Chart (1952). This chart has proved to be quite accurate for computational checking of the Sasamori emissivities and was used by Spaeth (1975) and Warner (1974) as a systematic guide for integration of the radiative transfer formula developed by Martin (1972, 1974), who adapted the Sasamori formulas to the particular layers of interest in gridpoint computations of the FNWC primitive equation model (Fig. 2).

The essential long-wave flux formulas required for use in the FNWC heating package are the following:

$F_{10}^*$ = net IR flux at earth, k=10

$F_6^*$ = net IR flux at level k=6

$F_2^*$ = net IR flux at level k=2

F610 = net IR-flux divergence in the layer (6,10)

F26 = net IR-flux divergence in the layer (2,6)

To get the IR-flux divergences in the layers (6,10) and (2,6), the differences $F_6^* - F_{10}^*$ and $F_2^* - F_6^*$ must be computed. The detailed scheme for making such computations with various combinations of cloud cover CL(1) and CL(2) is similar to that developed by Martin (1974) and as reproduced in detail by Spaeth (1975).

In order to make IR net-flux calculations along the path of integration, there must be a physically sound representation of the emissivity ($\varepsilon_{wc}$) as a function of both water-vapor and $CO_2$ absorber masses in layers along the sounding. For a further discussion of the emissivity formulas used in the quadrature scheme, refer to Spaeth's Appendix A (1975).

B. NET FLUX FORMULATION

1. At Level k=10

The radiative sounding as depicted in Table I(b), was computed as the combination of parameters U(k,10), C(k,10) and $T_k$ for each required level, k=10,8,...,2,1,0. Cloud parameters CL(1) and CL(2) are also listed at each gridpoint and in general are non-zero. The grid area was then considered to be composed of areal fractions (weights) defined in Eqs. 2-6(a,...,d) and denoted by the symbols W(0,0), W(1,1), W(1,0), W(0,1).

The composite net flux $F_{10}^*(CL_1, CL_2)$ at level k=10 at each gridpoint is then constructed by using the appropriate weight factor to multiply the corresponding reference net flux $F_{10}^*$ computations,defined for the special cloud-cover cases,$F_{10}^*(0,0)$, $F_{10}^*(1,0)$, $F_{10}^*(0,1)$, $F_{10}^*(1,1)$. As a result, the composite net flux may be written

$$F_{10}^*(CL_1,CL_2) = W(0,0)F_{10}^*(0,0)+W(1,0)F_{10}^*(1,0)+W(0,1)F_{10}^*(0,1) + W(1,1)F_{10}^*(1,1) \qquad (3\text{-}1)$$

Spaeth (1975) has listed these reference net flux formulations in his

Eqs. 3-6,7,8. Using the definitions of W(0,0), W(1,0), W(0,1), W(1,1) $F_{10}^{*}(CL_1,CL_2)$ can be shown to assume the form

$$\begin{aligned} F_{10}^{*}(CL_1,CL_2) = {} & [1-CL(2)]\{(B_{10}-B_6)-.5[\varepsilon_{wc}(8,10)(B_{10}-B_8) \\ & + (\varepsilon_{wc}(8,10)+\varepsilon_{wc}(6,10))(B_8-B_6)]\} \\ & + (1-CL(2))(1-CL(1))\{B_6-.5[(\varepsilon_{wc}(6,10) \\ & + \varepsilon_{wc}(4,10))(B_6-B_4)+(\varepsilon_{wc}(4,10) \\ & + \varepsilon_{wc}(2,10))(B_4-B_2)+(\varepsilon_{wc}(2,10) \\ & + \varepsilon_{wc}(1,0))(B_2-B_1)+\tilde{\varepsilon}_{wc}((0,10),T_1)*B_1]\} \\ & + CL(2)\{(B_{10}-B_9)[1-.5\varepsilon_{wc}(9,10)]\} \ . \end{aligned} \qquad (3\text{-}2)$$

Here

$$B_k = 1.170403 \times 10^{-7} T_k^{4} \qquad (3\text{-}3)$$

is the Stefan-Boltzmann blackbody flux in ly $day^{-1}$ at temperature $T_k$.

Further, $\varepsilon_{wc}(U_k,C_k, 10)$ is the combined water-vapor and $CO_2$ emissivity along the path from level 10 to level k. This emissivity is considered by Sasamori to be temperature independent for $T \geq 210K$, whereas $\tilde{\varepsilon}_{wc}$ represents the temperature dependent emissivity applicable for $T < 210K$ (see pp. 136-137, Spaeth, 1975).

The reference net fluxes $F_{10}^{*}$ of Eq. 3-1 are associated with (1) clear skies in both layers, (2) overcast in the upper layer only, (3) overcast in the lower layer only and (4) overcast in both layers, respectively.

2. Net Flux $F_6^{*}$

The formula for $F_6^{*}(CL_1,CL_2)$ has been developed by Spaeth (Eq. 3-10, 1975) in a manner analogous to the derivation of the weighted

$F_{10}^*$. The result is reproduced for completeness after (pp. 48, Spaeth, 1975).

$$F_6^* = [1-CL(1)]\{B_8-.5[\varepsilon_{wc}(6,8)(B_8-B_6)+\varepsilon_{wc}(4,6)(B_6-B_4) + (\varepsilon_{wc}(4,6)+\varepsilon_{wc}(2,6))(B_4-B_2)+(\varepsilon_{wc}(2,6)+\varepsilon_{wc}(1,6))(B_2-B_1) + \tilde{\varepsilon}_{wc}((0,6),T_1)*B_1]\}+(1-CL(1))(1-CL(2))\{(B_{10}-B_8)[1. -.5(\varepsilon_{wc}(6,8)+\varepsilon_{wc}(6,10))]\}+CL(1)\{(B_8-B_6)* [1-.5\varepsilon_{wc}(6,8)]\}+CL(1)(1-CL(2))\{(B_{10}-B_8)* [1-.5(\varepsilon_{wc}(6,8)+\varepsilon_{wc}(6,10))]\} . \quad (3-4)$$

3. Net Flux $F_2^*$

The net flux at level k=2 can be calculated in a similar fashion to $F_{10}^*$ and $F_6^*$, with the formulation of the individual reference net fluxes $F_2^*$ as previously described. The formula for $F_2^*(CL_1,CL_2)$ is developed analogous to that for $F_{10}^*(CL_1,CL_2)$ and $F_6^*(CL_1,CL_2)$.

$$F_2^* = [1-CL(1)]\{B_8-.5[\varepsilon_{wc}(2,4)(B_4-B_2)+(\varepsilon_{wc}(2,4) + \varepsilon_{wc}(2,6))(B_6-B_4)+(\varepsilon_{wc}(2,6)+\varepsilon_{wc}(2,8))* (B_8-B_6)+\varepsilon_{wc}(1,2)(B_2-B_1)+\tilde{\varepsilon}_{wc}((0,2), T_1)*B_1)]\} + (1-CL(1))(1-CL(2))*\{(B_{10}-B_8)[1-.5(\varepsilon_{wc}(2,8) + \varepsilon_{wc}(2,10))]\}+CL(1)\{B_4-.5[\varepsilon_{wc}(2,4)(B_4-B_2) + \varepsilon_{wc}(1,2)(B_2-B_1)+\tilde{\varepsilon}_{wc}((0,2), T_1)*B_1]\} \quad (3-5)$$

A new parameter, the total outgoing long-wave radiation to space (FF2) can be readily defined from the expression for $F_2^*$ by setting to zero the terms of Eq. 3-5 representing the downward flux through level k=2. These terms are just those denoted by the symbols $\tilde{\varepsilon}_{wc}((0,2),T_1)*B_1$

and $\varepsilon_{wc}(1,2)*(B_2-B_1)$. If the long-wave radiative model including its cloud parameterization is realistic, the modeled outgoing flux to space (FF2) should compare reasonably with that observed by NIMBUS III satellite during the same period, after Raschke et al (1973). The most nearly comparable satellite climatological period was 16-31 July 1969. These satellite observations were obtained from the NIMBUS III satellite atlas of Raschke et al (1973) for the July dates indicated and used for comparison with the model values of FF2, point for point (at 5° latitude intervals) along the same four meridians of Fig. 1. Also the latitudinally-distributed mean satellite fluxes were compared with the corresponding averaged values of FF2. The results showing the comparisons of the latitudinally-averaged distribution of the model computations of FF2 and the corresponding satellite observations are listed by latitude in Table V.

## C. APPLICATIONS TO HEAT BALANCE COMPUTATIONS

### 1. At Upper and Lower Boundaries

In order to compute the heat balance at the top of the earth-tropospheric system the composite $F_2^*$ and the total insolation absorbed below level k=2 at each gridpoint are required. Moreover, a radiative balance is computed at the surface for each gridpoint using the earth's absorbed insolation (Section IV) and the composite net flux loss $F_{10}^*$.

In order to consider the possibility of a heat balance at the earth's surface, rather than merely a radiative balance, it is necessary to add a term representing combined sensible and latent heat transfer across the air-sea interface (Section V). This latter transfer rate at each gridpoint was adapted from the FNWC primitive equation model, after

the discussion of Kaitala (1974), and based upon the FNWC data of 16 July 1974.

2. Intermediate Levels

Consideration of the radiation balance in the atmosphere requires computation of the long-wave cooling effects caused by the flux divergences F26 and F610. F26 and F610 are defined as

$$F26 = F_2^* - F_6^* \tag{3-6}$$

$$F610 = F_6^* - F_{10}^* \tag{3-7}$$

where the symbols (2,6) and (6,10) indicate the layer boundaries involved in the balance consideration for the indicated layer.

In order to compute F26 and F610 at each gridpoint, complete listings of IR net fluxes $F_{10}^*$, $F_6^*$, $F_2^*$, associated with each set of reference cloud amounts (0,0), (1,0), (0,1), (1,1) have been computed at each gridpoint together with the weighted set of fluxes $F_{10}^*(CL_1, CL_2)$, $F_6^*(CL_1, CL_2)$, $F_2^*(CL_1, CL_2)$. These cloud-weighted values have been constructed using the weighting scheme of Eqs. 2-6, 3-1, 3-4 and 3-5. A sample gridpoint printout of the net fluxes and flux divergences has been included in Table II.

The determination of the heat balance by layers has been deferred to Section VI, where the results are displayed in cross-sectional form for the 2/3-CL case.

D. STATISTICAL RESULTS AND COMPARISONS

1. Net Flux $F_{10}^*$ (0,0)

A statistical test of the $F_{10}^*(0,0)$ numerical results was conducted by utilizing a linear regression program for relating the

predictand $F_{10}^{*}(0,0)$ against the simultaneous values of $X_1 = B_{10}$ and $X_2 = B_{10}\sqrt{e}$ as predictors, using all 93 gridpoint data as samples. The regression program was based on the BMD02R in the Biomedical set of programs (Dixon (1973)). The result was cast in the form of the well-known Brunt net flux equation (1932):

$$F_{10}^{*} = B_{10}(a+b\sqrt{e}) \tag{3-8}$$

where

$$B_{10} = St*T_{10}^{4} \tag{3-9}$$

is the Stefan-Boltzmann blackbody flux at the surface temperature $T_{10}$ and e is the surface vapor pressure in mb. The multiple correlation coefficient $R_M(F_{10}^{*}|X_1,X_2)$ was higher than 0.99 in the 16 July case, as was also true for the data periods of Warner (16 October 1973) and Meyers (16 April 1974), (Table III).

Since $F_{10}^{*}$ may be defined as

$$F_{10}^{*} = B_{10} - F_d \tag{3-10}$$

Eq. 3-10 can then be solved for $F_d$.

$$F_d = B_{10}[(1-a) - b\sqrt{e}] \tag{3-11}$$

for the clear-sky case. It must be recalled that the computation of $F_d$ included both the effects of water vapor and of $CO_2$. Since there is no direct relationship of $\sqrt{e}$ upon the quasi-constant absorber mass of $CO_2$, the radiative effect of the $CO_2$ in Eq. 3-11 must be included in the term involving $(1-a)\ B_{10}$.

A cross-seasonal comparison of the coefficients 1-a and -b of Eq. 3-11 is presented in Table III, comparing the clear-sky results of $F_d$ for 16 July 1975 with those of Meyers and Warner at climatological intervals of three months earlier and later, respectively.

The high multiple correlation coefficients indicate that an oceanic version of the Brunt downward flux equation is valid for each tested season. $F_d$ depends most strongly upon $B_{10}$ while only slightly on $B_{10}\sqrt{e}$. This is an apparent result of the nearly constant relative humidity over the large oceanic regimes. Moreover, the weak dependence of $F_d$ upon $B_{10}\sqrt{e}$ is most evident at the data-time 16 July 1974, when the coefficient -b is so small as to be statistically insignificant. This result is due primarily to the relatively weak gradients of both $\sqrt{e}$ and in the radiative soundings aloft corresponding to 16 July 1974, as compared with the adjacent seasons.

2. Modification of $F_{10}^*$ for Cloudiness $CL_1$, $CL_2$

A second statistical test was performed based on a possible relationship between the cloudy-sky and the clear-sky cases of $F_{10}^*$. The ratio $Y = F_{10}^*(CL_1,CL_2)/F_{10}^*(0,0)$ was used as the predictand in this case. The predictor CL was the total opaque cloud cover at each gridpoint, defined as (after Quinn, 1971, and Spaeth, 1975):

$$CL = CL(1) + CL(2)(1-CL(1)) \qquad (3\text{-}12)$$

This regression was run utilizing $F_{10}^*(CL_1, CL_2)$ in the numerator, computed using the amounts of CL(1) and CL(2) as calculated from Smagorinsky's formulation and then utilizing $F_{10}^*(CL_1', CL_2')$ computed from the

| | | | | | |
|---|---|---|---|---|---|
| CL(1) = 0.0 | CL(2) = 0.0 | WT = 0.7587 | $F_{10}^{*}$ = .1829 | $F_{6}^{*}$ = .3013 | $F_{2}^{*}$ = .3970 ly/min |
| CL(1) = 1.0 | CL(2) = 0.0 | WT = 0.0 | $F_{10}^{*}$ = .1020 | $F_{6}^{*}$ = .0984 | $F_{2}^{*}$ = .2610 ly/min |
| CL(1) = 0.0 | CL(2) = 1.0 | WT = 0.2413 | $F_{10}^{*}$ = .0572 | $F_{6}^{*}$ = .2656 | $F_{2}^{*}$ = .3643 ly/min |
| CL(1) = 1.0 | CL(2) = 1.0 | WT = 0.0 | $F_{10}^{*}$ = .0572 | $F_{6}^{*}$ = .0635 | $F_{2}^{*}$ = .2610 ly/min |
| COMPOSITE TOTALS | | | $F_{10}^{*}$ = .1525 | $F_{6}^{*}$ = .2921 | $F_{2}^{*}$ = .3891 ly/min |

Table II. A sample listing of gridpoint values of the terrestrial radiation fluxes computed at gridpoint (2,2) using the equations detailed in Sec. III (full-CL case). All net fluxes have been converted to ly $min^{-1}$.

2/3-CL parameterization. The general form of the regression formula required is shown in Eq. 3-13 below, with CL given in Eq. 3-12

$$F_{10}^{*}(CL) = F_{10}^{*}(0,0)(1-d(CL)) \qquad (3\text{-}13)$$

A cross-seasonal comparison of the coefficient d for the 2/3-CL and full-CL cases using the results of this study and those of Meyers and Warner, and of the resulting multiple correlation coefficients are presented in Table IV. There seems to be little clear-cut variation in the statistics of Table IV between the results of adjacent seasons, and little statistical preference between the full-CL and the 2/3-CL cases. The high correlation coefficients of Table IV, for all seasons considered, indicate the general capability of the IR radiative model employed in this study to account for the effective net radiation at the surface.

The mean values of $F_{10}^{*}$ over the 93 gridpoint soundings for 16 July 1974, as applicable in Tables III and IV were as follows:

| Full-CL Statistics | 2/3-CL Statistics |
|---|---|
| $\overline{F_{10}^{*}(CL)} = .0774$ ly $min^{-1}$ | $\overline{F_{10}^{*}(CL')} = .0966$ ly $min^{-1}$ |
| $\overline{F_{10}^{*}(0,0)} = .1449$ ly $min^{-1}$ | $\overline{F_{10}^{*}(0,0)} = .1449$ ly $min^{-1}$ |
| $\overline{CL} = .5890$ | $\overline{CL'} = .4306$ |

The superior bar symbol denotes the sample mean. These results indicate that the surface net flux is decreased by the ratio .4658 with $\overline{CL} = .5890$, and by the ratio .3333 with $\overline{CL'} = .4306$. These results indicate that the downward flux $F_d(CL)$ is 46.6 percent larger at the surface than $F_d(0,0)$ when full-CL amounts are used in the cloud parameterization model. In the 2/3-CL parameterization the mean downward

| | 16 April 1974 | 16 July 1974 | 16 October 1973 |
|---|---|---|---|
| 1-a | .6557 | .8129 | .6834 |
| -b | .0209 | -.0094 | .0161 |
| $\overline{F_d}$ | .4527 | .5471 | .4716 |
| $R_M$ | .9969 | .9950 | .9973 |

Table III. Cross-seasonal comparisons of the coefficients 1-a and -b from Eq. 3-11, as well as mean values from the Brunt equation and the resulting multiple correlation coefficients have been included.

| | 16 April 1974 | | 16 July 1974 | | 16 October 1973 | |
|---|---|---|---|---|---|---|
| | 2/3-CL | full-CL | 2/3-CL | full-CL | 2/3-CL | full-CL |
| d | -.73 | -.75 | -.74 | -.81 | -.72 | -.73 |
| $R_M$ | .9916 | .9945 | .9942 | .9920 | .9974 | .9972 |

Table IV. Cross-seasonal comparison of the coefficient d from Eq. 3-13 and the resulting multiple correlation coefficients for both the 2/3-CL and the full-CL cases.

flux at the surface $F_d(CL')$ is increased by only 33.3 percent when compared to $F_d(0,0)$.

## E. COMPARISONS OF FF2 WITH SATELLITE CLIMATOLOGY

Comparison was made of computed-model values of FF2 with satellite measurements of total long-wave flux to space (after Raschke et al, 1973) for the NIMBUS III period of 16-31 July 1969. FF2 is used here instead of $F_2^*$ since the downward flux at k=2 is not measured by the satellite. The computation of FF2 was previously discussed. FF2 for 16 July 1974 was computed for both full-CL and 2/3-CL cases at all 93 gridpoints. These FF2 values were then interpolated to whole multiples of 5° latitude along each of the four meridians and the results were then averaged zonally to get a mean latitudinal distribution valid for each 5° latitude interval considered in this study.

Table V shows both of the latitudinally-distributed FF2 cloud-model values compared with those extracted from Raschke et al (1973). Raschke's results were obtained by interpolation from charts using the same oceanic meridians as those used in this study. Latitudinally distributed total opaque cloud cover CL by Eq. 3-12 are also listed for both full-CL and 2/3-CL cases at each latitude. In the bottom line of each column in Table V is listed the cosine-weighted mean of each set of the column values for the listed latitude range. It should be noted that the Raschke results do not correspond to specifically known CL values. Table V suggests that the model results for FF2, both full-CL and 2/3-CL, are reasonably close to the corresponding values derived from Raschke. A close examination of this table shows that in the regions 20S to 5N and 25N to 45N both sets of model results

| Lat | RADIATIVE STATISTICS FF2 full-CL | FF2 2/3-CL | F2(RAS) | CLOUD STATISTICS full-CL CL Avg | 2/3-CL CL' Avg |
|---|---|---|---|---|---|
| 20S | .377 | .382 | .40 | .398 | .269 |
| 15 | .386 | .390 | .42 | .456 | .306 |
| 10 | .400 | .403 | .42 | .396 | .258 |
| 5 | .378 | .384 | .39 | .616 | .498 |
| 0 | .357 | .366 | .38 | .615 | .445 |
| 5 | .341 | .354 | .36 | .737 | .534 |
| 10 | .357 | .367 | .34 | .651 | .460 |
| 15 | .369 | .377 | .35 | .622 | .430 |
| 20 | .384 | .389 | .37 | .638 | .431 |
| 25 | .390 | .393 | .40 | .559 | .375 |
| 30 | .372 | .378 | .39 | .601 | .425 |
| 35 | .378 | .382 | .38 | .555 | .383 |
| 40 | .356 | .360 | .36 | .546 | .387 |
| 45 | .333 | .338 | .36 | .671 | .566 |
| 50 | .284 | .298 | .35 | .652 | .475 |
| 55 | .210 | .229 | .33 | .948 | .819 |
| 60 | .269 | .286 | .33 | .635 | .459 |
| 65 | .196 | .219 | .33 | .862 | .590 |
| Wt Avg | .352 | .360 | .374 | .552 | .405 |

Table V. Comparison of zonally-averaged longwave flux to space, FF2, as found by this study for both full-CL and 2/3-CL cloud cases for 16 July 1974, and by Raschke et al (1973) based upon NIMBUS III measurements. Also included are composite cloud amount fractions used in the two cloud models of this study. Flux values in ly $min^{-1}$.

are slightly less than given by Raschke, while in the region 10N to 20N both sets of values are slightly higher than Raschke. From 20S to 45N the agreement between FF2 and F2(RAS) is quite close. From 50N and higher the correspondence to F2(RAS) is not as good and perhaps this is due to the high amounts of cloud cover experienced on this day in this region. This could be particularly true since the model calculations are for a single day, whereas Raschke's calculations are based upon 16-day averaged values. Additional limitations of the comparisons made here are obvious, when it is recalled that between latitudes 20S-5S and between 60N-65N there are fewer than four meridional lines available for computing the listed zonal values in Table V. For all other latitudinal-average values, four meridional lines were used in the averaging. While the results from Table V are not used to make a final choice of cloud-cover parameterization for use in the radiation model, there is evidence of slightly closer agreement of FF2 with F2(RAS) using the 2/3-CL parameterization.

## F. COMPARISONS OF CROSS-SEASONAL RESULTS OF $F_{10}^*$

Table VI depicts the latitudinally distributed values of $F_{10}^*(CL')$ and of CL' at the earth's surface obtained using the 2/3-CL parameterization. A seasonal comparison of the model computed $F_{10}^*$ is made with data obtained from Meyers (1975) for the 16 April 1974 case and from Warner (1974) for 16 October 1973. It is clearly shown that $F_{10}^*(CL')$ is a decreasing function of cloud cover. The most noteworthy aspect of Table VI is the belt of high values of $F_{10}^*$ for 16 July 1974 in the latitudinal band 20S to 10S. If the associated CL values are examined, it is noted that the composite cloud values were very low

| Lat. | 16 April 1974 $F_{10}^{*}$(CL') | CL' | 16 July 1974 $F_{10}^{*}$(CL') | CL' | 16 October 1973 $F_{10}^{*}$(CL') | CL' |
|---|---|---|---|---|---|---|
| 20S | .0736 | .842 | .1509 | .269 | .0927 | .628 |
| 15 | .0667 | .838 | .1328 | .306 | .0823 | .629 |
| 10 | .0710 | .752 | .1346 | .258 | .0807 | .607 |
| 5 | .0690 | .647 | .0935 | .498 | .0747 | .707 |
| 0 | .0779 | .659 | .1014 | .445 | .0952 | .489 |
| 5 | .0802 | .591 | .0945 | .534 | .1011 | .471 |
| 10 | .0863 | .639 | .1022 | .460 | .1015 | .459 |
| 15 | .0919 | .548 | .1033 | .430 | .0988 | .486 |
| 20 | .0847 | .536 | .0941 | .431 | .1011 | .437 |
| 25 | .0939 | .473 | .0983 | .375 | .1056 | .383 |
| 30 | .0981 | .446 | .0918 | .425 | .1037 | .448 |
| 35 | .1115 | .520 | .0924 | .383 | .1087 | .484 |
| 40 | .1162 | .408 | .0854 | .387 | .1218 | .325 |
| 45 | .0995 | .467 | .0705 | .566 | .1188 | .301 |
| 50 | .0795 | .674 | .0637 | .475 | .1037 | .381 |
| 55 | .1082 | .555 | .0377 | .819 | .0921 | .452 |
| 60 | .0538 | .816 | .0852 | .459 | .0856 | .450 |
| 65 | .0816 | .796 | .0613 | .590 | .0346 | .885 |
| Wt Avg. | .0773 | .596 | .0848 | .405 | .0853 | .462 |

Table VI. Cross-seasonal comparison of the zonally-averaged net fluxes at the surface $F_{10}^{*}$ and zonally-averaged CL' based on 2/3-CL parameterization for the three mid-seasonal dates 16 April 1974, 16 July 1974, and 16 October 1973. Flux values are in ly $min^{-1}$.

and this seems to be consistent with the high values for $F_{10}^*$. Furthermore, the low CL values would appear to be consistent with the northward migration of the ITCZ during mid-summer. There is a tendency in each season for a relative maximum value of $F_{10}^*$ to be located in the subtropics (latitudes 15-25N). There is further evidence of a high latitude (55-65N) minimum $F_{10}^*$ associated with a concentration of maximum cloud cover CL'. The analysis does seem to be consistent across seasons. Similar conclusions were reached for the full-CL model, although they were not included in Table VI. In general, it is felt that the results of the $F_{10}^*$ analysis yield no conclusive results in regard to the appropriateness of the choice of full-CL or the 2/3-CL parameterization models.

## IV. SOLAR RADIATION

### A. PARTITION OF SOLAR INSOLATION

The solar constant assumed in this study at level k=0 (top of atmosphere) was 2.00 ly $min^{-1}$ (Joseph, 1971). This flux was depleted by 4% to account for the attenuation caused by oxygen and ozone above the tropopause. This left the value S = 1.92 ly $min^{-1}$ at level k=2 to be used in this study as the effective solar constant.

Equation (4-1) was then utilized to compute the effective solar insolation at the tropopause (k=2) as follows:

$$F(2) = S \left[\frac{r}{r_m}\right]^{-2} \text{Cos } z \qquad (4\text{-}1)$$

where S = effective solar constant at k=2

Cos z = cosine of the zenith angle for the Julian date used

$r/r_m$ = ratio of the actual earth-sun distance to the mean earth-sun distance for the Julian date used in this study.

The Smithsonian Meteorological Tables (List, 1958) gives the ratio $r/r_m$ and the solar declination $\delta$ for 16 July 1974, 0000GMT, as these values are employed in Eq. 4-1. These values are, respectively:

$$\frac{r}{r_m} = 1.01644$$

$$\delta = 21.5\text{N latitude}$$

$\delta$ is used in evaluating the cosine of the solar zenith angle, given by

$$\text{Cos } z = \text{Sin } \phi \text{ Sin } \delta + \text{Cos } \phi \text{ Cos } \delta \text{ Cos } h \qquad (4\text{-}2)$$

where $\phi$ is the latitude and h is the hour angle of the sun relative to the meridional data lines. For example, Fig. 1 makes it clear that for

line 1 h = 55°

line 2 h = 10°

lines 3,4 h = 35°

at the times of the synoptic charts (0000GMT and 1200GMT, as applicable). Sin $\phi$ was computed according to the standard polar stereographic projection formula applicable to the FNWC base chart given by

$$\text{Sin } \phi = \frac{r_E^2 - [(I-32)^2 + (J-32)^2]}{r_E^2 + [(I-32)^2 + (J-32)^2]} \qquad (4\text{-}3)$$

where $r_E^2 = 973.752$. Thus Sin $\phi$ assumes the following functional form in terms of the FNWC grid-coordinate I (Fig. 1):

Lines 1, 3, 4

$$\text{Sin } \phi = \frac{973.752 - 2(32-I)^2}{973.752 + 2(32-I)^2} \qquad (4\text{-}4(a))$$

Line 2

$$\text{Sin } \phi = \frac{973.752 - (32-I)^2}{973.752 + (32-I)^2} \qquad (4\text{-}4(b))$$

or, conversely I is given in terms of $\phi$ by

Lines 1, 3, 4

$$I = 32 - 22.065\left[\frac{\text{Cos } \phi}{1 + \text{Sin } \phi}\right] \qquad (4\text{-}4(c))$$

Line 2

$$I = 32 - 31.205\left[\frac{\text{Cos } \phi}{1 + \text{Sin } \phi}\right] \qquad (4\text{-}4(d))$$

I = 1,..., 25 for Lines 1, 2

I = 9,..., 25 for Line 3

I = 63,...,38 for Line 4

For lines 1, 2, and 3 the gridpoint soundings correspond to 0000GMT 16 July when solar noon occurs at the 180th meridian. Line 4 gridpoint soundings correspond to 1200GMT, 16 July, when solar noon was at the Greenwich meridian.

A very simple partition of solar insolation was utilized in this study after Joseph (1971). It consisted of dividing the insolation F(2) into two parts at level k=2. One part was considered to include all wavelengths $\lambda > .9$ μm where absorption by water vapor and carbon dioxide bands are the most prevalent attenuation processes in clear air. This part of the solar spectrum was termed F(A) energy and was considered subject to water-vapor absorption but not to Rayleigh scattering. For those wavelengths $\lambda \leq .9$ μm, absorption of the solar insolation energy by water vapor was considered negligible. This part of the solar insolation was denoted F(S) suggestive of the fact that it was subject only to Rayleigh scattering attenuation in clear air. The two partitions are formulated after Joseph (1971) as follows:

$$F(A) = .349\ F(2) \qquad (4\text{-}5(a))$$

$$F(S) = .651\ F(2) \qquad (4\text{-}5(b))$$

In this study, the introduction of two cloud decks produced cloud-reflectivity effects upon both the F(A) and F(S) solar energy insolations. However, in the clear areas around any gridpoint the absorption-attenuation only applies to the F(A) insolation, while only Rayleigh scattering-attenuation applies to the F(S) insolation.

B. DISPOSITION OF F(S) INSOLATION

In the disposition of the F(S) insolation, Joseph (1971) determined that Rayleigh scattering reflectance to space by clear skies (after

Coulson, 1959) could be effectively approximated by least squares in the following form

$$\alpha(R) = .085 + .25074\ [\log\ (\frac{\pi}{P_o}\ \text{Sec}\ z)] \qquad (4\text{-}6)$$

where $P_o = 1013.25$ mb. In Equation 4-6, $\pi/P_o \doteq 1$ in view of the fact that the mean sea level pressure $\pi$ is close to 1000 mb. Also

$$\text{Sec}\ z = (\text{Cos}\ z)^{-1}$$

with Cos z given by Equation 4-2.

The surface albedo $\alpha(G)$ is another reflective parameter utilized in this study. Over oceanic areas the following formula for $\alpha(G)$ after Gates et al (1971), was utilized:

$$\alpha(G) = \max\ \{.06,\ .06 + .54\ (.7 - \text{Cos}\ z)\}\ . \qquad (4\text{-}7)$$

1. Clear Sky Case

In the clear sky (0,0) case the F(S) insolation was subjected to Rayleigh scattering-reflectance $\alpha(R)$ by the atmosphere, as well as to reflectance $\alpha(R)$ by the earth's surface. Considering the likelihood of a succession of multiple reflections between earth and atmosphere, the F(S) insolation actually penetrating the earth's surface after scattering is given by

$$ISl0(0,0) = F(S)[1-\alpha(R)][1+\alpha(R)\alpha(G)+....(\alpha(R)\alpha(G))^{n}$$
$$+...]*(1-\alpha(G)) \qquad (4\text{-}8(a))$$

that is, by

$$ISl0(0,0) = F(S)[1-\alpha(R)][1-\alpha(G)]/[1-\alpha(R)\alpha(G)] \qquad (4\text{-}8(b))$$

2. Cloudy-Sky Cases

In the three cases in which clouds were present, F(S) insolation absorbed by the ground at each gridpoint was (Arakawa, 1972):

$$ISlO(1,1) = F(S)(1-R(1))(1-R(2))(1-\alpha(G)) \\ *\{1-[(R(1)R(2) + R(2)\alpha(G) + R(1)\alpha(G) \\ + 2R(1)R(2)\alpha(G)]\}^{-1} \qquad (4\text{-}9)$$

As indicated by the notation (1,1), denoting CL(1) = CL(2) = 1.0, Eq. 4-9 is the formula used in calculating F(S) insolation absorbed by the ground in the case where overcast clouds are present at both levels of Fig. 2. Also in Eq. 4-9, constant cloud-reflectance values were chosen, namely R(1) = .54 for the mid-level clouds between k=4 and 6, and R(2) = .66 for the low-level clouds between k=8 and 9. Both cloud-reflectance values are as suggested by C. D. Rodgers (1967).

For all the other cloud cases, the following changes were applied to Eq. 4-9. In the (1,0) case (CL(1) = 1.0, CL(2) = 0.0), the desired result is obtained by setting R(2) = 0 in (4-9), from which it follows that

$$ISlO(1,0) = F(S)(1-R(1))(1-\alpha(G))/[1-R(1)\alpha(G)] \qquad (4\text{-}10)$$

In the case (0,1), one sets R(1) = 0.0 in (4-9) so that (4-9) is simplified to

$$ISlO(0,1) = F(S)(1-R(2))(1-\alpha(G))/[1-R(2)\alpha(G)] \qquad (4\text{-}11)$$

Note that with a cloud overcast present, the Rayleigh clear-sky scattering $\alpha(R)$ does not appear in Eqs. 4-9, 4-10 or 4-11, but is included in the cloud reflectances (Rogers, 1967).

3. Composite F(S) Insolation

Equations (4-8), (4-9), (4-10), and (4-11) were utilized in the computation of the cloud-weighted F(S) insolation penetrating the earth's surface considering the areal-weights of the cloud combinations denoted by (0,0), (1,1), (1,0) and (0,1) about a gridpoint. The resultant F(S) insolation penetrating the earth's surface denoted by ISl0 is therefore expressible as

$$\begin{aligned} ISl0(CL(1), CL(2)) = {} & ISl0(0,0)\ W(0,0) \\ & + ISl0(1,1)\ W(1,1) \\ & + ISl0(1,0)\ W(1,0) \\ & + ISl0(0,1)\ W(0,1) \end{aligned} \qquad (4\text{-}12)$$

Here the weighting factors W(0,0), W(1,1), W(1,0) and W(0,1) are as computed in Eq. 2-6(a,...,d) respectively. Note that Table VII lists the radiative computations as they apply to the disposition of F(S) insolation. The four individual computations of ISl0 as applicable to the possible overcast-clear layer cases are made under that heading while the composite value of ISl0 appears in the final line of the same column of Table VII. The difference

$$REFS = F(S) - ISl0 \qquad (4\text{-}13)$$

in each case represents F(S)-insolation reflection to space while

$$STRAN = \frac{ISl0}{(1 - \alpha(G))} \qquad (4\text{-}14)$$

has been computed as that portion of the F(S)-insolation incident at the sea surface just prior to absorption by the surface. Note that

no absorption in air has been included in the computations of Table VII, and that the only absorption permitted is that implicit on IS10. The final line under each column of Table VII depicts the composite dispositions computed by means of the weighting scheme of Eq. 4-12 as applicable to the case 2/3-CL.

Table VII. A sample listing of F(S) insolational disposition computed at gridpoint (2,2) using equations listed in Sec. IV.B. Insolational values in ly $min^{-1}$.

| $(CL_1, CL_2)$ | Weighting | IS10 | REFS | STRAN |
|---|---|---|---|---|
| (0,0) | .8391 | .3203 | .1639 | .4117 |
| (1,0) | .0000 | .1969 | .2873 | .2531 |
| (0,1) | .1609 | .1501 | .3342 | .1929 |
| (1,1) | .0000 | .110 | .3742 | .1414 |
| COMPOSITE VALUES | | .2969 | .2217 | .3815 |

C. DISPOSITION OF F(A) INSOLATION

The fractional portion of the solar insolation subject to absorption by atmospheric water vapor and carbon dioxide are covered in the following subsections.

1. Clear-Sky Case (0,0)

The Manabe-Möller absorptivity function provided the necessary absorptivity values for the key layers in this case. The form of this absorptivity function is

$$\underline{a}(2, k) = .271[U(2, k) \text{ Sec } z]^{.303} \qquad (4\text{-}15)$$

Here $\underline{a}$ is the absorptivity applied to the pressure-scaled water vapor mass between levels 2 and k (Fig. 2) along the zenith slant-path angle z.

The resultant absorbed insolational energy in the partular layer (2,6) is then given by the Manabe-Möller relation

$$A(2,6) = 0.271F(A)[U(2,6)\ \text{Sec}\ z]^{.303} \tag{4-16}$$

The two layers of interest in which absorption was computed were (2,6) and (2,10). The absorbed insolation in the layer (6,10) was then computed by

$$A(6,10) = A(2,10) - A(2,6) \tag{4-17}$$

Water vapor mass above level 2 was assumed negligible in the F(A) disposition of the solar insolation.

By subtracting A(2,10) from F(A), the direct transmission of F(A) insolation impinging at the earth's surface was determined. The transmission of F(A) insolation is then further reduced by the transmissivity of $(1-\alpha(G))$, after surface-reflectance, which leads to the earth-absorbed result

$$IA10(0,0) = F(A)\{1-.271[U(2,10)\ \text{Sec}\ z]^{.303}\}(1-\alpha(G)) \tag{4-18}$$

The transmitted energy impinging upon the earth just prior to absorption is

$$TRANA(0,0) = IA10(0,0)/[1-\alpha(G)] \tag{4-19}$$

2. Cloudy Cases

In order to compute meaningful dispositions of F(A) insolation in cloudy-sky cases, cloud reflectivities and cloud absorptivities after C. D. Rodgers (1967) were utilized. The reflectance-values used

are different from those suggested by Rodgers for the F(S) wavelengths. The cloud reflectivities used here are RA(1) = .46 and RA(2) = .50. In this case there are also cloud-absorptivities to be considered. These were taken as A(1) = .20 and A(2) = .30, respectively. In the following discussions the cloud conditions are considered totally overcast in the layer or layers indicated when the notations ((1,1), (0,1), and (1,0)) are utilized.

Schematic representation of the computations performed in the various cases ((1,1), (0,1), (1,0)) are displayed in Fig. 3. This figure indicates the theoretical parameters required in computing the disposition of incoming F(A)-insolation from level k=2 to the earth's surface (k = 10). The equations which relate to the parameters in Fig. 3 and the other cloud configurations are listed in Appendix B of Spaeth's study (1975).

The symbols A24, A46, A68, A89, and A910, etc., represent the insolation absorbed in the layers concerned. Symbols F2, F4, F6, F8 and F9, etc., depict the streams of insolation passing through the indicated level. A vertical arrow implies the direction of insolation passage, i.e., ↓ denotes downward insolation, ↑ upward-reflected insolation, and ↓↓ downward-reflected insolation. The absorption quantity A(6,8)↓↓, for example, indicates absorbed energy remaining in (6,8) from a downward reflected beam.

Since multiple reflections occur between the earth's surface and a cloud base, or between cloud-layers in this model (Fig. 3), the insolational amount reaching the lowermost reflecting surface is affected by the downward reflected beams. Additional insolational amounts remaining after more than two reflections are negligible, and

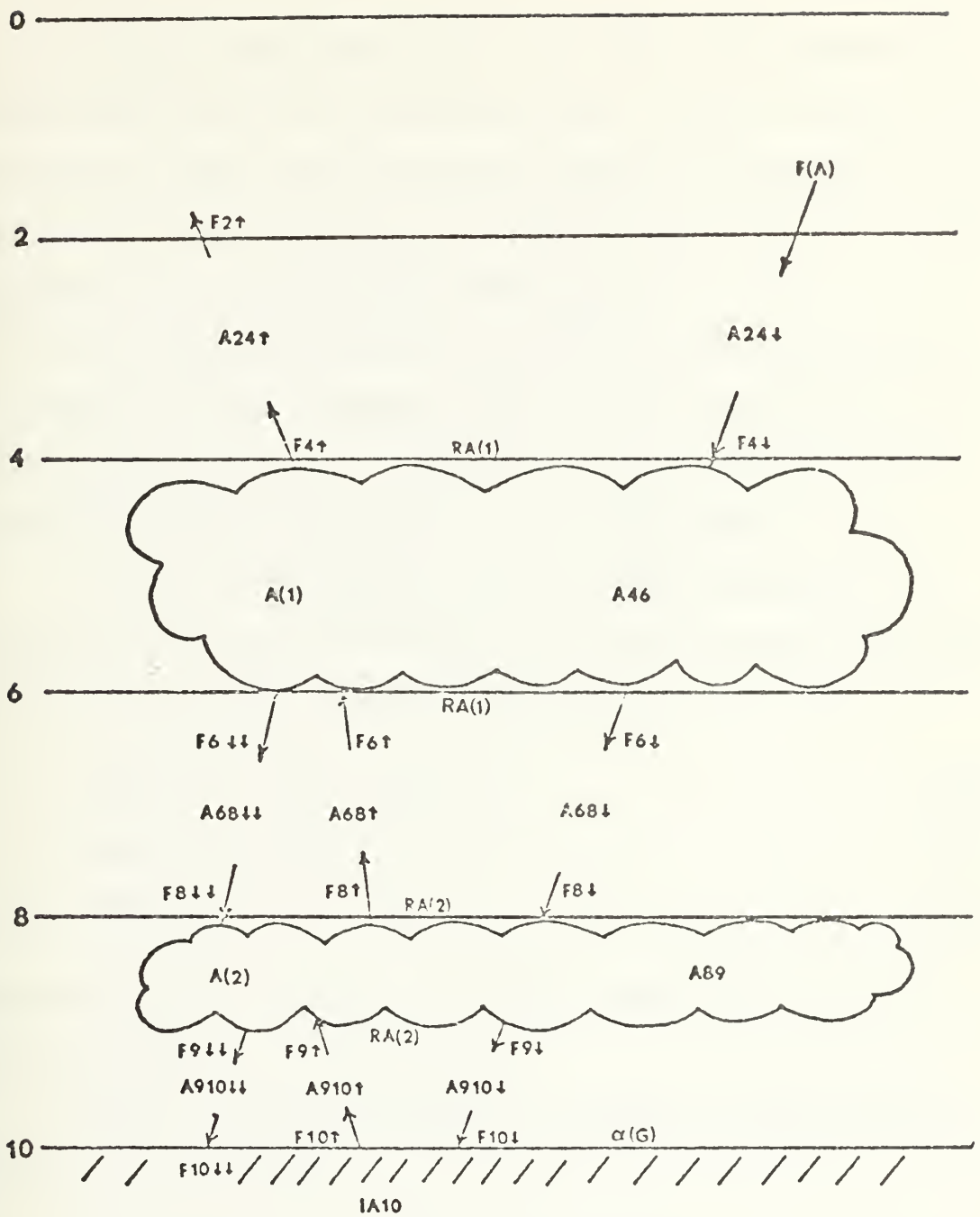


Figure 3. Schematic representation of F(A)-insolation disposition in the case of two overcast layers (cloud-case (1,1)).

are not included in the model computations. Note that insolation reflected upward from a lower interface, either cloud-top or ground, to the base of a higher cloud deck was not subjected to absorption by or transmission through the cloud. This simplification resulted in slightly reduced F(A) insolation-reflectance to space.

A final point to note is that there are three contributions to the absorption of solar insolation within a layer between any two reflecting surfaces. In Fig. 3, these contributions are identified by arrows which indicate the portion of path being crossed.

For each of the possible overcast-cloud combinations, the transmitted F(A) insolation arriving at the earth's surface may be defined using the following notation (TRANA) as

$$TRANA(1,1) = F1O\downarrow + F1O\downarrow\downarrow \tag{4-20}$$

$$TRANA(1,0) = F1O\downarrow + F1O\downarrow\downarrow \tag{4-21}$$

$$TRANA(0,1) = F1O\downarrow + F1O\downarrow\downarrow \tag{4-22}$$

where the right side parameters of (4-20), (4-21), and (4-22) are derived in Appendix B of Spaeth (1975).

The F(A) insolation absorbed by the earth in each cloud-case considered is derived from

$$IA1O(1,1) = F1O\downarrow\ (1-\alpha(G)) + F1O\downarrow\downarrow \tag{4-23}$$

$$IA1O(1,0) = F1O\downarrow\ (1-\alpha(G)) + F1O\downarrow\downarrow \tag{4-24}$$

$$IA1O(0,1) = F1O\downarrow\ (1-\alpha(G)) + F1O\downarrow\downarrow \tag{4-25}$$

In the last three equations, the quantity $F1O\downarrow\downarrow$ is small enough in each case, that no further reflections from the earth were considered.

3. Composite F(A) Layer-Absorptions and Surface-Absorption Insolation

As has been previously discussed, the standard grid-area weighting scheme of this study was applied to obtain composite values of the absorbed F(A) insolation in key layers and also within the earth's surface. The weighting factors applied to the corresponding overcast-combination absorption quantities provided the following composite results:

$$\begin{aligned} A26(CL(1),CL(2)) = {} & A26(0,0)\ W(0,0) + A26(1,0)\ W(1,0) \\ & + A26(0,1)\ W(0,1) \\ & + A26(1,1)\ W(1,1) \end{aligned} \tag{4-26}$$

$$\begin{aligned} A610(CL(1),CL(2)) = {} & A610(0,0)\ W(0,0) + A610(1,0)\ W(1,0) \\ & + A610(0,1)\ W(0,1) \\ & + A610(1,1)\ W(1,1) \end{aligned} \tag{4-27}$$

$$\begin{aligned} IA10(CL(1),CL(2)) = {} & IA10(0,0)\ W(0,0) + IA10(1,0)\ W(1,0) \\ & + IA10(0,1)\ W(0,1) \\ & + IA10(1,1)\ W(1,1) \end{aligned} \tag{4-28}$$

The weighting factors W(0,0),...,W(1,1) were first listed in Eqs. 2-6 (a,...,d). Also A26(0,0), A610(0,0), IA10(0,0) are given in each clear-sky case (0,0) about each gridpoint by Eqs. 4-16, 4-17 and 4-18, respectively.

The results for the absorption in layers (2,6), (6,10) and at the surface are shown in Table VIII for the four cloud cases [(0,0), (1,0), (0,1), (1,1)] and for the composite case based on the weighting factors W(0,0),...,W(1,1).

Table VIII. A sample listing of F(A) disposition parameters computed at gridpoint (2,2) using equations listed in Sec. IV.C. Values listed are in ly $min^{-1}$.

| $(CL_1, CL_2)$ | Weighting | A26 | A610 | AI10 | REFA | TRANA |
|---|---|---|---|---|---|---|
| (0,0) | .7587 | .0509 | .0670 | .1103 | .0314 | .1418 |
| (1,0) | 0.0 | .0821 | .0335 | .0424 | .1017 | .0538 |
| (0,1) | .2413 | .0529 | .1215 | .0211 | .0641 | .0267 |
| (1,1) | 0.0 | .0821 | .0567 | .0102 | .1107 | .0129 |
| COMPOSITE VALUES | | .0514 | .0801 | .0888 | .0393 | .1260 |

In the computational scheme indicated by the entries of Table VIII, the reflected F(A) insolation to space has been depicted by the symbol REFA, and its values follow from

$$REFA = F(A) - A26 - A610 - IA10 \tag{4-29}$$

whereas the TRANA dispositions are given by Eqs. 4-19,...4-22, respectively, or by its weighted-mean value in the case of the composites (last line, Table VIII).

4. Absorptivity (ABA) by Layers

Here the (fractional) absorptivity as well as the actual insolation values absorbed in the layers are considered. In the computation of absorptivity, which is fractional absorption, the total undepleted insolation at the top (k=0) is used. The following equation was utilized in this calculation:

$$FADJ = 2.00(r/r_m)^{-2} \text{ Cos } z \tag{4-30}$$

The absorptivity of the troposphere ABA was computed from the ratio of the insolation absorbed in the troposphere to the insolation incident at the top of the atmosphere rather than at k=2:

$$ABA = \frac{A(2,6) + A(6,10)}{FADJ} \qquad (4\text{-}31)$$

D. ALBEDO (ALB) OF THE EARTH-TROPOSPHERE SYSTEM

In considering the planetary albedo, the reflected insolation of the earth-troposphere system in both the F(A) and F(S) insolational regions must be recalled by the program. Thus REF is computed at each gridpoint as the sum of the reflected insolation energy in F(A) (denoted REFA in Eq. 4-29) and the reflected part of F(S), previously denoted REFS in Eq. 4-13:

$$REF = REFS + REFA \qquad (4\text{-}32)$$

Finally the planetary albedo is related to FADJ through

$$ALB = \frac{REF}{FADJ} \qquad (4\text{-}33)$$

E. COMPOSITE ABSORPTIVITY (ABG) BY THE EARTH-SURFACE; COMPOSITE ATMOSPHERIC TRANSMISSIVITY (ATRAN)

1. Absorptivity (ABG) of Earth

By summing the weighted values of F(S) and F(A) portions of the incoming insolation entering the earth, the total insolation absorbed at the earth's surface was computed. This quantity when divided by the extraterrestrial insolation gave the fractional absorptivity (ABG) of the

earth's surface. The equation for ABG was

$$ABG = \frac{IA10 + IS10}{FADJ} \qquad (4\text{-}34)$$

where IA10, IS10, and FADJ were defined previously by Eqs. 4-28, 4-12, and 4-30, respectively.

2. Transmissivity (ATRAN) of the Troposphere

Also computed with the total insolational energy TRAN, incident at the earth's surface just before absorption by the surface. This calculation is given by

$$TRAN = TRANA + STRAN \qquad (4\text{-}35)$$

Here STRAN = (IS10/(1-α(G)) as previously defined in Eq. 4-14, and α(G) is given in Eq. 4-7. TRANA has also been defined as the weighted value of TRANA(0,0), TRANA(1,1), TRANA(1,0), and TRANA(0,1) given by Eqs. 4-19,...,22. Note also in justification of STRAN that the four cases for IS10 of Eqs. 4-8,...,11 each have the common factor (1-α(G)) in the numerator and therefore each transmitted F(S)-insolational component available at the earth just before absorption needs only to be divided by (1-α(G)). TRAN may thus be viewed as the total insolational energy incident at a pyrheliometer located at earth. The (fractional) transmissivity of the troposphere (ATRAN) is then computed from

$$ATRAN \equiv TRAN/FADJ \qquad (4\text{-}36)$$

Note finally that the major dispositions of the total insolation at the indicated map times have now been identified by the fractional values, ALB, ABA or ABG, and ATRAN, each of which is a fractional value representing the reflectivity (albedo), absorptivity of air or earth, or atmospheric transmissivity as the case may be.

3. Computational Check

The computational scheme utilized in this model was checked continuously by summing the fractional values ALB, ABA, and ABG at each gridpoint. The value in each case must total .96, since as previously noted the attenuation of solar insolation was taken as four percent as it passed through the stratosphere.

F. STATISTICAL ANALYSIS

In order to substantiate some of the computations performed in this section, several of the most important items computed were statistically analyzed using linear regression computer programs from the BMD set of statistical programs (Dixon, 1973).

1. Clear Sky Cases

Using ALB (0,0,z) which is the clear sky case of albedo, as the predictand, and $\log_{10}$Sec z as the predictor, the following best-fit equation resulted

$$\text{ALB}(0,0,z) = .07856 + .38689 \log_{10}\text{Sec } z$$
$$R_M = .9618 \qquad (4\text{-}37)$$

where $R_M$ represents the multiple correlation coefficient.

This result was expected over the ocean where $\alpha(G)$ and $\alpha(R)$ involved logarithmic dependence on Sec z. The sample-average values of ALB and $\log_{10}$Sec z were

$$\overline{\text{ALB}(0,0)} = .1295 \qquad \overline{\log_{10}\text{Sec } z} = .1316$$

Other clear-sky regression tests made use of the water-vapor mass path length (M) defined by

$$M = (U \text{ Sec } z)^{1/2} \log_{10}(U \text{ Sec } z) \tag{4-38}$$

This parameterization of water vapor mass is similar to that developed by Hanson (1971), who used a similar M as a predictor in his empirical formulations of ABA for both clear and partly cloudy sky cases. In this study the two regressions attempted using M as a predictor were with ABA(0,0,M) and ATRAN(0,0,M) as predictands. The best-fit equations resulting were

$$ABA(0,0,M) = .1028 + .0281\ M$$

$$R_M = .9922 \tag{4-39}$$

$$ATRAN(0,0,M) = .7976 - .0338\ M$$

$$R_M = .8796 \tag{4-40}$$

The absorptivity in the form given by (4-39) agrees closely in form with that obtained by Spaeth based on 16 January 1974 data and with that of Hanson (1971) based on pyrheliometric data. The means of ABA(0,0,M) and ATRAN(0,0,M) for the original 93 gridpoint sample were

$$\overline{ABA(0,0,M)} = .1433$$

$$\overline{ATRAN(0,0,M)} = .7488$$

$$\overline{M} = 1.44376 \text{ (gm cm}^{-2})^{1/2}$$

2. Statistical Relationships Between ALB, ABA and ATRAN in the Cloudy and Clear Sky Cases

In addition to computing the clear-sky value of ALB, it was also possible to compute the composite cloud value of ALB. A regression was

formed showing the relationship between the ratio ALB(CL(1), CL(2))/ ALB(0,0) as the predictand and the total opaque cloud cover(CL) as the predictor. CL in this model is specified by Eq. 3-12, and gives a good approximation of the effective total cloud cover by the two layers of cloud amounts $CL_1$ and $CL_2$ by Eq. 2-4 used in this model. As explained earlier in this study, a one-third reduction of both CL(1) and CL(2) after initial determination by Eq. 2-4 was also tried in all computations involving cloud amounts. This test represented an attempt at tuning the cloud model for radiative calculations, and gave results in closer agreement with the latest literature on satellite reflectances. Thus all subsequent regressions of ALB(CL)/ALB(0,0) upon CL, computed after Eq. 3-12, will include best-fit equations formulated using a CL based upon the 2/3-CL model (Eq. 2-5) and the full-CL model (Eq. 2-4).

A small letter subscript 'a' in the equation number or symbol will indicate those computations using 2/3-CL amounts while a small letter subscript 'b' will indicate those utilizing the full-CL model.

The first regression equations tested were those for $ALB_a(CL')$ and $ALB_b(CL)$ for the respective cases of 2/3-CL and full-CL cases. The results are given in (4-41a,b). The symbol $R_M$ once again signifies the multiple correlation of the statistical regressions.

$$ALB_a(CL(1)CL(2)) = ALB(0,0)[1 + 2.9915\ CL + .5873\ CL^2]$$

$$R_M = .9858 \qquad (4\text{-}41(a))$$

$$ALB_b(CL(1)CL(2)) = ALB(0,0)[1 + 2.7654\ CL + .8308\ CL^2]$$

$$R_M = .9846 \qquad (4\text{-}41(b))$$

The sample means of the values in Eqs. 4-41(a,b) are

| Eq. 4-41a | | Eq. 4-41b | |
|---|---|---|---|
| $\overline{ALB_a(CL(1),CL(2))}$ | = .3163 | $\overline{ALB_b(CL(1),CL(2))}$ | = .3893 |
| $\overline{ALB(0,0)}$ | = .1295 | $\overline{ALB(0,0)}$ | = .1295 |
| $\overline{CL}_a$ | = .4320 | $\overline{CL}_b$ | = .5890 |

The high value of the correlation coefficient in Eq. 4-41 shows strong dependence of ALB upon CL in either cloud parameterization case. Also note that ALB(CL(1),CL(2)) values computed here are clearly higher than reported by Raschke et al (1973), where ALB = .26 for essentially the same set of gridpoints during the NIMBUS III, period 16-31 July 1969. The 2/3-CL cloud parameterization gives albedo results which are closer to Raschke's results, suggesting that the full-CL amounts of Smagorinsky (Eq. 2-4) are too high for radiational computations. A second regression was developed between ABA(CL)/ABA(0,0) versus CL. The following best-fit equation resulted:

$$ABA_a(CL(1),CL(2)) = ABA(0,0)[1+.4667CL - .0148CL^2]$$

$$R_M = .9565 \qquad (4\text{-}42(a))$$

$$ABA_b(CL(1),CL(2)) = ABA(0,0)[1+.5606CL - .1238CL^2]$$

$$R_M = .9597 \qquad (4\text{-}42(b))$$

Mean statistics for these regression cases are

| Eq. 4-42a | | Eq. 4-42b | |
|---|---|---|---|
| $\overline{ABA_a(CL(1),CL(2))}$ | = .1721 | $\overline{ABA_b(CL(1),CL(2)}$ | = .1827 |
| $\overline{ABA(0,0)}$ | = .1433 | $\overline{ABA(0,0)}$ | = .1433 |
| $\overline{CL}_a$ | = .4320 | $\overline{CL}_b$ | = .5890 |

From the means of (4-42), it is seen that the model specifies an increase in atmospheric (solar) absorptivity with increasing cloud cover. This result is in agreement with studies of Warner (1974) and Spaeth (1975) and with the earlier study of London (1957).

An analogous statistical regression was then developed for the cloudy-sky transmissivity relative to the clear-sky transmissitivity. The resulting regressions were

$$\text{ATRAN}_a(\text{CL}(1),\text{CL}(2)) = \text{ATRAN}(0,0)[1-.6522\text{CL}]$$

$$R_M = .9982 \qquad (4\text{-}43(a))$$

$$\text{ATRAN}_b(\text{CL}(1),\text{CL}(2)) = \text{ATRAN}(0,0)[1-.6647\text{CL}]$$

$$R_M = .9977 \qquad (4\text{-}43(b))$$

and the corresponding mean values of the transmissivities are listed below:

| Eq. 4-43a means | | Eq. 4-43b means | |
|---|---|---|---|
| $\overline{\text{ATRAN}_a(\text{CL}(1),\text{CL}(2))}$ | = .5389 | $\overline{\text{ATRAN}_b(\text{CL}(1),\text{CL}(2))}$ | = .4576 |
| $\overline{\text{ATRAN}(0,0)}$ | = .7488 | $\overline{\text{ATRAN}(0,0)}$ | = .7488 |

The parameter ATRAN(CL')/ATRAN(0,0) given by (4-43a) is in very good agreement with the statistical result of Savino-Angstrom, which was

$$Q = Q_o(1 - .66\text{CL})$$

for the tropical ocean areas. The coefficient of CL in the last result is known to be a decreasing function of latitude (Budyko, 1958).

Similarly, the parameters ALB(CL')/ALB(0,0) and ABA(CL')/ABA(0,0) behave consistently with respect to increasing CL, with somewhat more realistic mean values for $\overline{\text{ALB}(\text{CL}')}$ and $\overline{\text{ABA}(\text{CL}')}$ than for the corresponding

full-CL parameterization. Hence, in the mean, the statistical analyses performed seem to show agreement with observational results of other investigators. Comparative computations of the atmospheric transmissivity, particularly in the 2/3-CL case appear to give better agreement with ground-based pyrheliometry.

A major test still to be made is the comparison of the latitudinal-distribution of $ALB_a(CL)$ and $ALB_b(CL)$ with that of the satellite albedo of Raschke et al (1973).

## G. ALBEDO COMPARISONS WITH PUBLISHED RESULTS

The tropospheric albedo computations of the solar-insolation model of this section have been presented for both full-CL and 2/3-CL cases, respectively. These albedos have been interpolated to whole multiples of 5° latitude between 20S and 65N. These computations were made for each of the four oceanic meridians and the resulting albedos averaged across the meridians are presented as a function of latitude in Table IX for both the full-CL and 2/3-CL cases, where comparison is also made with satellite albedos of Raschke et al (1973). For sake of consistency the Raschke albedo data have been extracted from atlas presentations for the period 16-31 July 1969 to 5° latitude grids, on the same four meridians, before applying the zonal-averaging process. The total opaque cloud-cover amounts for the two cases are listed under the headings "full-CL" and "2/3-CL" corresponding to the composite cloud-cover formula, Eq. 3-12.

The primary results to be noted in Table IX are the quasi-constant values of ALB(RAS) between 20S,...,35N, with individual latitudinal values not greatly different from the tropical-subtropical mean of

Table IX. Comparison of zonally-averaged albedos as computed by this study for both full-CL and 2/3-CL models for 16 July 1974 with those of Raschke et al (1973), and the corresponding values of full-CL and of 2/3-CL, each as a function of latitude. The bottom line lists the cosine-weighted average of the parameter listed in the tabular column above.

| Lat. | Albedo full-CL | Albedo 2/3-CL | Albedo Raschke | Full-CL Avg. | 2/3-CL Avg. |
|---|---|---|---|---|---|
| 20S | .335 | .296 | .20 | .398 | .269 |
| 15 | .347 | .296 | .18 | .456 | .306 |
| 10 | .320 | .268 | .16 | .396 | .258 |
| 5 | .392 | .345 | .26 | .616 | .498 |
| 0 | .372 | .303 | .24 | .615 | .445 |
| 5 | .404 | .324 | .21 | .737 | .534 |
| 10 | .368 | .292 | .25 | .651 | .460 |
| 15 | .359 | .282 | .24 | .622 | .430 |
| 20 | .362 | .281 | .22 | .638 | .431 |
| 25 | .330 | .259 | .21 | .559 | .375 |
| 30 | .337 | .272 | .21 | .601 | .425 |
| 35 | .325 | .259 | .24 | .555 | .383 |
| 40 | .317 | .257 | .25 | .546 | .387 |
| 45 | .365 | .341 | .32 | .671 | .566 |
| 50 | .391 | .309 | .34 | .652 | .475 |
| 55 | .536 | .463 | .37 | .948 | .819 |
| 60 | .356 | .288 | .40 | .635 | .459 |
| 65 | .413 | .323 | .39 | .862 | .590 |
| Wt.Avg. | .364 | .302 | .25 | .552 | .405 |

$\overline{ALB(RAS)} \doteq .22$. For most of this latitude range the computed values of ALB(2/3-CL) exceed those observed by Raschke (Table IX) by the fractional amounts .05 to .10. From 40N poleward ALB(RAS) and ALB(2/3-CL) are in fairly close agreement, with individual values close to the local average of 0.35. Note that at latitudes 60, 65N, the ALB(RAS) results are slightly greater than ALB(2/3-CL) which may be due to an effect associated with the large mean zenith angle at these latitudes.

As noted earlier in Table V, at latitude 55N there is a localized maximum of CL' associated with the largest computed value of ALB(2/3-CL) = .463. The later value is not verified by the two-week average observation of ALB(RAS) = .37. Overall, the computed values of ALB(CL) exceed those of ALB(RAS), latitude-by-latitude, in much the same degree as indicated by cosine-weighted means of Table IX, which are also listed below:

$$\overline{ALB(full\text{-}CL)} = .36$$

$$\overline{ALB(2/3\text{-}CL)} = .30$$

$$\overline{ALB(RAS)} = .25$$

To summarize, there is a well-defined preference for the 2/3-CL over the full-CL model in giving albedos closer to those observed by satellite for the same general period (16-31 July 1969) as reported by Raschke et al (1973). An area of difficulty even with the 2/3-CL model occurs in tropical and subtropical latitudes where Von der Haar and Hanson (1969) have reported the reality of smaller than suspected cloud-covers and of smaller values of the resultant global-albedo. At these latitudes (tropical and subtropical) it seems doubtful that the

large-scale CL'-parameterization, following Smagorinsky, is as applicable as in higher latitudes. Rather some method of specifying the distribution (at gridpoints) of isolated cumulus towers may be appropriate. Finally, it is questionable whether vertically-structured convective cloud elements will have the high reflective capability attributed here to clouds which are depicted as existing in horizontal layers with a constant reflectivity $.5 \leq R \leq .65$ as specified in the radiation model. It may well be that the vertical shafts between convective elements may be a more efficient focus of solar energy to the earth than is perceived by ascribing a constant cloud albedo to the cloud-layer. An alternative approach would be to reduce the two-cloud layering in the tropics to a single layer of clouds.

At any rate with the two-layered cloud-model considered in this study, the only feasible selection from the results deduced here is the 2/3-CL parameterization. This selection is carried over into the computations of Section VI. A further test of the cloud-parameterization effect on the computation of net radiation of the earth-atmosphere system, by comparison with that observed by satellite, is made in Section VII. D.

## V. SENSIBLE AND LATENT HEAT TRANSPORT AT THE SEA-AIR INTERFACE

### A. GENERAL PURPOSE

The model used here to describe the turbulent transports of sensible and latent heat across the sea-air interface was basically that already in use in the operational FNWC primitive equation model. This model has been discussed in detail by Kesel and Winninghoff (1972) and by Kaitala (1974). The primary purpose of the adaptation of the turbulent flux model in this study was to test the magnitudes and directions of these transfer rates in comparison with those of the radiational transfer model which has been discussed here in Sections III and IV. The final purpose of the inclusion of the turbulent flux model was to conduct a diagnostic computation of the heat balance within the oceanic and atmospheric layers for 16 July 1974 under the combined operation of the radiational and turbulent flux models.

### B. WINDSPEED COMPUTATION IN THE TURBULENT FLUX MODEL

At all of the 93 gridpoints tested, the geostrophic windspeed $V_g$ was computed by use of the standard formula

$$V_g = \frac{g}{f} \frac{\Delta Z}{2(d/m)} \tag{5-1}$$

with

$$f = \left(\frac{4\pi}{86,400}\right) \text{Sin } \phi \tag{5-2}$$

$$m = \frac{1.86603}{1+\text{Sin } \phi}$$

and

$$\Delta Z = \sqrt{(Z_4 - Z_2)^2 + (Z_3 - Z_1)^2} \tag{5-3}$$

In Eq. 5-1, d = 381.0 km is the nominal FNWC grid-spacing (true at 60N) and $(\frac{2d}{m})$ is the true-earth spacing used in the centered-difference computations of the contour gradient (cf., Fig. 4).

In (5-1) and (5-3) $\Delta Z$ is the contour-difference, centered in most cases on the gridpoint under consideration. However, at the map edge gridpoints of the meridians, it was only possible to compute a forward-differenced version of $V_g$ (cf., Fig. 4). Thus at edge-point "0", Eq. (5-4) below was used. The spacing $\frac{d}{m}$ in Eq. 5-4 is then taken as one-half that in (5-1), so that

$$V_g = \frac{g}{f} \frac{\Delta Z}{(d/m)} \tag{5-4}$$

with

$$\Delta Z = \sqrt{(Z_4 - Z_0)^2 + (Z_3 - Z_0)^2} \tag{5-5}$$

All geostrophic windspeeds were then converted to surface windspeeds using the following empiricism due to Langlois and Kwok (1969)

$$V_s = .8\ V_g + 2.2 \tag{5-6}$$

where $V_s$ = surface windspeed (mps) and $V_g$ is the 1000 mb geostrophic windspeed. The factor 2.2 in (5-6) is an empiricism introduced to include the effects of gustiness upon the measured (steady-state) windspeed.

In the interval of $\pm$ 10 degrees of latitude, the value of the Coriolis parameter was arbitrarily set at $f = \pm .25 \times 10^{-4} sec^{-1}$, following Kaitala (1974), while for $|\phi| > 10°$, the actual value of f for the particular latitude was used.

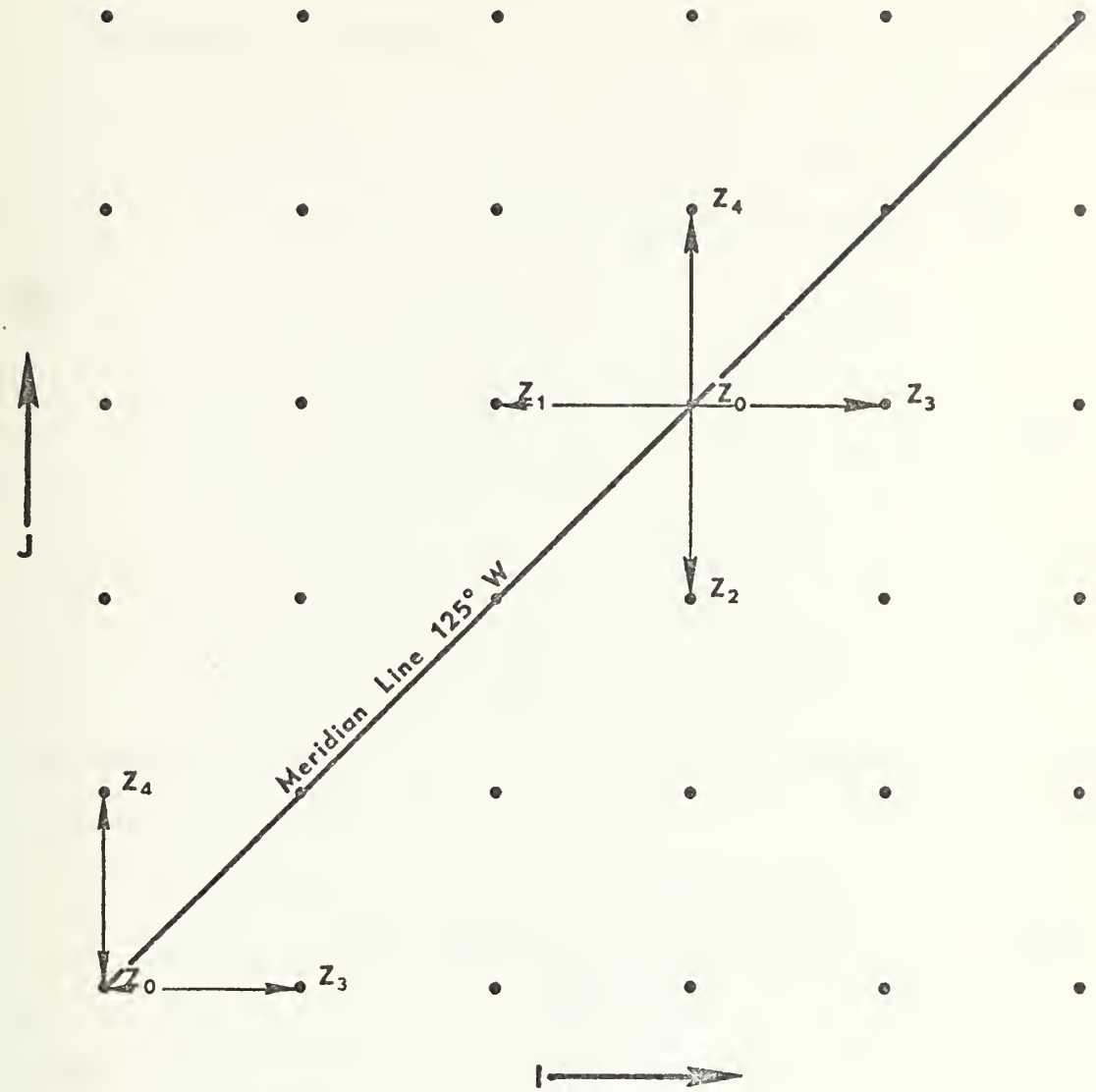


Figure 4. Section of FNWC polar stereographic meridian illustrating the method of obtaining contour gradients in the vicinity of a gridpoint. The values of contour-heights correspond to the 1000 mb D-values in the neighborhood of the gridpoint.

C. SENSIBLE HEAT TRANSPORT

The details of the adaptation of the FNWC model for sensible heat transport $H_\Gamma$ utilized in this study follow the description of Spaeth (1975). The formulation of $H_\Gamma$ is given below in terms of bulk parameters of the surface and of the planetary boundary layer (10,8) of Fig. 2:

$$H_\Gamma = \rho_{10} C_p C_D V_s (T_g - T_x)$$
$$\rho_{10} = \rho_{10} (R_d T_{10})^{-1} \qquad (5\text{-}7)$$

where $C_p = .239 \text{ cal gm}^{-1} (\text{deg. K})^{-1}$

and $C_D = 1.4 \times 10^{3}$ (after Weiler and Burling, 1967)

The equation utilized in this study to compute $T_x$ may be shown to be (Spaeth, 1975)

$$T_x = \frac{C_D V_s T_g + \frac{2 \tilde{K} \theta_9}{\Delta Z} - 2 \tilde{K} \gamma_c}{\frac{2\tilde{K}}{\Delta Z} + C_D V_s} \qquad (5\text{-}8)$$

where

$$\theta_9 = T_9 \left(\frac{1000}{900}\right)^{.286} \qquad (5\text{-}9)$$

$$\tilde{K} = \frac{K^*}{1 + a^* \left(\frac{\theta_9 - \theta_g}{Z_9 - Z_{10}}\right)} \qquad (5\text{-}10)$$

$$\Delta Z = Z_9 - Z_{10} = \frac{R_d}{g} \bar{T} \left(\ln \frac{10}{9}\right) \qquad (5\text{-}11)$$

In 5-7(c), the turbulent parameters $K^*$ and $a^*$ have been determined empirically by FNWC

$$K^* \doteq 10^5 \text{cm}^2\text{sec}^{-1}$$

$$a^* \doteq 5 \times 10^4 \text{cm(deg.K)}^{-1}$$

$T_g - T_x$ in Eq. 5-7 is the temperature lapse for the thin layer between the surface and the top of the constant flux layer (cf., Fig. 5). The formula for $T_x$ deduced here required a constant value of sensible heat $H_\Gamma$ within the constant flux layer (CFL) at each gridpoint with $H_\Gamma$ then decreasing linearly with pressure to $H_\Gamma = 0$ at k=8, and then remaining zero above k=8. This linear decrease of $H_\Gamma$ with pressure is compatible with the condition of constant convergence of the sensible heat flux per gram in the turbulent boundary layer (x,8)。 Thus, the constant value of the convergence of sensible heat as given by Eq. 5-7 within the layer (8,10) may then be considered to be applicable at level k=9 as depicted in Fig. 5(a), after Spaeth (1975).

After computing $T_x$ by Eq. 5-8, $H_\Gamma$ was then computed at each gridpoint using the bulk transfer equation 5-7. The gridpoint values of $H_\Gamma$ are used later in calculations of heat balance in Sections VI and VIII.

## D. EVAPORATIVE HEAT TRANSPORT

Similar to the case of sensible heat convergence, the latent heat transport by turbulence was assumed to be subject to constant evaporative flux convergence throughout the layer 800-1000 mb. The total amount of latent heat removed by evaporation from the ocean surface was essentially as modeled by Kaitala (1974) using bulk transfer theory. It should be recognized, however, that the condensation and consequent

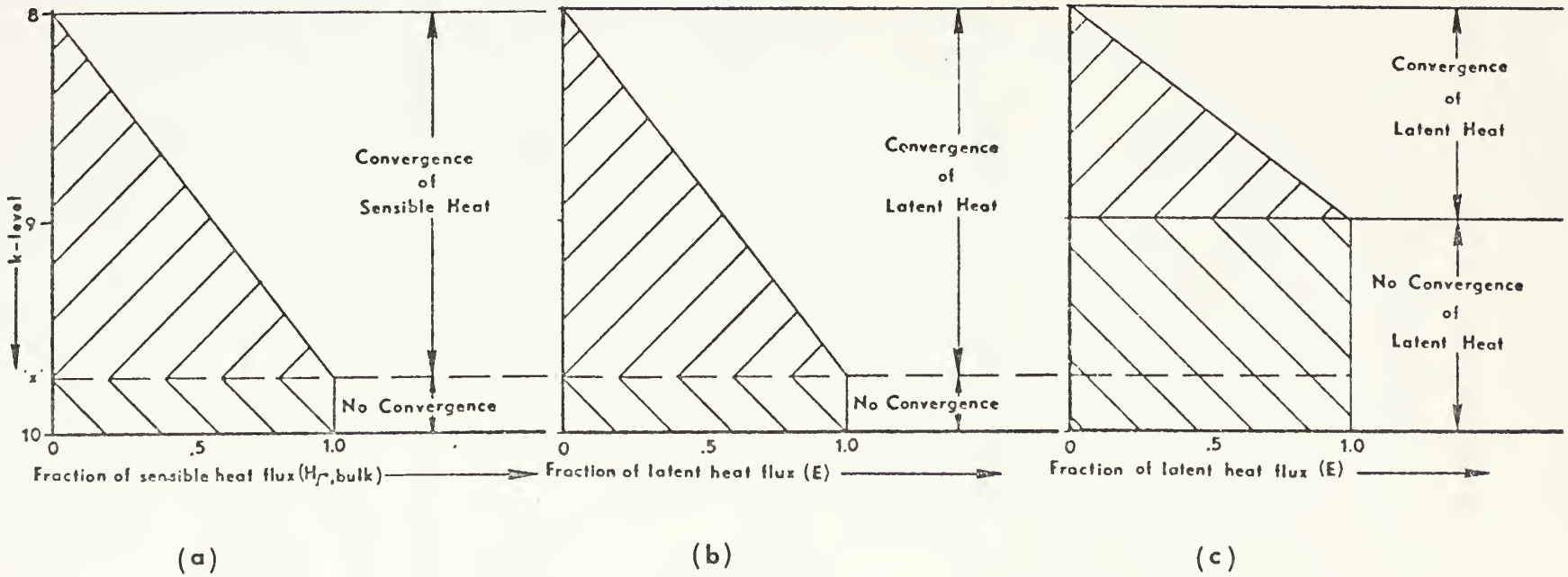


Figure 5. Schematic representation of the distribution of convergence of turbulent fluxes (a) sensible heat flux used in this study, (b) convergence of latent-heat flux used in this study and (c) convergence of latent-heat flux after Kaitala (1974). Note 'x' is the level of the top of the constant flux layer.

realized latent heat may occur at arbitrary levels, i.e., in general at levels higher than k=8. Thus, in following the FNWC model, we have not introduced E as a heating rate at level k=9.

The basis of the turbulent latent heat model adopted is shown in Fig. 5(b), where

$$E_{(900)} = 1/2\ E\ (\text{Bulk}) \tag{5-12}$$

and where the surface layer bulk transfer of latent heat is given by

$$E \equiv E(\text{Bulk}) = L\rho_{10}\ C_D\ V_s\ (q_s - q_x) \tag{5-13}$$

Evaporation at level k=9 may also be computed using

$$E_{(900)} = L\rho_{10}\ \tilde{K}\ \frac{(q_x - q_9)}{(Z_9 - Z_{10})} \tag{5-14}$$

where $\tilde{K}$ is given in Eq. 5-10. In (5-13) and (5-14), L is the latent heat of vaporization.

$$L = 596.73 - .601\ T_{10}$$

in $\text{cal}(\text{gm})^{-1}$. In Eqs. 5-13, 5-14 and 5-15 $q_9$ and $q_x$ are the mixing ratios at the levels k=9 and at x, respectively, whereas $q_s$ is the saturation mixing ratio at the surface temperature $T_g$. The factor 1/2 which appears in the right side of (5-12) reemphasizes the concept of constant latent-heat convergence in the layer (x,8), (cf., Fig. 5(b)).

The solution for $q_x$ is obtained by combining Eqs. (5-12), (5-13), and (5-14) in the form

$$q_x = \frac{C_D\ V_s\ q_{10} + 2\ \frac{\tilde{K}}{\Delta Z}\ q_9}{C_D\ V_s + 2\ \frac{\tilde{K}}{\Delta Z}} \tag{5-15}$$

where $\Delta Z = Z_9 - Z_{10}$ .

Application of Eqs. 5-13 and 5-15 makes possible the computation of E at each gridpoint. As in the case for $T_x$, the factor of $2\tilde{K}$ of Eq. 5-15 was taken to conform to the value $\tilde{K}$ as used by Kaitala (1974) so that the turbulent transport results obtained here will be compatible with those computed operationally by the FNWC primitive equation model. As already noted, this was accomplished in this study by using a value of $2K^* = 2 \times 10^5 cm^2 sec^{-1}$ as equivalent to the K*-value of Kaitala (1974). Thus computation of E by Eqs. 5-13 and 5-15 was equivalent to that using Kaitala's scheme (1974), the only change being that the vertical distribution of E implicit in Fig. 5(b) is slightly different from that of the constancy of E everywhere in the planetary boundary layer, as postulated by Kaitala (1974).

## E. LARGE-SCALE TURBULENT HEAT FLUX ACROSS THE SEA-AIR INTERFACE

The values of $H_\Gamma$ represent the sensible heating rates for the atmospheric layer (8,10) and were computed for each gridpoint along the four meridians. The values of $H_\Gamma$ in general turned out to be large and positive in the Southern Hemisphere reflecting the computed positive values of $T_g - T_x$. In the Northern Hemisphere, $H_\Gamma$ was predominantly negative (cf., Figs. 7,...,10) and therefore contributes negatively to the net atmospheric heat budget in the layer (8,10).

The latent heat term (E) was large and positive relative to $H_\Gamma$ in the Southern Hemisphere and in the latitude band 0-25N. Regardless of localized variations in the sign of $H_\Gamma$, combined values of $E + H_\Gamma$ seemed to give reasonable heating rates in the atmosphere in these latitudes. On the other hand, the combined $E + H_\Gamma$ acts as heat-loss contribution to the troposphere in Northern Hemisphere latitudes $\phi \geq 30N$ and is of

the same sign as the sensible heat-loss contribution (in these latitudes) applied to the layer (8,10).

In those latitudes (Southern Hemisphere and the Trade Wind Belt) where $E + H_{\Gamma}$ acts as a positive contribution to the heat budget of the tropospheric column, it is not specified in this study precisely where the latent heat source E will be realized. The use of the equations of conservation of mass, momentum and of water-vapor mass, would resolve the latter question, but this was considered beyond the scope of the present work.

The turbulent flux computations of Section VI for $H_{\Gamma}$ and E just outlined represent minor modifications of the FNWC turbulent boundary layer model which has been appended to the major concept of this study namely the radiative model. The purpose for inclusion of the E, $H_{\Gamma}$ computations has been primarily for consistency tests, that is, to determine whether net radiative flux at the surface is of the proper magnitude, relative to $E + H_{\Gamma}$.

## VI. MERIDIONAL CROSS-SECTIONAL DEPICTION OF THE HEAT-BALANCE COMPUTATIONS

### A. GENERAL

The general design of this section is to utilize all of the computational concepts discussed in Sections III, IV, and V in the computations for a single time-step in the heating model developed for use in the FNWC prediction model. After testing FF2 and ALB with the corresponding values of Raschke et al (1973), it was decided that only the computations by the 2/3-CL parameterization would be displayed in the meridional cross-sections (Figs. 6,7,8,9,10). The appropriate calculations were performed at each gridpoint of the four meridians used for presentation purposes in this section. However, the same type of computations using the full-CL parameterization were also made, but not presented in this section.

### B. GEOGRAPHICAL REPRESENTATION OF THE HEAT-BALANCE DISTRIBUTION

The FNWC gridpoint processed analyses for 0000GMT, 16 July 1974 were used at the three Pacific cross-sections, while that for 1200GMT, 16 July 1974, were used for the single Atlantic meridian. This was done so that the set of gridpoints was considered to be subject to the actual radiative-transfer calculations involved for these specific times. Figure 6 depicts in symbolic language the key to the computational entries in Figs. 7,8,9 and 10. This symbolic list presents initially the computations made at each gridpoint (I,J) radiative sounding data in the form of Table I(b). The computations proceed from the top of the troposphere to the ocean surface and include the sensible and latent

heat transfers, by the means of the computational procedure of Section V. For purposes of climatological data comparison, Figs. 7,8,9 and 10 were developed by interpolating gridpoint results to whole 5° latitude increments. The interpolation routine to this gridpoint spacing made use of the Lagrangian cubic interpolation scheme (after Spaeth, 1975).

$$Q(I) = Q_1 \frac{(I-2)(I-3)(I-4)}{(1-2)(1-3)(1-4)} + Q_2 \frac{(I-1)(I-3)(I-4)}{(2-1)(2-3)(2-4)}$$

$$+ Q_3 \frac{(I-1)(I-2)(I-4)}{(3-1)(3-2)(3-4)} + Q_4 \frac{(I-1)(I-2)(I-3)}{(4-1)(4-2)(4-3)} \qquad (6\text{-}1)$$

Finally for ease in reconciling the magnitudes of all heat-transfer rates, the time-dependent solar disposition rates have been averaged to 24-hourly rates.

## C. EXPLANATION OF SYMBOLIC TERMS

### 1. Cross-Section at Level k=2 (Fig. 6)

The discussion of all insolation parameters discussed previously in Section IV dealt with the specific time of day that corresponded to the hour angle h for the instantaneous time t under consideration. The incident solar insolation dealt with is then

$$F(S) = S \left(\frac{r}{r_m}\right)^{-2} \text{Cos } z \qquad (6\text{-}2)$$

In order to avoid reference to specific map times t, the instantaneous solar hour-angles were h = 55°, 10°, 35°, and 35°, respectively for cross-sections 1,2,3 and 4, as depicted in Figs. 7,8,9 and 10.

QAVE represents the 24-hour average of F(2) and appears as the first input symbol in Fig. 6. Its value is considered to be more

representative climatologically for the data day under consideration than F(2).

QAVE is derived by the formula

$$QAVE = F(2)\ \frac{\overline{\overline{\overline{\overline{\overline{Cos\ z}}}}}}{Cos\ z} \tag{6-3}$$

where

$$\overline{\overline{\overline{\overline{\overline{Cos\ z}}}}} = [H\sin\phi\ \sin\delta + \cos\phi\ \cos\delta\ \sin H]/\pi \tag{6-4}$$

and

$$H = \arccos[-\tan\phi\ \tan\delta] \tag{6-5}$$

Here $\delta = 21.5°$ is the solar declination for 16 July 1974, and H is the hour angle at local sunset at latitude $\phi$. $\overline{\overline{\overline{\overline{\overline{Cos\ z}}}}}$ in (6-3) is equal to the 24-hour average cosine of the zenith angle, Eq. 4-2. The 24-hour time averaging period yielding QAVE gives heating results consistent in magnitude with the terrestrial-flux divergences, which change only slightly with time of day. This conversion to expected daily-averaged solar disposition quantities is compatible with the determination of a heat budget for the given date (16 July 1974).

Other parameters needed for level k=2 are

$$QREF = REF(t)\ \left(\frac{\overline{\overline{\overline{\overline{\overline{Cos\ z}}}}}}{Cos\ z}\right) \tag{6-6}$$

where

$$REF(t) = F(2)\ -A26\ -A610\ -(IA10+IS10) \tag{6-7}$$

REF(t) is the instantaneous solar reflected insolation at a gridpoint and QREF is its 24-hour average, assuming that the planetary albedo

remains constant for the 24-hour period, although it was calculated for the indicated solar time t. This assumption requires that the cloud amounts computed at the indicated synoptic times are representative of the entire day.

The same principle will be used with regard to all other solar parameters in the conversion from time-dependent values at solar time t to 24-hour averaged values. Superior bars ( $\overline{\ }$ ) are not used in presenting the averaged values shown in the cross-sectional key, Fig. 6. The 24-hour average earth-troposphere system balance, BALT, is computed from

$$BALT = QAVE - (QREF + F_2^*) \qquad (6\text{-}8)$$

for the tropopause level k=2 at the indicated latitude. Net terrestrial fluxes, such as $F_2^*$, were considered to be constant throughout the 24-hour period, a valid assumption if the cloud cover remains quasi-constant for the period.

2. Cross-Section in Layer (2,6)

The following definitions apply for the layer (2,6) as referred to in Fig. 6. All the heat transfers shown in this layer are assumed to be of radiative character only, as in the corresponding version of the FNWC heating model. The averaged radiative cooling rate is given by

$$BAL\ 26 = Q26 - F26 \qquad (6\text{-}9)$$

where F26 = terrestrial cooling rate in layer (2,6)

and Q26 = daily solar absorption in layer (2,6)

is defined relative to A26(t) by a cosine transformation similar to Eq. 6-3.

3. Cross-Section in Layer (6,10)

The 24-hour average radiative cooling in the layer (6,10) is given by

$$BAL\ 610 = Q610 - F610 \tag{6-10}$$

where Q610 is the sum of Q68 and Q810. BAL 68 has been taken as one-half of BAL610. However, the heat balance in the layer (8,10) has been modified for inclusion of $H_\Gamma$, as given by Eq. 5-7.

$$BAL810 = Q810 - F810 + H_\Gamma = BAL68 + H_\Gamma \tag{6-11}$$

Here $H_\Gamma$ is the sensible heat-flux convergence in the layer (8,10). F610 is the sum of F68 and F810, the terrestrial flux losses for the respective layers.

4. Cross-Section at Air-Sea Interface (k=10)

The heat balance at the earth's surface (BALB) is as defined in the following equation

$$BALB = QABG - F_{10}^{*} - (H_\Gamma + E) \tag{6-12}$$

QABG is the 24-hour average insolation absorbed by the surface defined by

$$QABG = QABG(t)\ \overline{(Cos\ z/Cos\ z)} \tag{6-13}$$

$H_\Gamma$ and E were computed, respectively, from Eqs. 5-7 and 5-13 and considered constant for the computational day, 16 July 1974.

D. MERIDIONAL CROSS-SECTIONS OF THE VERTICAL HEAT BALANCE FOR 16 JULY 1974

Figs. 7,8,9 and 10 as previously explained represent the single time step of heating computations for each of the four meridians used in this study. The four figures have been divided into (a) tropical results and (b) mid-to-high-latitude results. While the results depicted in these cross-sections are exhibited as representing daily-averaged values, they are actually based upon heat-computations at the specific map times of 0000GMT and 1200GMT on 16 July 1974. Therefore, for these results to be meaningful as a stepwise part of the heat package subroutine of FNWC, the solar radiative absorption and reflectance terms would have to be recoverable as a function of GMT, i.e.,

$$F(2,t) = QAVE \quad (\text{Cos } z/\overline{\text{Cos } z}) \tag{6-14}$$

$$REF(t) = QREF \quad (\text{Cos } z/\overline{\text{Cos } z}) \tag{6-15}$$

etc. Thus solar disposition terms may then be utilized in connection with the one-hour time stepwise application of the thermodynamic equation of the set of primitive equations used in the FNWC prediction process, for the 2/3-CL parameterization used throughout this section.

The full-CL heat-balance cross-sections were also computed, but have not been presented here for the sake of brevity. However, certain key radiative heating (cooling) rates have been summarized in zonally-averaged form for both cloud parameterizations for the purposes of presenting the mean latitudinal comparisons (Section VII) of the purely radiative heat budget of the FNWC data as it was applicable to 16 July 1974.

| k | | | |
|---|---|---|---|
| | LAT. | | latitude of the gridpoints in 5° increments |
| | a) | QAVE | 24-hour averaged insolation at level k=2 |
| | b) | QREF | Reflected average insolation at level k=2 |
| | c) | $F_2$* | Net Outgoing long-wave flux at level k-2 |
| 2 | d) | BALT | averaged earth-tropospheric gain or loss (a-b-c) |
| | e) | Q26 | averaged solar insolation absorbed by layer (2,6), positive heating |
| | f) | F26 | IR flux loss by layer (2,6) |
| 6 | g) | BAL26 | averaged radiative cooling in layer (2,6) (e-f) |
| | | 2/3 CL(1) | upper layer (4,6) cloud amount |
| | | 2/3 CL(2) | lower layer (8,9) cloud amount |
| | h) | Q68 | averaged solar insolation absorbed by layer (6,8) |
| | i) | F68 | IR flux loss by layer (6,8) |
| | j) | BAL68 | averaged radiative cooling in layer (6,8) (h-i) |
| 8 | | | |
| | k) | Q810 | averaged solar insolation absorbed by layer (8,10) |
| | ℓ) | F810 | IR flux loss by layer (8,10) |
| | m) | $H_\Gamma$ | sensible heat gain in layer (8,10) |
| | n) | BAL810 | averaged heat balance in layer (8,10) (k-ℓ+m) |
| 10 | | | |
| | o) | QABG | averaged solar insolation absorbed by surface |
| | p) | $F_{10}$* | net long-wave flux at earth's surface |
| | q) | $E+H_\Gamma$ | combined heat loss due to evaporative and sensible heat transport |
| | r) | BALB | averaged warming or cooling at earth's surface (o-p-q) |

Figure 6. Key to meridional cross-sections for Figs. 7,...,10. All radiative and turbulent transfer values are in ly $min^{-1}$ for the levels or layers considered. The reduced cloud amounts 2/3 CL(1) and 2/3 CL(2) are given by Eq. (2-5).

| -20.0 | -15.0 | -10.0 | -5.0 | 0.0 | 5.0 | 10.0 | 15.0 | 20.0 | 25.0 |
|---|---|---|---|---|---|---|---|---|---|
| 0.4062 | 0.4465 | 0.4842 | 0.5189 | 0.5504 | 0.5783 | 0.6025 | 0.6227 | 0.6390 | 0.6512 |
| -.1329 | -.1324 | -.1166 | -.1146 | -.1400 | -.1866 | -.2222 | -.2201 | -.1774 | -.1381 |
| 0.3894 | 0.3916 | 0.3967 | 0.3886 | 0.3630 | 0.3451 | 0.3345 | 0.3401 | 0.3652 | 0.3957 |
| -.1161 | -.0775 | -.0291 | 0.0157 | 0.0474 | 0.0466 | 0.0458 | 0.0625 | 0.0953 | 0.1173 |
| 0.0274 | 0.0311 | 0.0334 | 0.0377 | 0.0454 | 0.0523 | 0.0573 | 0.0567 | 0.0484 | 0.0393 |
| 0.0932 | 0.0970 | 0.0972 | 0.0972 | 0.1035 | 0.1118 | 0.1194 | 0.1186 | 0.1064 | 0.1089 |
| -.0658 | -.0660 | -.0639 | -.0596 | -.0582 | -.0595 | -.0621 | -.0619 | -.0581 | -.0697 |
| 0.0 | 0.0 | 0.0 | 0.011 | 0.121 | 0.220 | 0.288 | 0.247 | 0.077 | 0.0 |
| 0.196 | 0.157 | 0.024 | 0.006 | 0.063 | 0.243 | 0.375 | 0.373 | 0.284 | 0.166 |
| 0.0211 | 0.0228 | 0.0218 | 0.0225 | 0.0239 | 0.0281 | 0.0318 | 0.0340 | 0.0358 | 0.0354 |
| 0.0649 | 0.0686 | 0.0654 | 0.0649 | 0.0616 | 0.0611 | 0.0609 | 0.0573 | 0.0846 | 0.0933 |
| -.0438 | -.0458 | -.0436 | -.0424 | -.0377 | -.0330 | -.0290 | -.0333 | -.0488 | -.0579 |
| 0.0211 | 0.0228 | 0.0218 | 0.0225 | 0.0239 | 0.0281 | 0.0318 | 0.0340 | 0.0358 | 0.0354 |
| 0.0649 | 0.0686 | 0.0654 | 0.0649 | 0.0616 | 0.0611 | 0.0609 | 0.0573 | 0.0846 | 0.0933 |
| 0.1477 | 0.0541 | 0.0108 | -.0069 | -.0162 | -.0092 | -.0085 | -.0180 | -.0301 | -.0342 |
| 0.1039 | 0.0083 | -.0328 | -.0493 | -.0540 | -.0422 | -.0376 | -.0513 | -.0788 | -.0921 |
| 0.2036 | 0.2372 | 0.2906 | 0.3215 | 0.3172 | 0.2830 | 0.2592 | 0.2777 | 0.3414 | 0.4028 |
| 0.1664 | 0.1573 | 0.1687 | 0.1615 | 0.1363 | 0.1112 | 0.0933 | 0.0868 | 0.0896 | 0.1002 |
| 0.9019 | 0.5559 | 0.2531 | 0.0965 | 0.0553 | 0.0901 | 0.0790 | -.0009 | -.0640 | -.0698 |
| -.8644 | -.4760 | -.1312 | 0.0635 | 0.1256 | 0.0817 | 0.0868 | 0.1917 | 0.3158 | 0.3724 |

Figure 7(a). 125°W Longitudinal cross-section for tropical latitudes. Refer to Fig. 6 for key. Values computed from data for 16 July 1974 for 2/3-CL case only.

| 30.0 | 35.0 | 40.0 | 45.0 | 50.0 | 55.0 |
|---|---|---|---|---|---|
| 0.6593 | 0.6634 | 0.6638 | 0.6606 | 0.6543 | 0.6545 |
| -.1167 | -.0983 | -.0878 | -.3156 | -.2721 | -.2717 |
| 0.4020 | 0.4038 | 0.3791 | 0.3357 | 0.2947 | 0.2784 |
| 0.1407 | 0.1613 | 0.1969 | 0.0093 | 0.0875 | 0.1043 |
| 0.0355 | 0.0313 | 0.0347 | 0.0363 | 0.0457 | 0.0474 |
| 0.1090 | 0.0982 | 0.0960 | 0.1093 | 0.1143 | 0.1065 |
| -.0734 | -.0669 | -.0613 | -.0730 | -.0684 | -.0591 |
| 0.0 | 0.0 | 0.0 | 0.002 | 0.296 | 0.400 |
| 0.075 | 0.0 | 0.0 | 0.843 | 0.496 | 0.389 |
| 0.0325 | 0.0226 | 0.0144 | 0.0460 | 0.0323 | 0.0272 |
| 0.0930 | 0.0867 | 0.0631 | 0.0818 | 0.0508 | 0.0484 |
| -.0605 | -.0640 | -.0487 | -.0359 | -.0187 | -.0212 |
| 0.0325 | 0.0226 | 0.0144 | 0.0460 | 0.0323 | 0.0272 |
| 0.0930 | 0.0867 | 0.0631 | 0.0818 | 0.0508 | 0.0484 |
| -.0370 | -.0352 | -.0342 | 0.0212 | 0.0044 | -.0123 |
| -.0974 | -.0993 | -.0830 | -.0147 | -.0143 | -.0334 |
| 0.4419 | 0.4384 | 0.5124 | 0.2164 | 0.2716 | 0.2807 |
| 0.1070 | 0.1322 | 0.1569 | 0.0627 | 0.0786 | 0.0752 |
| -.0766 | -.0229 | 0.0241 | 0.1111 | 0.0556 | 0.0107 |
| 0.4114 | 0.3790 | 0.3315 | 0.0427 | 0.1275 | 0.1948 |



Figure 7(b). 125°W Longitudinal cross-section for higher latitudes. Refer to Fig. 6 for key. Values computed from data for 16 July 1974 for 2/3-CL case only.

| 0.0 | 5.0 | 10.0 | 15.0 | 20.0 | 25.0 |
|---|---|---|---|---|---|
| 0.5504 | 0.5783 | 0.6024 | 0.6228 | 0.6390 | 0.6511 |
| -.0953 | -.1019 | -.1047 | -.1537 | -.1632 | -.1469 |
| 0.3865 | 0.3900 | 0.4036 | 0.3933 | 0.4017 | 0.4064 |
| 0.0688 | 0.0864 | 0.0942 | 0.0757 | 0.0740 | 0.0979 |
| 0.0379 | 0.0384 | 0.0359 | 0.0359 | 0.0331 | 0.0316 |
| 0.1039 | 0.1029 | 0.1050 | 0.1133 | 0.1133 | 0.1098 |
| -.0659 | -.0644 | -.0691 | -.0774 | -.0302 | -.0782 |
| 0.053 | 0.033 | 0.0 | 0.0 | 0.0 | 0.0 |
| 0.116 | 0.145 | 0.168 | 0.339 | 0.365 | 0.296 |
| 0.0242 | 0.0265 | 0.0289 | 0.0331 | 0.0380 | 0.0384 |
| 0.0711 | 0.0748 | 0.0809 | 0.0753 | 0.0815 | 0.0833 |
| -.0472 | -.0483 | -.0520 | -.0422 | -.0435 | -.0449 |
| 0.0242 | 0.0265 | 0.0289 | 0.0331 | 0.0380 | 0.0384 |
| 0.0711 | 0.0748 | 0.0809 | 0.0753 | 0.0815 | 0.0833 |
| -.0089 | -.0093 | -.0120 | 0.0335 | 0.0337 | 0.0287 |
| -.0561 | -.0576 | -.0640 | -.0087 | -.0093 | -.0162 |
| 0.3690 | 0.3850 | 0.4041 | 0.3668 | 0.3666 | 0.3957 |
| 0.1402 | 0.1376 | 0.1369 | 0.1293 | 0.1255 | 0.1300 |
| 0.1027 | 0.1044 | 0.0726 | 0.3894 | 0.3821 | 0.3545 |
| 0.1259 | 0.1429 | 0.1946 | -.1519 | -.1410 | -.0839 |

Figure 8(a). 170°W Longitudinal cross-section for tropical latitudes. Refer to Fig. 6 for key. Values computed from data for 16 July 1974 for 2/3-CL case only.

| 30.0 | 35.0 | 40.0 | 45.0 | 50.0 | 55.0 | 60.0 | 65.0 |
|---|---|---|---|---|---|---|---|
| 0.6593 | 0.6634 | 0.6638 | 0.6606 | 0.6544 | 0.6460 | 0.6371 | 0.6308 |
| -.1356 | -.1448 | -.1483 | -.1205 | -.2167 | -.3743 | -.1914 | -.2125 |
| 0.4053 | 0.3901 | 0.3576 | 0.3706 | 0.3413 | 0.2303 | 0.3121 | 0.2194 |
| 0.1185 | 0.1285 | 0.1578 | 0.1695 | 0.0964 | 0.0414 | 0.1336 | 0.1990 |
| 0.0332 | 0.0371 | 0.0441 | 0.0360 | 0.0358 | 0.0637 | 0.0395 | 0.0645 |
| 0.1106 | 0.1097 | 0.1117 | 0.1132 | 0.1160 | 0.1352 | 0.1092 | 0.1059 |
| -.0774 | -.0726 | -.0676 | -.0772 | -.0802 | -.0715 | -.0698 | -.0414 |
| 0.0 | 0.0 | 0.069 | 0.0 | 0.022 | 0.629 | 0.189 | 0.569 |
| 0.247 | 0.280 | 0.236 | 0.184 | 0.514 | 0.914 | 0.375 | 0.049 |
| 0.0365 | 0.0371 | 0.0341 | 0.0335 | 0.0404 | 0.0327 | 0.0251 | 0.0144 |
| 0.0837 | 0.0871 | 0.0873 | 0.0952 | 0.0901 | 0.0402 | 0.0619 | 0.0261 |
| -.0472 | -.0500 | -.0532 | -.0618 | -.0497 | -.0074 | -.0369 | -.0118 |
| 0.0365 | 0.0371 | 0.0341 | 0.0335 | 0.0404 | 0.0327 | 0.0251 | 0.0144 |
| 0.0837 | 0.0871 | 0.0873 | 0.0952 | 0.0901 | 0.0402 | 0.0619 | 0.0261 |
| 0.0004 | -.0173 | -.0409 | -.0416 | -.0335 | -.0214 | -.0230 | -.0338 |
| -.0467 | -.0572 | -.0941 | -.1035 | -.0831 | -.0289 | -.0599 | -.0456 |
| 0.4174 | 0.4072 | 0.4028 | 0.4369 | 0.3210 | 0.1425 | 0.3560 | 0.3250 |
| 0.1273 | 0.1064 | 0.0712 | 0.0668 | 0.0453 | 0.0147 | 0.0790 | 0.0613 |
| 0.1478 | 0.0223 | -.1244 | -.0851 | -.0622 | -.0378 | -.0211 | -.0303 |
| 0.1422 | 0.2785 | 0.4560 | 0.4553 | 0.3378 | 0.1655 | 0.2981 | 0.2941 |

Figure 8(b). 170°W Longitudinal cross-section for higher latitudes. Refer to Fig. 6 for key. Values computed from data for 16 July 1974 for 2/3-CL case only.

| -5.0 | 0.0 | 5.0 | 10.0 | 15.0 | 20.0 | 25.0 |
|---|---|---|---|---|---|---|
| 0.5193 | 0.5504 | 0.5783 | 0.6025 | 0.6227 | 0.6390 | 0.6512 |
| -.1841 | -.2242 | -.2645 | -.2234 | -.2216 | -.2387 | -.2254 |
| 0.3531 | 0.3316 | 0.3178 | 0.3656 | 0.3935 | 0.3991 | 0.3855 |
| -.0176 | -.0055 | -.0040 | 0.0135 | 0.0076 | 0.0011 | 0.0403 |
| 0.0458 | 0.0536 | 0.0590 | 0.0465 | 0.0401 | 0.0423 | 0.0471 |
| 0.1231 | 0.1282 | 0.1328 | 0.1200 | 0.1203 | 0.1187 | 0.1240 |
| -.0772 | -.0746 | -.0739 | -.0734 | -.0802 | -.0764 | -.0770 |
| 0.232 | 0.336 | 0.406 | 0.123 | 0.0 | 0.0 | 0.019 |
| 0.454 | 0.553 | 0.667 | 0.579 | 0.602 | 0.654 | 0.574 |
| 0.0304 | 0.0316 | 0.0327 | 0.0382 | 0.0437 | 0.0474 | 0.0440 |
| 0.0774 | 0.0685 | 0.0632 | 0.0793 | 0.0929 | 0.1074 | 0.0925 |
| -.0470 | -.0369 | -.0305 | -.0410 | -.0492 | -.0599 | -.0485 |
| 0.0304 | 0.0316 | 0.0327 | 0.0382 | 0.0437 | 0.0474 | 0.0440 |
| 0.0744 | 0.0685 | 0.0632 | 0.0793 | 0.0929 | 0.1074 | 0.0925 |
| -.0201 | -.0106 | -.0098 | 0.0057 | 0.0047 | -.0129 | -.0098 |
| -.0671 | -.0475 | -.0404 | -.0352 | -.0445 | -.0728 | -.0584 |
| 0.2272 | 0.2094 | 0.1892 | 0.2558 | 0.2735 | 0.2629 | 0.2906 |
| 0.0743 | 0.0665 | 0.0585 | 0.0870 | 0.0873 | 0.0657 | 0.0764 |
| 0.0059 | 0.0407 | 0.0296 | 0.1514 | 0.1405 | 0.0175 | 0.0467 |
| 0.1470 | 0.1020 | 0.1011 | 0.0173 | 0.0457 | 0.1797 | 0.1674 |



Figure 9(a). 145°E Longitudinal cross-section for tropical latitudes. Refer to Fig. 6 for key. Values computed from data for 16 July 1974 for 2/3-CL case only.

| 30.0 | 35.0 | 40.0 | 45.0 | 50.0 | 55.0 |
|---|---|---|---|---|---|
| 0.6593 | 0.6634 | 0.6638 | 0.6606 | 0.6544 | 0.6460 |
| -.3017 | -.2741 | -.2943 | -.3234 | -.1030 | -.3392 |
| 0.3177 | 0.3479 | 0.3155 | 0.3134 | 0.3197 | 0.1899 |
| 0.0399 | 0.0414 | 0.0540 | 0.0237 | 0.2316 | 0.1170 |
| 0.0673 | 0.0547 | 0.0529 | 0.0414 | 0.0391 | 0.0855 |
| 0.1419 | 0.1291 | 0.1209 | 0.1039 | 0.1020 | 0.1225 |
| -.0745 | -.0744 | -.0680 | -.0625 | -.0629 | -.0370 |
| 0.362 | 0.155 | 0.231 | 0.113 | 0.080 | 0.914 |
| 0.698 | 0.683 | 0.707 | 0.857 | 0.020 | 0.377 |
| 0.0377 | 0.0443 | 0.0408 | 0.0455 | 0.0210 | 0.0196 |
| 0.0651 | 0.0890 | 0.0811 | 0.0843 | 0.0639 | 0.0244 |
| -.0274 | -.0447 | -.0404 | -.0379 | -.0429 | -.0048 |
| 0.0377 | 0.0443 | 0.0408 | 0.0455 | 0.0210 | 0.0196 |
| 0.0651 | 0.0890 | 0.0811 | 0.0843 | 0.0639 | 0.0244 |
| -.0212 | -.0286 | -.0296 | 0.0017 | -.0337 | -.0303 |
| -.0485 | -.0733 | -.0699 | -.0370 | -.0766 | -.0351 |
| 0.2146 | 0.2459 | 0.2349 | 0.2045 | 0.4702 | 0.1821 |
| 0.0457 | 0.0408 | 0.0322 | 0.0455 | 0.0901 | 0.0189 |
| -.1139 | -.1293 | -.0835 | 0.0315 | -.0368 | -.0462 |
| 0.2828 | 0.3343 | 0.2860 | 0.1319 | 0.4170 | 0.2097 |



Figure 9(b). 145°E Longitudinal cross-section for higher latitudes. Refer to Fig. 6 for key. Values computed from data for 16 July 1974 for 2/3-CL case only.

| -20.0 | -15.0 | -10.0 | -5.0 | 0.0 | 5.0 | 10.0 | 15.0 | 20.0 | 25.0 |
|---|---|---|---|---|---|---|---|---|---|
| 0.4062 | 0.4465 | 0.4842 | 0.5189 | 0.5504 | 0.5783 | 0.6025 | 0.6227 | 0.6390 | 0.6512 |
| -.1180 | -.1434 | -.1542 | -.2471 | -.2215 | -.2264 | -.1822 | -.1352 | -.1684 | -.1913 |
| 0.3745 | 0.3888 | 0.4101 | 0.4104 | 0.3846 | 0.3621 | 0.3655 | 0.3795 | 0.3914 | 0.3852 |
| -.0864 | -.0858 | -.0802 | -.1386 | -.0557 | -.0102 | 0.0547 | 0.1080 | 0.0792 | 0.0746 |
| 0.0265 | 0.0275 | 0.0247 | 0.0266 | 0.0364 | 0.0439 | 0.0449 | 0.0418 | 0.0381 | 0.0396 |
| 0.0997 | 0.1035 | 0.1057 | 0.1107 | 0.1082 | 0.1151 | 0.1121 | 0.1057 | 0.1059 | 0.1065 |
| -.0732 | -.0761 | -.0809 | -.0841 | -.0718 | -.0712 | -.0672 | -.0639 | -.0678 | -.0670 |
| 0.030 | 0.0 | 0.0 | 0.0 | 0.005 | 0.127 | 0.116 | 0.040 | 0.0 | 0.0 |
| 0.319 | 0.455 | 0.491 | 0.902 | 0.722 | 0.629 | 0.392 | 0.228 | 0.376 | 0.452 |
| 0.0218 | 0.0282 | 0.0356 | 0.0470 | 0.0430 | 0.0390 | 0.0344 | 0.0320 | 0.0389 | 0.0422 |
| 0.0698 | 0.0886 | 0.1020 | 0.1275 | 0.1070 | 0.0881 | 0.0810 | 0.0821 | 0.0951 | 0.0962 |
| -.0479 | -.0603 | -.0664 | -.0805 | -.0640 | -.0491 | -.0466 | -.0501 | -.0562 | -.0540 |
| 0.0218 | 0.0282 | 0.0356 | 0.0470 | 0.0430 | 0.0390 | 0.0344 | 0.0320 | 0.0389 | 0.0422 |
| 0.0698 | 0.0886 | 0.1020 | 0.1275 | 0.1070 | 0.0881 | 0.0810 | 0.0821 | 0.0951 | 0.0962 |
| 0.0620 | 0.0134 | 0.0056 | -.0026 | -.0074 | -.0090 | -.0193 | -.0231 | -.0214 | -.0166 |
| 0.0143 | -.0470 | -.0598 | -.0831 | -.0714 | -.0581 | -.0659 | -.0731 | -.0777 | -.0706 |
| 0.2179 | 0.2191 | 0.2339 | 0.1511 | 0.2065 | 0.2300 | 0.3063 | 0.3815 | 0.3546 | 0.3358 |
| 0.1355 | 0.1083 | 0.1004 | 0.0447 | 0.0626 | 0.0708 | 0.0913 | 0.1096 | 0.0954 | 0.0863 |
| 0.5070 | 0.2010 | 0.1497 | -.0206 | 0.0392 | 0.0126 | -.0355 | -.0107 | -.0311 | 0.0093 |
| -.4246 | -.0902 | -.0163 | 0.1270 | 0.1047 | 0.1465 | 0.2504 | 0.2826 | 0.2904 | 0.2402 |

Figure 10(a). 35°W Longitudinal cross-section for tropical latitudes. Refer to Fig. 6 for key. Values computed from data for 16 July 1974 for 2/3-CL case only.

| 30.0 | 35.0 | 40.0 | 45.0 | 50.0 | 55.0 | 60.0 |
|---|---|---|---|---|---|---|
| 0.6593 | 0.6634 | 0.6638 | 0.6606 | 0.6544 | 0.6460 | 0.6370 |
| -.1928 | -.1993 | -.1808 | -.1777 | -.2505 | -.2654 | -.1909 |
| 0.3874 | 0.3881 | 0.3901 | 0.3286 | 0.2347 | 0.2178 | 0.2591 |
| 0.0791 | 0.0760 | 0.0928 | 0.1542 | 0.1591 | 0.1629 | 0.1871 |
| 0.0392 | 0.0374 | 0.0364 | 0.0514 | 0.0752 | 0.0767 | 0.0547 |
| 0.1098 | 0.1089 | 0.1117 | 0.1151 | 0.1231 | 0.1259 | 0.1087 |
| -.0705 | -.0715 | -.0754 | -.0637 | -.0479 | -.0492 | -.0540 |
| 0.0 | 0.0 | 0.0 | 0.187 | 0.670 | 0.770 | 0.449 |
| 0.451 | 0.468 | 0.404 | 0.239 | 0.106 | 0.072 | 0.037 |
| 0.0436 | 0.0445 | 0.0420 | 0.0307 | 0.0188 | 0.0160 | 0.0160 |
| 0.0951 | 0.0946 | 0.0971 | 0.0752 | 0.0363 | 0.0265 | 0.0295 |
| -.0515 | -.0500 | -.0551 | -.0445 | -.0173 | -.0106 | -.0135 |
| 0.0436 | 0.0445 | 0.0420 | 0.0307 | 0.0188 | 0.0160 | 0.0160 |
| 0.0951 | 0.0946 | 0.0971 | 0.0752 | 0.0363 | 0.0265 | 0.0295 |
| -.0154 | -.0075 | -.0138 | -.0365 | -.0436 | -.0406 | -.0167 |
| -.0670 | -.0576 | -.0689 | -.0810 | -.0611 | -.0512 | -.0302 |
| 0.3399 | 0.3375 | 0.3623 | 0.3698 | 0.2907 | 0.2719 | 0.3594 |
| 0.0873 | 0.0901 | 0.0841 | 0.0631 | 0.0392 | 0.0388 | 0.0915 |
| 0.0161 | 0.0580 | 0.0195 | -.0764 | -.1040 | -.0699 | 0.0028 |
| 0.2365 | 0.1894 | 0.2586 | 0.3831 | 0.3556 | 0.3030 | 0.2650 |

Figure 10(b). 35°W Longitudinal cross-section for higher latitudes. Refer to Fig. 6 for key. Values computed from data for 16 July 1974 for 2/3-CL case only.

## VII. THE LATITUDINAL DISTRIBUTION OF RADIATIONAL BALANCE TERMS OF THE OCEAN-ATMOSPHERE SYSTEM

### A. GENERAL

The latitudinally distributed results of the purely radiative contributions, over the ocean-atmosphere system, are presented in Figs. 12(a,b) for the 2/3-CL and 13(a,b) for the full-CL cases, respectively. These cross-sections show the results after averaging over the four meridians considered in this study. The results are displayed in the format of Fig. 11. Radiative transfers Q68 and Q810 have been combined with F68 and F810 of Fig. 6 to compute layer-average radiational warming rates in the layer (6,10). The turbulent transfer heating rates $E + H_T$ to the atmosphere (and the corresponding cooling rates in the ocean) which were included in the results of Figs. 7,8,9, and 10 are now omitted in the radiative composites presented in Figs. 12 and 13.

In obtaining latitudinally-distributed means of radiative heating rates at each five-degree multiple of latitude $\phi$, all values of each radiative parameter listed in Figs. 12 and 13 at latitude $\phi$ in the range 20S,...,65N (5 degree increments) were simply averaged over the four meridians providing the zonally-averaged value at $\phi$. At $\phi$ = 65N there was only one contribution to the latitudinal average, while in the Southern Hemisphere latitudes 20, 15 and 10S, only two values (on $\lambda$ = 125W and $\lambda$ = 35W) of each parameter contributed to the means listed in Figs. 12 and 13. At 5S, there were three sets of radiative parameters entering into $\overline{Q(\phi)}$. Otherwise, there were four values of each radiative

parameter entering into the computed radiative mean values $\overline{Q(\phi)}$ of the cross-sections. Therefore, near the northern and southern boundaries of Figs. 12 and 13, the listed values may not be equally representative, although the general trend should be reliable. Fig. 14, using data extracted from Figs. 12 and 13, tends to confirm this statement.

Figs. 12, 13 and 14 are also useful in determining the relative merits of the 2/3-CL model as compared to the full-CL model.

B. EARTH-TROPOSPHERE SYSTEM RADIATIONAL BALANCE SUMMARY

The latitudinally averaged distributions of the three key radiative parameters, $R_s$, $R_a$ and R as functions of latitude for both the 2/3-CL and full-CL cases are shown in Fig. 14. The radiative-balance parameters were defined (after Malkus, 1962) as $R_s(\phi)$, the mean radiative-energy transfer rate across the top of the ocean-tropospheric system at k=2 (referred to as BALT in Fig. 11); $R_a(\phi)$, the meridional mean radiative cooling rate in the troposphere (BAL26 + BAL610 in Fig. 11); and $R(\phi)$, the mean radiative warming (cooling) rate at the earth surface (BAL10 in Fig. 11). The relationship between these radiative parameters is

$$R_s = R_a + R \tag{7-1}$$

The 16 July portion of Tables X, XI and XII list the zonally-averaged values of $R_s$, R and $R_a$ as a function of latitude $\phi$ for the 2/3-CL and

the full-CL cases. Weighted averages for any Q-value are then computed using the following cosine weighting scheme (Eq. 7-2, Spaeth, 1975)

$$Q_{\text{Wt. Avg.}} = \frac{\sum_{i=1}^{18} \frac{k_i}{4} \left( \sum_{j=1}^{4} \frac{Q_{ji}}{k_i} \right) \text{Cos } \phi_i}{\sum_{i=1}^{18} \frac{k_i}{4} \text{ Cos } \phi_i} \qquad (7\text{-}2)$$

where $Q_{ji}$ = value on meridian j at latitude $\phi_i$ and $k_i$ is the number k=1, ...,4 of meridional observations available for the meridional averages at $\phi_i$. Note that i=1,...,18 corresponds to the 18 latitudes $\phi_i$= -20., ...,65. degrees. Tables X, XI, and XII also depict the comparative cross-seasonal values of $R_s$, R, and $R_a$ by latitudes for both 2/3-CL and full-CL parameterizations for 16 April 1974, 16 July 1974, and 16 October 1973, respectively.

In Fig. 14, the net-flux terms across the interfaces k=2 and k=10 are $R_s(\phi)$ and $R(\phi)$. At k=2 net-flux values obtained from the 2/3-CL model (denoted $R_{s1}$) exceed those by the full-CL model ($R_{s2}$) at all latitudes. There is a localized maximum value of both $R_{s1}$ and $R_{s2}$ in the latitude zone 40 to 50N, with localized minima at latitudes 45 and 55N. Table IX indicates the existence of maximum CL at these two latitudes (45 and 55N) suggestive of polar frontal-zone cloudiness and higher than normal global albedo. The peak hemispheric values of $R_{s1}$ and $R_{s2}$ then occur finally at latitudes 65N in this study. If computational data extended further poleward, the overall maximum $R_s$ could possibly occur at latitudes higher than 65N, in view of the high declination of the sun on 16 July 1974. The same general pattern in the zonal mean radiative balance $R(\phi)$ at sea-level exists for both the 2/3-CL and full-CL

| k | LAT | | latitude of the gridpoints in 5° increments |
|---|---|---|---|
| | a) | QAVE | 24-hour averaged mean insolation at level k=2 |
| | b) | QREF | mean reflected average insolation at level k=2 |
| | c) | $F_2^*$ | mean net outgoing long-wave flux at level k=2 |
| 2 | d) | BALT | mean averaged earth tropospheric gain rate (a-b-c) |
| | e) | Q26 | mean averaged solar insolation absorbed by layer (2,6) |
| | f) | F26 | mean IR flux loss by layer (2,6) |
| | g) | BAL26 | mean averaged radiative cooling rate, layer (2,6) (e-f) |
| | | $(CL_1)$ | upper layer (2,6) cloud amount |
| | | $(CL_2)$ | lower layer (8,9) cloud amount |
| 6 | | | |
| | h) | Q610 | mean averaged solar insolation absorbed by layer (6,10) |
| | i) | F610 | mean IR flux loss by layer (6,10) |
| | j) | BAL610 | mean averaged radiative cooling rate, layer (6,10) (h-i) |
| 10 | | | |
| | k) | QABG | mean averaged solar insolation absorbed by surface |
| | ℓ) | $F_{10}^*$ | mean net long-wave flux at earth's surface |
| | m) | BAL10 | mean averaged radiational warming (cooling) rate at earth's surface (k-ℓ) |

Figure 11. Key to latitudinal distribution of radiational cross-section for Figs. 12 and 13. All radiational values have been averaged over a 24-hour day and are expressed in ly $min^{-1}$ for the levels or layers considered. The values are averages taken over the meridians (125°W, 170°W, 145°E, and 35°W) used in this study. The cloud-amounts (in parentheses) are by the 2/3-cloud model in Fig. 12 and by the full-CL model in Fig. 13.

| -20.0 | -15.0 | -10.0 | -5.0 | 0.0 | 5.0 | 10.0 | 15.0 | 20.0 | 25.0 |
|---|---|---|---|---|---|---|---|---|---|
| 0.4062 | 0.4465 | 0.4842 | 0.5191 | 0.5504 | 0.5783 | 0.6025 | 0.6227 | 0.6390 | 0.6512 |
| -.1254 | -.1379 | -.1354 | -.1819 | -.1702 | -.1949 | -.1831 | -.1827 | -.1869 | -.1754 |
| 0.3820 | 0.3902 | 0.4034 | 0.3840 | 0.3664 | 0.3537 | 0.3673 | 0.3766 | 0.3894 | 0.3932 |
| -.1012 | -.0817 | -.0546 | -.0468 | 0.0138 | 0.0297 | 0.0521 | 0.0635 | 0.0627 | 0.0825 |
| 0.0269 | 0.0293 | 0.0291 | 0.0367 | 0.0433 | 0.0484 | 0.0462 | 0.0436 | 0.0405 | 0.0394 |
| 0.0964 | 0.1003 | 0.1015 | 0.1104 | 0.1109 | 0.1156 | 0.1141 | 0.1145 | 0.1111 | 0.1123 |
| -.0695 | -.0710 | -.0724 | -.0736 | -.0676 | -.0672 | -.0679 | -.0708 | -.0706 | -.0730 |
| 0.015 | 0.0 | 0.0 | 0.081 | 0.128 | 0.196 | 0.131 | 0.072 | 0.019 | 0.005 |
| 0.258 | 0.306 | 0.258 | 0.454 | 0.364 | 0.421 | 0.379 | 0.336 | 0.420 | 0.372 |
| 0.0429 | 0.0510 | 0.0574 | 0.0666 | 0.0613 | 0.0631 | 0.0667 | 0.0714 | 0.0800 | 0.0800 |
| 0.1347 | 0.1572 | 0.1674 | 0.1799 | 0.1541 | 0.1436 | 0.1510 | 0.1588 | 0.1843 | 0.1826 |
| -.0918 | -.1062 | -.1100 | -.1133 | -.0928 | -.0804 | -.0843 | -.0874 | -.1043 | -.1026 |
| 0.2107 | 0.2282 | 0.2622 | 0.2333 | 0.2755 | 0.2718 | 0.3063 | 0.3249 | 0.3314 | 0.3562 |
| 0.1509 | 0.1328 | 0.1346 | 0.0935 | 0.1014 | 0.0945 | 0.1022 | 0.1033 | 0.0941 | 0.0983 |
| 0.0598 | 0.0954 | 0.1277 | 0.1597 | 0.1741 | 0.1773 | 0.2042 | 0.2216 | 0.2373 | 0.2580 |

Figure 12(a). Zonally-averaged radiational cross-section for tropical latitudes with 2/3-CL model. Refer to Fig. 11 for key. All values listed are daily averages in ly $min^{-1}$ and are computed from data for 16 July 1974.

| 30.0 | 35.0 | 40.0 | 45.0 | 50.0 | 55.0 | 60.0 | 65.0 |
|---|---|---|---|---|---|---|---|
| 0.6593 | 0.6634 | 0.6638 | 0.6606 | 0.6544 | 0.6481 | 0.6371 | 0.6308 |
| -.1867 | -.1791 | -.1778 | -.2343 | -.2106 | -.3127 | -.1911 | -.2123 |
| 0.3781 | 0.3825 | 0.3606 | 0.3371 | 0.2976 | 0.2291 | 0.2856 | 0.2194 |
| 0.0945 | 0.1018 | 0.1254 | 0.0892 | 0.1462 | 0.1064 | 0.1603 | 0.1990 |
| 0.0438 | 0.0401 | 0.0420 | 0.0413 | 0.0490 | 0.0683 | 0.0471 | 0.0645 |
| 0.1178 | 0.1115 | 0.1101 | 0.1104 | 0.1138 | 0.1225 | 0.1090 | 0.1059 |
| -.0740 | -.0713 | -.0681 | -.0691 | -.0648 | -.0542 | -.0619 | -.0414 |
| 0.091 | 0.039 | 0.075 | 0.075 | 0.267 | 0.678 | 0.319 | 0.569 |
| 0.367 | 0.358 | 0.337 | 0.531 | 0.284 | 0.438 | 0.206 | 0.049 |
| 0.0752 | 0.0743 | 0.0657 | 0.0779 | 0.0563 | 0.0478 | 0.0410 | 0.0288 |
| 0.1685 | 0.1787 | 0.1643 | 0.1683 | 0.1206 | 0.0697 | 0.0914 | 0.0522 |
| -.0933 | -.1044 | -.0986 | -.0904 | -.0643 | -.0220 | -.0504 | -.0234 |
| 0.3534 | 0.3698 | 0.3781 | 0.3069 | 0.3384 | 0.2193 | 0.3577 | 0.3250 |
| 0.0918 | 0.0924 | 0.0861 | 0.0595 | 0.0633 | 0.0369 | 0.0852 | 0.0613 |
| 0.2616 | 0.2774 | 0.2920 | 0.2474 | 0.2751 | 0.1824 | 0.2724 | 0.2637 |

Figure 12(b). Zonally-averaged radiational cross-section for mid to high latitudes with 2/3-CL model. Refer to Fig. 11 for key. All values listed are daily averages in ly $min^{-1}$ and are from data for 16 July 1974.

| -20.0 | -15.0 | -10.0 | -5.0 | 0.0 | 5.0 | 10.0 | 15.0 | 20.0 | 25.0 |
|---|---|---|---|---|---|---|---|---|---|
| 0.4062 | 0.4465 | 0.4842 | 0.5191 | 0.5504 | 0.5783 | 0.6025 | 0.6227 | 0.6390 | 0.6512 |
| -.1418 | -.1615 | -.1614 | -.2068 | -.2086 | -.2435 | -.2307 | -.2330 | -.2410 | -.2236 |
| 0.3768 | 0.3860 | 0.4000 | 0.3780 | 0.3572 | 0.3410 | 0.3572 | 0.3687 | 0.3845 | 0.3895 |
| -.1124 | -.1010 | -.0772 | -.0656 | -.0154 | -.0062 | 0.0145 | 0.0211 | 0.0136 | 0.0380 |
| 0.0272 | 0.0294 | 0.0291 | 0.0375 | 0.0449 | 0.0509 | 0.0480 | 0.0448 | 0.0409 | 0.0396 |
| 0.0975 | 0.1005 | 0.1016 | 0.1145 | 0.1175 | 0.1261 | 0.1210 | 0.1182 | 0.1122 | 0.1128 |
| -.0702 | -.0711 | -.0725 | -.0768 | -.0726 | -.0752 | -.0730 | -.0734 | -.0712 | -.0731 |
| 0.022 | 0.0 | 0.0 | 0.121 | 0.193 | 0.295 | 0.197 | 0.108 | 0.029 | 0.007 |
| 0.384 | 0.456 | 0.396 | 0.563 | 0.523 | 0.627 | 0.565 | 0.576 | 0.627 | 0.556 |
| 0.0469 | 0.0561 | 0.0627 | 0.0690 | 0.0650 | 0.0667 | 0.0721 | 0.0791 | 0.0903 | 0.0897 |
| 0.1438 | 0.1713 | 0.1809 | 0.1834 | 0.1587 | 0.1442 | 0.1572 | 0.1714 | 0.2044 | 0.2012 |
| -.0969 | -.1152 | -.1181 | -.1144 | -.0937 | -.0775 | -.0852 | -.0923 | -.1141 | -.1115 |
| 0.1901 | 0.1993 | 0.2309 | 0.2052 | 0.2319 | 0.2170 | 0.2516 | 0.2657 | 0.2666 | 0.2980 |
| 0.1355 | 0.1141 | 0.1175 | 0.0798 | 0.0811 | 0.0707 | 0.0790 | 0.0791 | 0.0679 | 0.0755 |
| 0.0547 | 0.0852 | 0.1134 | 0.1255 | 0.1508 | 0.1464 | 0.1725 | 0.1866 | 0.1987 | 0.2225 |

Figure 13(a). Similar to Fig. 11(a) except full-CL model (after Smagorinsky, Eq. 2-4) is used in all radiative calculations.

| 30.0 | 35.0 | 40.0 | 45.0 | 50.0 | 55.0 | 60.0 | 65.0 |
|---|---|---|---|---|---|---|---|
| 0.6593 | 0.6634 | 0.6638 | 0.6606 | 0.6544 | 0.6481 | 0.6371 | 0.6308 |
| -.2313 | -.2243 | -.2191 | -.2668 | -.2663 | -.3615 | -.2363 | -.2714 |
| 0.3720 | 0.3785 | 0.3559 | 0.3326 | 0.2843 | 0.2101 | 0.2693 | 0.1955 |
| 0.0560 | 0.0607 | 0.0888 | 0.0612 | 0.1038 | 0.0766 | 0.1315 | 0.1640 |
| 0.0452 | 0.0408 | 0.0433 | 0.0426 | 0.0531 | 0.0754 | 0.0530 | 0.0738 |
| 0.1230 | 0.1137 | 0.1135 | 0.1139 | 0.1246 | 0.1392 | 0.1212 | 0.1264 |
| -.0777 | -.0728 | -.0702 | -.0713 | -.0714 | -.0639 | -.0681 | -.0525 |
| 0.136 | 0.058 | 0.113 | 0.113 | 0.396 | 0.884 | 0.499 | 0.854 |
| 0.538 | 0.528 | 0.488 | 0.629 | 0.424 | 0.552 | 0.271 | 0.055 |
| 0.0812 | 0.0823 | 0.0719 | 0.0822 | 0.0601 | 0.0441 | 0.0394 | 0.0248 |
| 0.1762 | 0.1919 | 0.1727 | 0.1722 | 0.1164 | 0.0486 | 0.0759 | 0.0240 |
| -.0950 | -.1096 | -.1009 | -.0899 | -.0563 | -.0045 | -.0365 | 0.0008 |
| 0.3014 | 0.3159 | 0.3294 | 0.2688 | 0.2747 | 0.1670 | 0.3083 | 0.2507 |
| 0.0729 | 0.0730 | 0.0697 | 0.0465 | 0.0434 | 0.0223 | 0.0724 | 0.0453 |
| 0.2286 | 0.2429 | 0.2598 | 0.2224 | 0.2313 | 0.1447 | 0.2359 | 0.2154 |

Figure 13(b). Similar to Fig. 11(b) except full-CL model (after Smagorinsky, Eq. 2-4) is used in all radiative calculations.

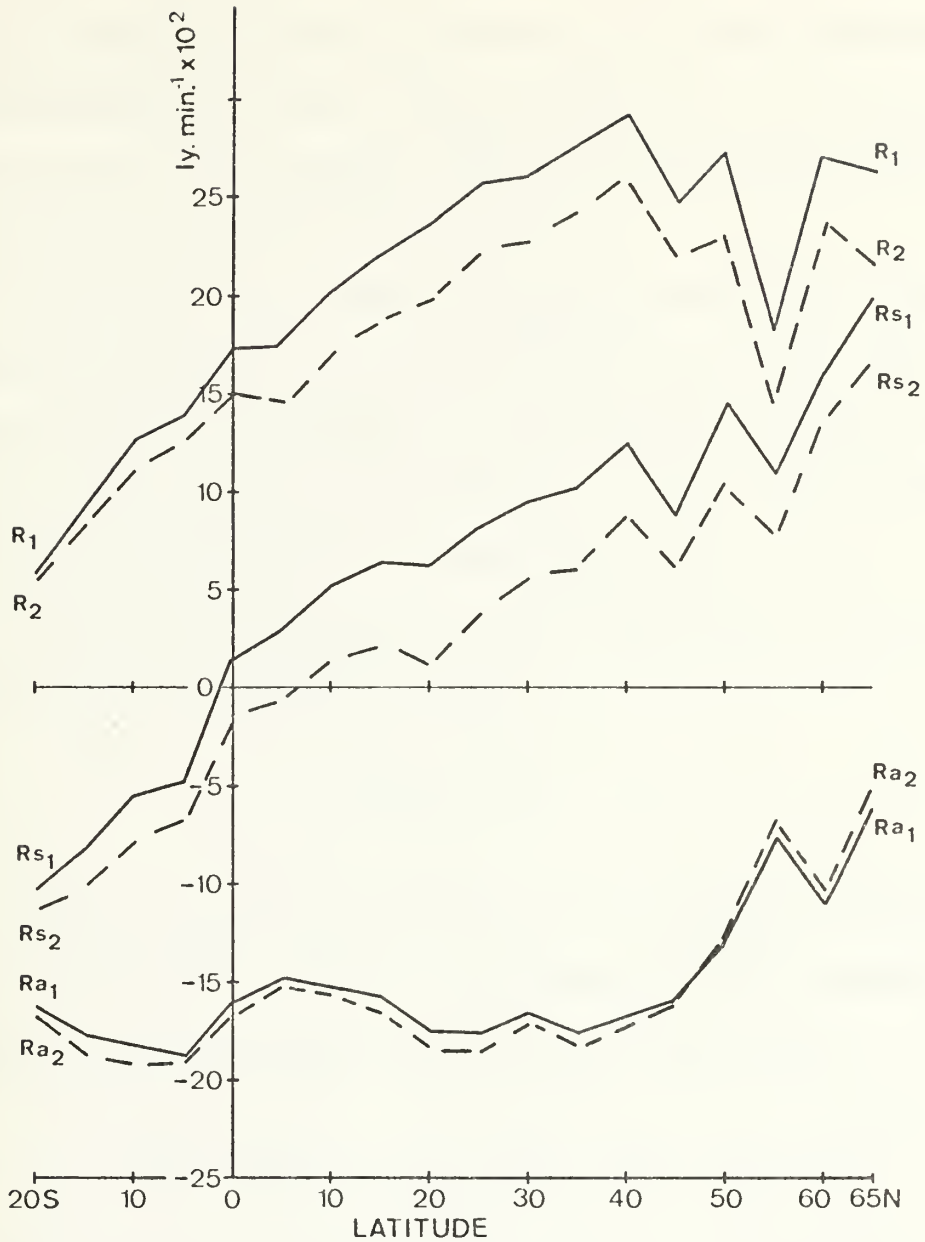


Figure 14. Radiational balance at the tropopause ($R_s$), at the ocean surface (R), and in the tropospheric column ($R_a$). Solid lines denote computations made with the 2/3-CL (subscripted "1") cloud model and dashed lines correspond to the full-CL model, (subscripted "2"). All computations for for 16 July 1974 in ly $min^{-1}$ x $10^2$.

cases. However, the sea-level maximum in the 40-50N latitude zone is more pronounced than that at latitude 65N. It is to be noted that $R_1$ for the 2/3-CL case is greater than $R_2$ over the entire range of latitudes under consideration in Fig. 14.

In particular Fig. 14 for 16 July 1974, shows that the quasi-constant difference $R_{s1} - R_{s2}$ from the bottom line of Table X(b) is .0346 ly $min^{-1}$. Likewise, Fig. 14 shows that the net-flux difference $R_1(\phi) - R_2(\phi)$ is closely approximated by .0303 ly $min^{-1}$, the result of the cosine-weighted difference from Table XI(b).

From the flux-divergence equation 7-1 pertaining to the radiative cooling of the tropospheric columns

$$R_a = R_s - R$$

the values of $R_{a1}$ and $R_{a2}$ turn out to be nearly equal, regardless of cloud configuration. From the considerations of the preceding paragraph, the cosine-weighted mean difference $R_{a1} - R_{a2}$ is

$$\overline{R_{a1}} - \overline{R_{a2}} = (\overline{R_{s1}} - \overline{R_{s2}}) - (\overline{R_1} - \overline{R_2}) = .0043 \text{ ly } min^{-1}$$

which also results from Table XII(b). This is a relatively small difference considering the mean cooling rates involved. Fig. 14 makes this same result evident upon examination of the curves of $R_{a1}$ and $R_{a2}$. There are consistent features in both the $R_{a1}$ and $R_{a2}$ curves, such as the minimum values in the latitude zones -10, to the equator and 20N to 30N, which make the general results on $R_{a1}$ and $R_{a2}$ appear credible.

C. CROSS-SEASONAL EFFECTS

Tables X and XI show the three cross-seasonal dates affecting $R_s$ and R centered on 16 July 1974. It is clear that $R_{s1}$ is a relative cross-seasonal minimum at all $\phi \leq 5N$ for 16 July 1974. A similar effect applies to $R_{s2}$ thrugh the same time sequence. Intra-seasonal maximum results apply poleward of 10N to the cross-seasonal comparisons of R at the earth's surface in either cloud-case.

For all $\phi \leq 5$ degrees of latitude in Tables X and XI, there is a systematic trend toward minimal values of both $R_{s1}$ and R, at 16 July 1974. The same effect applies to $R_{s2}$ and $R_2$ on this date. For this limited geographical range near the Southern Hemisphere border, the 16 October date having a solar declination $\delta = -8.5°$ latitude corresponds to the largest positive values of both $R_s$ and R in either cloud configuration. These cross-seasonal results appear to afford qualitative support to the radiational model tested here.

D. COMPARISONS OF NET FLUX AT THE TOP OF THE MODEL ATMOSPHERE WITH SATELLITE OBSERVATIONS

Based upon observations of Raschke et al (1973) of F2(RAS) and of the albedo ALB(RAS) over the latitude-range of this study, the net flux parameter at the top of the atmosphere was defined for the NIMBUS III data-period (16-31 July 1969) at k=0

$$RN(RAS) = QAVE^* \frac{2.00}{1.92} (1-ALB(RAS)) - F2(RAS) \qquad (7-3)$$

Raschke's computed values of the RN for this data period used a slightly different solar constant than that employed in this study (S = 2.00 ly $min^{-1}$). Hence for purposes of consistency in comparisons, our average

extraterrestrial insolation, QAVE*(2.00/1.92) was used in the definition of RN(RAS) in Eq. 7-3.

Values of RN(RAS) were computed after Raschke at each five-degree latitude intersection on the four meridians where comparisons with the present model computations were possible. For the corresponding radiative model computations of this study, the following analog to Eq. 7-3 was adopted.

$$\text{RNMOD} = \text{QAVE}^* \frac{2.00}{1.92} (1-\text{ALBMOD}) - \text{FF2} \qquad (7\text{-}4)$$

FF2 represents a parameter analogous to F2(RAS), values of which were compared in Section III.E. on a latitudinal basis. Likewise, albedo values were compared on a latitudinal basis in Section IV.G.

The computational values of RNMOD for 16 July 1974 were computed using both the 2/3-CL and the full-CL cloud parameterizations. After obtaining averages across the four meridians, the latitudinal comparisons are depicted in Table XIII.

Comparison of RN(RAS) with RNMOD in Table XIII shows that values of RNMOD are somewhat smaller than the values of RN(RAS) at all latitudes $\phi \leq 45N$. The positive difference

$$\text{RN(RAS)} - \text{RNMOD} \qquad \phi \leq 45N$$

occurs because of the consistently small albedos of the Raschke observations. This difference is considerably larger for the full-CL case, when the model albedos were excessively high.

$R_s$-values for the earth-troposphere have been extracted from Table X and appear in columns four and five of Table XIII. Recall that

$$R_s = QAVE\ (1\text{-}ALBMOD) - F_2^* \tag{7-5}$$

In comparing Eqs. 7-4 and 7-5, it is clear that the incoming insolation used in the computation of $R_s$ has been reduced by 4% of an amount which is approximately

$$\overline{QAVE} - \overline{QREF} = .4148 \text{ ly min}^{-1} \tag{7-6}$$

when cosine-averaged over all latitudes considered in this study. Table XIII indicates that

$$\bar{R}_{s1} - \overline{RN(MOD\text{-}2/3)} = .025 \text{ ly min}^{-1}$$

holds for the 2/3-CL case. This difference may be reconciled with the net-flux differences of Eqs. 7-5 and 7-4, through the differenced equation

$$\bar{R}_{s1} - \overline{RN(MOD\text{-}2/3)} = (\overline{FF2} - \overline{F_2^*}) - .04(\overline{QAVE} - \overline{QREF}) \tag{7-7}$$

which requires that

$$(\overline{FF2} - \overline{F_2^*}) = .025 + .04(\overline{QAVE} - \overline{QREF}) \tag{7-8}$$

in ly $\text{min}^{-1}$ for the 2/3-CL case.

The result of Eq. 7-8 shows the average IR-flux divergence across the layer k=2 to k=0 by the $F_2^*$ model of Eq. 3-5. The water-vapor and

$CO_2$ absorber masses of the stratosphere are therefore not quite in radiative equilibrium, because these same absorber masses do not have a compensating solar absorption effect in the present model. The 4% solar absorption by ozone and oxygen are not sufficient to compensate for the added water vapor-$CO_2$ flux-divergence in the terrestrial waves.

| | Mid-Seasonal Dates | | | | | |
|---|---|---|---|---|---|---|
| | (a) | | (b) | | (c) | |
| | 16 April 1974 | | 16 July 1974 | | 16 October 1973 | |
| LAT. | $R_{s1}$ | $R_{s2}$ | $R_{s1}$ | $R_{s2}$ | $R_{s1}$ | $R_{s2}$ |
| 20S | -.0229 | -.0469 | -.1012 | -.1124 | .0764 | .0384 |
| 15 | -.0119 | -.0418 | -.0817 | -.1010 | .0785 | .0400 |
| 10 | -.0002 | -.0358 | -.0546 | -.0772 | .0803 | .0430 |
| 5 | .0171 | -.0235 | -.0468 | -.0656 | .0814 | .0480 |
| 0 | .0353 | -.0079 | .0138 | -.0154 | .0893 | .0567 |
| 5 | .0283 | .0243 | .0297 | -.0062 | .0696 | .0388 |
| 10 | .0198 | -.0364 | .0521 | .0145 | .0484 | .0164 |
| 15 | .0225 | -.0335 | .0635 | .0211 | .0170 | -.0030 |
| 20 | .0204 | -.0368 | .0627 | .0136 | -.0011 | -.0322 |
| 25 | -.0256 | -.0126 | .0825 | .0380 | -.0281 | -.0588 |
| 30 | .0547 | .0293 | .0945 | .0560 | -.0573 | -.0840 |
| 35 | .0488 | .0301 | .1018 | .0607 | -.0743 | -.0916 |
| 40 | .0540 | .0296 | .1254 | .0888 | -.0916 | -.1036 |
| 45 | .0427 | .0096 | .0892 | .0612 | -.1131 | -.1212 |
| 50 | -.0055 | -.0362 | .1461 | .1038 | -.1347 | -.1395 |
| 55 | .0016 | -.0146 | .1063 | .0766 | -.1307 | -.1302 |
| 60 | -.0428 | -.0591 | .1603 | .1315 | -.1525 | -.1493 |
| 65 | -.0089 | -.0374 | .1990 | .1640 | -.1169 | -.1096 |
| Wt.Avg. | .0027 | -.0153 | .0536 | .0190 | -.0081 | -.0320 |

Table X. Cross-seasonal comparison of zonally-averaged values of $R_s$ as a function of latitude. The averaged radiational values for the 2/3-CL cloud parameterization are denoted with a subscripted 1 and the full-CL values by a subscripted 2. (All values in ly $min^{-1}$).

| | Mid-Seasonal Dates | | | | | |
|---|---|---|---|---|---|---|
| | (a) | | (b) | | (c) | |
| | 16 April 1974 | | 16 July 1974 | | 16 October 1974 | |
| LAT. | $R_1$ | $R_2$ | $R_1$ | $R_2$ | $R_1$ | $R_2$ |
| 20S | .0813 | .0514 | .0598 | .0547 | .1742 | .1329 |
| 15 | .1015 | .0681 | .0954 | .0852 | .1845 | .1438 |
| 10 | .1299 | .0957 | .1277 | .1134 | .1911 | .1524 |
| 5 | .1438 | .1049 | .1397 | .1255 | .1756 | .1352 |
| 0 | .1164 | .1376 | .1741 | .1508 | .2117 | .1787 |
| 5 | .1858 | .1294 | .1773 | .1464 | .2017 | .1722 |
| 10 | .1911 | .1460 | .2042 | .1725 | .1886 | .1598 |
| 15 | .1933 | .1470 | .2216 | .1866 | .1657 | .1465 |
| 20 | .2018 | .1569 | .2373 | .1987 | .1611 | .1365 |
| 25 | .2079 | .1769 | .2580 | .2225 | .1490 | .1282 |
| 30 | .2153 | .1917 | .2016 | .2286 | .1179 | .0988 |
| 35 | .1889 | .1684 | .2774 | .2429 | .0870 | .0712 |
| 40 | .1824 | .1549 | .2920 | .2598 | .0791 | .0711 |
| 45 | .1670 | .1343 | .2474 | .2224 | .0547 | .0507 |
| 50 | .1256 | .0952 | .2751 | .2313 | .0341 | .0342 |
| 55 | .1062 | .0850 | .1824 | .1447 | .0112 | .0151 |
| 60 | .0818 | .0603 | .2724 | .2359 | -.0040 | .0017 |
| 65 | .0614 | .0206 | .2637 | .2154 | .0060 | .0119 |
| Wt. Avg. | .1684 | .1333 | .2119 | .1816 | .1370 | .1155 |

Table XI. Cross-seasonal comparison of zonally-averaged values of R as a function of latitude. The averaged values for the 2/3-CL case are denoted with a subscripted 1 and the full-CL case values by a subscripted 2. (All values in ly $min^{-1}$).

| | Mid-Seasonal Dates | | | | | |
|---|---|---|---|---|---|---|
| | (a) | | (b) | | (c) | |
| | 16 April 1974 | | 16 July 1974 | | 16 October 1973 | |
| LAT. | $R_{a1}$ | $R_{a2}$ | $R_{a1}$ | $R_{a2}$ | $R_{a1}$ | $R_{a2}$ |
| 20S | -.1042 | -.0983 | -.1613 | -.1671 | -.0900 | -.0942 |
| 15 | -.1134 | -.1099 | -.1772 | -.1863 | -.1061 | -.1039 |
| 10 | -.1297 | -.1315 | -.1824 | -.1906 | -.1107 | -.1093 |
| 5 | -.1267 | -.1284 | -.1869 | -.1912 | -.0941 | -.0872 |
| 0 | -.0811 | -.1455 | -.1604 | -.1663 | -.1225 | -.1219 |
| 5 | -.1575 | -.1671 | -.1476 | -.1527 | -.1322 | -.1334 |
| 10 | -.1713 | -.1824 | -.1522 | -.1582 | -.1402 | -.1434 |
| 15 | -.1708 | -.1805 | -.1582 | -.1657 | -.1488 | -.1495 |
| 20 | -.1814 | -.1937 | -.1749 | -.1853 | -.1621 | -.1687 |
| 25 | -.1823 | -.1895 | -.1756 | -.1846 | -.1772 | -.1869 |
| 30 | -.1606 | -.1622 | -.1673 | -.1727 | -.1753 | -.1828 |
| 35 | -.1401 | -.1383 | -.1757 | -.1824 | -.1613 | -.1628 |
| 40 | -.1284 | -.1253 | -.1667 | -.1711 | -.1707 | -.1748 |
| 45 | -.1243 | -.1247 | -.1595 | -.1612 | -.1679 | -.1718 |
| 50 | -.1311 | -.1314 | -.1291 | -.1277 | -.1688 | -.1736 |
| 55 | -.1046 | -.0996 | -.0762 | -.0684 | -.1419 | -.1453 |
| 60 | -.1246 | -.1194 | -.1123 | -.1046 | -.1486 | -.1511 |
| 65 | -.0703 | -.0580 | -.0648 | -.0517 | -.1226 | -.1215 |
| Wt. Avg. | -.1457 | -.1486 | -.1585 | -.1628 | -.1450 | -.1474 |

Table XII. Cross-seasonal comparison of the zonally-averaged values of $R_a$ as a function of latitude. The averaged values for the 2/3-CL are denoted with a subscripted 1 and the full-CL cases values by a subscripted 2. (All values in ly $min^{-1}$).

| LAT. | RNMOD 2/3-CL | RNMOD Full-CL | Ocean Troposphere $R_{s1}$ | Ocean Troposphere $R_{s2}$ | RN(RAS) |
|---|---|---|---|---|---|
| 20S | -.1144 | -.1256 | -.1012 | -.1124 | -.0594 |
| 15 | -.0928 | -.1121 | -.0817 | -.1010 | -.0362 |
| 10 | -.0618 | -.0844 | -.0546 | -.0772 | -.0038 |
| 5 | -.0554 | .0287 | -.0468 | -.0656 | .0182 |
| 0 | -.0042 | -.0345 | .0138 | -.0154 | .0616 |
| 5 | .0108 | -.0252 | .0297 | -.0062 | .1194 |
| 10 | .0374 | -.0002 | .0521 | .0145 | .1372 |
| 15 | .0572 | -.0102 | .0635 | .0211 | .1430 |
| 20 | .0577 | .0086 | .0627 | .0136 | .1500 |
| 25 | .0632 | .0348 | .0825 | .0380 | .1426 |
| 30 | .0873 | .0488 | .0945 | .0560 | .1484 |
| 35 | .0958 | .0546 | .1018 | .0607 | .1494 |
| 40 | .1148 | .0782 | .1254 | .0888 | .1561 |
| 45 | .0777 | .0504 | .0892 | .0612 | .1164 |
| 50 | .1244 | .0819 | .1461 | .1038 | .0965 |
| 55 | .0617 | .0317 | .1064 | .0766 | .0997 |
| 60 | .1323 | .1034 | .1603 | .1315 | .0715 |
| 65 | .1436 | .1082 | .1990 | .1640 | .0708 |
| Wt. Avg. | .0288 | .0027 | .0536 | .0190 | .0858 |

Table XIII. Comparison of the ocean-troposphere net radiation $R_s$ at k=2, with the model computed net radiation at the top of the atmosphere RNMOD and with climatology net radiation at the top of the atmosphere from Raschke et al (1973) RN(RAS). $R_s$ and RNMOD are shown for both cloud cases.

## VIII. ZONALLY-AVERAGED TROPOSPHERIC AND OCEANIC HEAT BUDGETS FOR 16 APRIL 1974

### A. THE TROPOSPHERIC HEAT BUDGET

By averaging over the tropospheric columns for the four meridians displayed in Figs. 7, 8, 9 and 10, latitude by latitude, the zonal distribution of $E + H_\Gamma$ results were obtained and are presented in Table XIV. Recall that $R_a$, the tropospheric radiative net cooling is listed in Table XII. The resulting heating rate of the troposphere may then be expressed as a function of $\phi$ by the right side of Eq. 8-1

$$Q_{va} + S_a = R_a + (E + H_\Gamma) \qquad (8\text{-}1)$$

| LAT. | 20S | 15 | 10 | 5 | 0 | 5 | 10 | 15 | 20 |
|---|---|---|---|---|---|---|---|---|---|
| $E+H_\Gamma$ | .7044 | .3784 | .2014 | .0273 | .0595 | .0592 | .0669 | .1296 | .0761 |
| LAT. | 25 | 30 | 35 | 40 | 45 | 50 | 55 | 60 | 65 |
| $E+H_\Gamma$ | .0852 | -.0066 | -.0180 | -.0411 | -.0047 | -.0344 | -.0358 | -.0092 | -.0303 |

Table XIV. Zonally-averaged values of $E + H_\Gamma$ as a function of latitude. (All values in ly $min^{-1}$).

$S_a$ is the storage heating rate of the column, and $Q_{va}$ is the required flux-divergence of heat compatible with the heat balance equation for the column, for the observed values of $R_a$, $E + H_\Gamma$ and $S_a$. Figure 15 depicts the three heating rates ($R_a$, $(E + H_\Gamma)$ and $(Q_{va} + S_a)$) as a function of latitude for the two cloud-model cases.

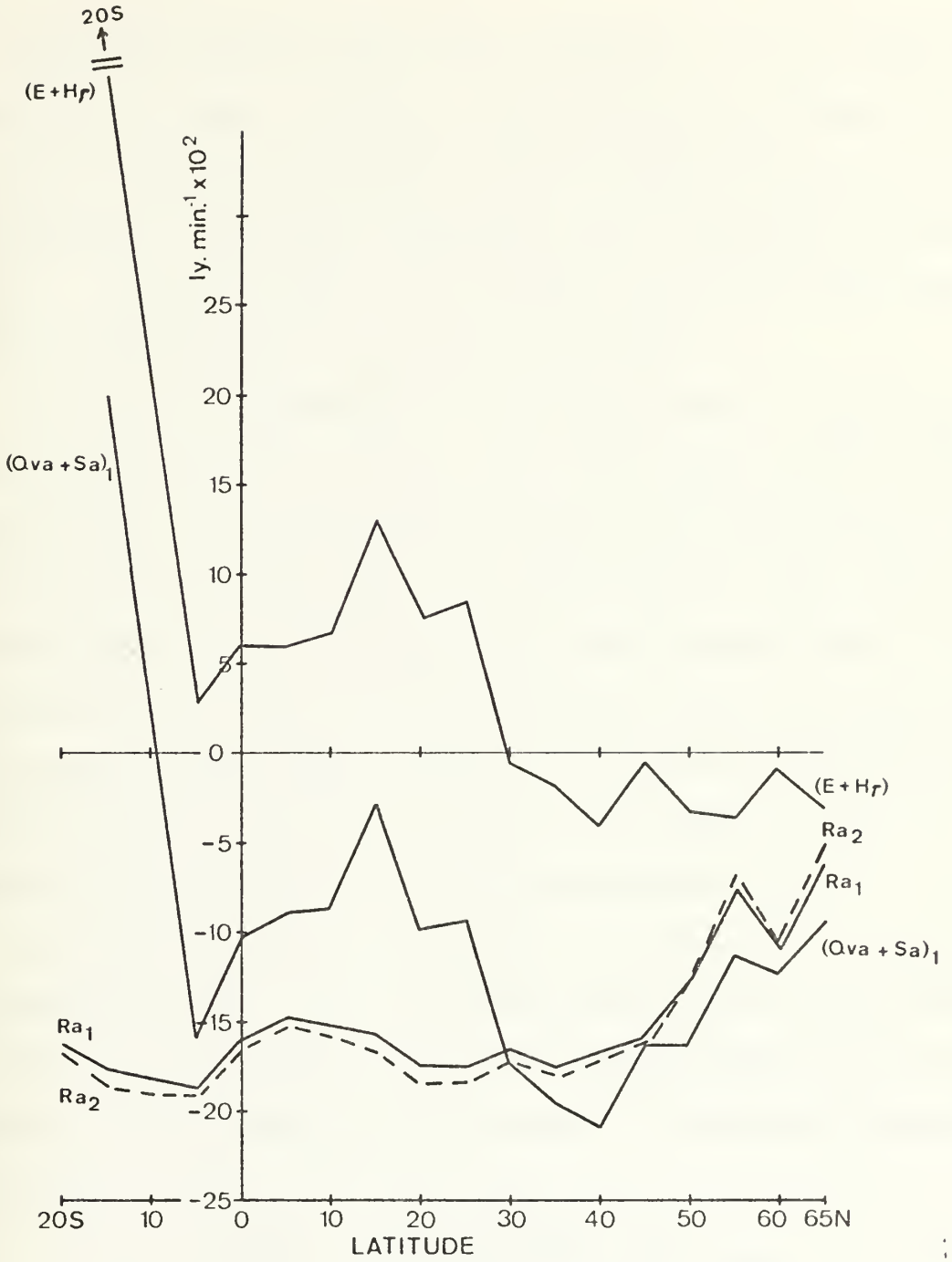


Figure 15. Latitudinal distribution of $R_a$, $E + H_\Gamma$, and of $Q_{va} + S_a$ as a function of latitude for the two cloud-model cases. Values of $E + H_\Gamma$ at 15 and 20S were off the upper scale of the ordinate and may be found in Table XIV. (Solid curves denote 2/3-CL case, dashed curve full-CL).

As noted in Section VII.B., the difference $R_{a1} - R_{a2}$ is almost negligible in this study, and there is little variation as a function of latitude. The distribution of $E + H_\Gamma$ as a function of latitude is also independent of cloud-model. Therefore, Fig. 15 shows only one curve for $E + H_\Gamma$. The curve of $(Q_{va} + S_a)_1$ is shown in Fig. 15, as the residual of the right side of Eq. 8-1 for the 2/3-CL case.

For ease of interpretation in Fig. 15, the curve of $(Q_{va} + S_a)_2$ for the full-CL case was not plotted. This curve follows closely parallel to that of $(Q_{va} + S_a)_1$ being slightly less than $(Q_{va} + S_a)_1$ in the latitude range 20S to 45N. From 45N to 65N the curve of $(Q_{va} + S_a)_2$ exceeds the curve of $(Q_{va} + S_a)_1$ by a small amount. This crossover effect is to be expected by examination of the corresponding crossover in the $R_{a1}$ and $R_{a2}$ curves at these higher latitudes. As is seen in Fig. 15, the net heating curve $Q_{va} + S_a$ follows the same basic pattern as the $E + H_\Gamma$ curve, since $R_a$ is relatively constant with latitude.

The cosine-weighted value $\overline{Q_{va} + S_a} = -.0512$ ly $min^{-1}$ for the average tropospheric column. $\overline{Q_{va}}$ has not been computed in this study; however, if $\overline{Q_{va} + S_a}$ is attributed solely to mean storage-cooling $\overline{S_a}$ of the troposphere, the daily storage rate corresponds to a temperature-change rate given by

$$\left(\overline{\frac{\partial T}{\partial t}}\right) = 4.1 \frac{\overline{R_a} + \overline{(E + H_\Gamma)}}{\Delta P \text{ mb}} \times 1440 \text{ °C/day} \qquad (8\text{-}2)$$

with $\Delta P$ mb $\doteq$ 800 mb in the troposphere. The resultant cooling rate by (8-2) in the troposphere, considering that zero lateral flux-divergence applies, is therefore approximately

$$\left(\overline{\frac{\partial T}{\partial t}}\right) = -.59°C \text{ (day)}^{-1}$$

averaged over the mean $cm^2$ tropospheric column.

B. THE LATITUDINALLY-AVERAGED HEAT BUDGET OF THE OCEAN

The latitudinally-averaged heat-budget of the ocean water-mass obeys the following thermodynamic relationship for both the 2/3-CL and full-CL cases.

$$Q_{vo} + S_o = R + (-(E + H_\Gamma)) \qquad (8\text{-}3)$$

Note that Eq. 8-3 is the analog of Eq. 8-1 for the ocean-mass, with $-(E + H_\Gamma)$ representing the average turbulent cooling rate for the water-mass by mixing across the sea-air interface.

The two terms of the right side of Eq. 8-3 have been computed for each meridian and then averaged zonally, with R and $E + H_\Gamma$ shown in Table XI and XIV, respectively. $Q_{vo} + S_o$ has been computed as the residual of these two terms at each latitude and is graphed in Fig. 16 for both cloud cases.

The primary ocean-mass heating-function is R, the radiative heating rate at the ocean-air interface. As discussed in Section VII, $R_1 > R_2$ for all latitudes considered in this study. Therefore, according to Eq. 8-3, $(Q_{vo} + S_o)_1$ must be greater than $(Q_{vo} + S_o)_2$ by the same amounts since $-(E + H_\Gamma)$ is constant for both cloud cases. This means that the internal heating rate of the ocean-mass, as given in Eq. 8-3, is greater in the 2/3-CL case than in the full-CL case for all latitudes considered in this study. $Q_{vo}$ is the required mean oceanic heat-flux divergence at latitude $\phi$, and $S_o$ is the heat-storage in the oceanic column.

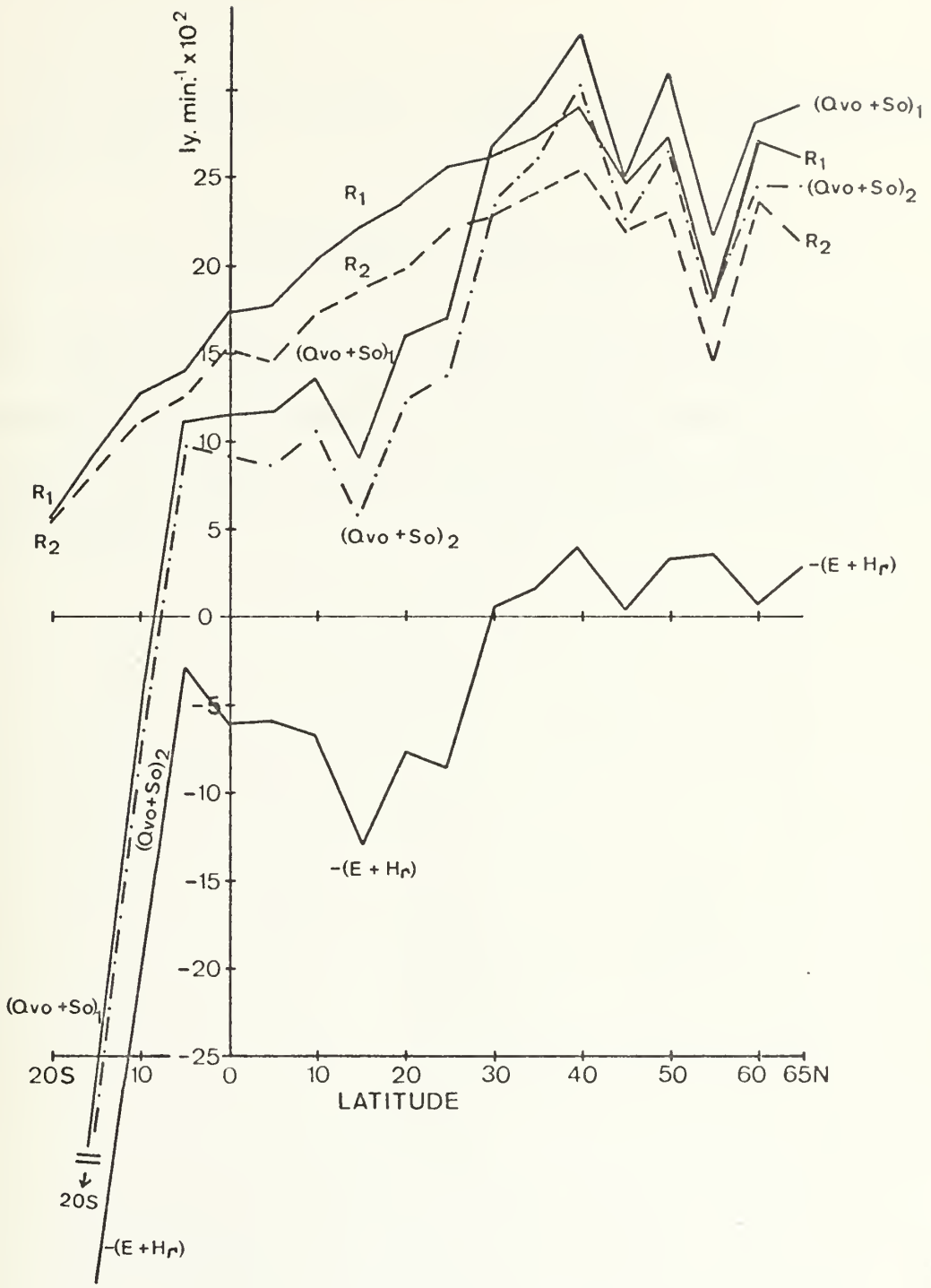


Figure 16. Latitudinal distribution of R, $-(E+H_\Gamma)$, and of $(Q_{vo}+S_o)$ as a function of latitude for the two cloud-model cases. The value of $-(E+H_\Gamma)$ at 15 and 20S were off the lower scale of the ordinate and may be inferred in Table XIV. (Solid curves denote 2/3-CL case; dashed or dot-dashed curves denote full-CL case).

The cosine-weighted average of $\overline{(Q_{vo} + S_o)}_1$ over the latitude range of Fig. 16 is

$$\overline{(Q_{vo} + S_o)}_1 = .0949 \text{ ly min}^{-1}$$

(cf., Tables XI, XIV) which corresponds to a mean heating rate in the water-mass column. It should be noted that this heating rate is considerably larger (and of opposite sign) than the corresponding atmospheric effect.

## IX. CONCLUSIONS

The present work continues the use of the radiational two-layer cloud model adapted from Spaeth's mid-winter study to FNWC gridpoint data valid over the four meridians for 16 July 1974. The use of the 2/3-CL parameterization, as compared to the full-CL after Smagorinsky (1960), for the specification of cloud-layer amounts gave the best verification for the computed global albedo as a function of latitude when compared with observations from NIMBUS III satellite climatology comparable to that of 16 July 1974. The use of the 2/3-CL parameterization also gave good verification of computed long-wave flux to space when compared to the latitudinal distribution of the same element as given by satellite climatology.

The chief shortcoming of the computed global albedo versus the satellite measured albedo occurred in tropical latitudes (20S - 20N). Here, it appears that cloud-elements do not behave as reflecting sheets for insolation but rather as focusing devices through the intra-cloud spaces. The use of 50-60% model cloud reflectances seems excessive in these latitudes. As a practical alternative it may be reasonable to tune the cloud reflectances until agreement of the computed global albedos with satellite measurements is achieved in the latitude range 20S - 20N.

In the topics, all analyses are subject to data-sparsity and hence are largely dependent upon climatology and a relatively few radiosonde reporting stations. An apparent weakness in this study is that of

overspecifying cloud-amounts through the use of Smagorinsky type formulas. This could be a result of inadequately resolved relative humidities, which in general might well be lower than inferred by the FNWC analyses.

One of the major positive results of the radiative model was the simulation of the proper sense of the cross-seasonal radiative heat balances at the top of the earth-atmosphere system. A similar positive result applied to cross-seasonal radiative balance at the ocean surface centered on 16 July 1974.

LIST OF REFERENCES


1. Arakawa, A., 1972: Design of the UCLA General Circulation Model, Numerical Simulation of Weather and Climate Tech. Rpt. No. 7, Department of Meteorology, University of California.

2. Budyko, M. I., 1956: The Heat Balance of the Earth's Surface, Leningrad, pp. 255 (Translated by N. A. Slepanova) translation distributed by U. S. Weather Bureau, Washington, D. C.

3. Coulson, K. L., 1959: Radiative Flux from the Top of Rayleigh Atmosphere, Ph.D. Dissertation, Department of Meteorology, University of California, pp. 60.

4. Dixon, W. J., 1973: Biomedical Computer Programs, University of California Press, pp. 773.

5. Fleagle, R. G., Businger, J. A., 1963: An Introduction to Atmospheric Physics, Academic Press, New York, pp. 346.

6. Gates, W. L., Batten, E. S., Khale, A. B., and Nelson, A. B., 1971: A Documentation of the Mintz-Arakawa Two-Level Atmospheric Circulation Model, Advance Research Projects Agency Report No. R-877-ARPA, Rand Corporation, Santa Monica, California, pp. 408.

7. Hanson, K. J., 1971: Studies of Cloud and Satellite Parameterization of Solar Irradiance at the Earth's Surface, paper presented at the Miami Workshop on Remote Sensing, Miami, Florida, 29-31 March 1971.

8. Joseph, J. H., 1971: "On the Calculation of Solar Radiation Fluxes in the Troposphere," Solar Energy, Vol. 13, Pergamon Press, London, pp. 251-261.

9. Kaitala, J. E., 1974: Heating Functions and Moisture Source Terms in the FNWC Primitive Equation Models, paper presented at the Continuing Education Program for Meteorological Specialists, Naval Postgraduate School, Monterey, California, 29 April 1974.

10. Kesel, P. G. Winninghoff, F. J., 1972: "The Fleet Numerical Weather Central Operational Primitive-Equation Model," Monthly Weather Review, Vol. 100, No. 5.

11. Langlois, W. E., Kwok, H. C. W., 1969: Description of the Mintz-Arakawa numerical general circulation model. Numerical Simulation of Weather and Climate Tech. Rpt. No. 3, Department of Meteorology, University of California.

12. Malkus, J. S., 1962: "Large Scale Interactions," The Sea, Vol. 1, Interscience Publishers.

13. Martin. F. L., 1972: Description of a Radiation Package for the Naval Postgraduate School General Circulation Model, Department of Meteorology, Naval Postgraduate School, Monterey, California.

14. Martin, F. L., 1974: Unpublished manuscript, Department of Meteorology, Naval Postgraduate School, Monterey, California.

15. Meyers, W. T., 1975: Radiational Parameterization for the FNWC Primitive Equation Model Using Data Over the Oceans for 16 April 1974, M. S. Thesis, Department of Meteorology, Naval Postgraduate School, Monterey, California (In progress).

16. Quinn, W. H., 1971: Studies of Parameterization of Solar Irradiance at the Earth's Surface, paper presented at the Miami Workshop on Remote Sensing, Miami, Florida, 29-31 March 1971.

17. Raschke, E., Von der Haar, T., Bandeen, W., Pasternak, M., 1973: The Annual Radiation Balance of the Earth-Atmosphere System during 1969-1970 from NIMBUS III Measurements," Journal of the Atmospheric Sciences, Vol. 30, No. 3, pp. 341-364.

18. Rodgers, C. D., 1967: "The Radiative Heat Budget of the Troposphere and Lower Stratosphere," Planetary Circulation Project Report N. A2, Department of Meteorology, Massachusetts Institute of Technology, pp. 99.

19. Sasamori, T., 1968: "The Radiative Cooling Calculation for Application to General Circulation Experiments," Journal of Applied Meteorology, Vol. 7, No. 5, pp. 721-729.

20. Smagorinsky, J., 1960: "On the Dynamical Prediction of Large Scale Condensation by Numerical Methods," Geophysical Monograph, No. 5, American Geophysical Union, Washington, D. C., pp. 71-78.

21. Smith, W. L., 1966: "Note on the Relationship between Total Precipitable Water and Surface Dew Point," Journal of Applied Meteorology, Vol. 5, No. 5, pp. 726-727.

22. Spaeth, W. T., Jr., 1974: Heat Budget Parameterization for the FNWC Primitive Equation Model Using Data for 16 January 1974, M. S. Thesis, Department of Meteorology, Naval Postgraduate School, Monterey, California.

23. Von der Haar, T. H., Hanson, K. J., 1969: Absorption of Solar Radiation in Tropical Regions," Journal of the Atmospheric Sciences, Vol. 26, No. 4, pp. 652-655.

24. Von der Haar, T. H., Oort, A. H., 1973: "New Estimate of Annual Poleward Energy Transport by Northern Hemisphere Oceans," Journal of Physical Oceanography, Vol. 3, No. 2, pp. 169-172.

25. Warner, M. W., 1974: Heat Budget Parameterization for the FNWC Primitive Equation Model Using Data for 16 October 1973, M. S. Thesis, Department of Meteorology, Naval Postgraduate School, Monterey, California.

26. Weiler, H., Burling, R. W., 1967: "Direct Measurements of Stress and Spectra of Turbulence in the Boundary Layer over the Sea," Journal of the Atmospheric Sciences, Vol. 24, pp. 653-664.

27. Yamamoto, G., 1952: "On a Radiation Chart," Science Rpts of the Tohoku University, Series No. 5, pp. 9-23.

INITIAL DISTRIBUTION LIST

| | | No. Copies |
|---|---|---|
| 1. | Defense Documentation Center<br>Cameron Station<br>Alexandria, Virginia 22314 | 2 |
| 2. | Library, Code 0212<br>Naval Postgraduate School<br>Monterey, California 93940 | 2 |
| 3. | Professor F. L. Martin, Code 51Mr<br>Department of Meteorology<br>Naval Postgraduate School<br>Monterey, California 93940 | 4 |
| 4. | Lt. Terry W. Beahan<br>406 Highland Road<br>Grayslake, Illinois 60030 | 2 |
| 5. | Department Chairman, Code 51<br>Department of Meteorology<br>Naval Postgraduate School<br>Monterey, California 93940 | 1 |
| 6. | Assoc. Prof. Robert. L. Haney, Code 51Hy<br>Department of Meteorology<br>Naval Postgraduate School<br>Monterey, California 93940 | 1 |
| 7. | Naval Weather Service Command<br>Naval Weather Service Headquarters<br>Washington Naval Yard<br>Washington, D. C. 20390 | 1 |
| 8. | Fleet Numerical Weather Central<br>Attn: Mr. Leo Clarke<br>Monterey, California 93940 | 2 |